EFFECTS OF IONIZING RADIATION ON THE ENVIRONMENT OF ^{14}N IN ORGANIC COMPOUNDS BY NUCLEAR QUADRUPOLE SPECTROSCOPY

By

KHALID JAMIL

A DISSERTATION PRESENTED TO THE GRADUATE SCHOOL
OF THE UNIVERSITY OF FLORIDA IN PARTIAL FULFILLMENT
OF THE REQUIREMENTS FOR THE DEGREE OF
DOCTOR OF PHILOSOPHY

UNIVERSITY OF FLORIDA

1993

To my late parents.

May God keep their souls in eternal peace and rest.

ACKNOWLEDGEMENTS

It is my pleasure to find an opportunity to express my gratitude to all those people who were kind to me, in one way or the other, during the entire course of this dissertation.

I would like to begin by acknowledging the chairman of my supervisory committee, Dr. D. E. Hintenlang, for introducing this area of research to me, providing apparatus and technical know-how, and assisting me financially from NQR project funds, when I needed it. I also extend my appreciation to him for being friendly and making himself available during all the working days and hours to discuss anything I wanted.

I am indebted to Dr. W. H. Ellis for his encouragement at various occasions during the progress of this work.

Dr. S. Anghaie, with whom I discussed not only science but also life in general, is sincerely acknowledged. His stimulating discussions and suggestions are greatly appreciated.

I am grateful to Dr. Hanrahan and Dr. Whitney for being on my dissertation supervisory committee and for their valuable suggestions to improve this dissertation.

Besides the committee members many friends need to be mentioned. Mian Wajahat Hussain's frequent visits to my apartment, which kept me feeling at Lahore, and his sincerity are greatly appreciated. I wish to thank Mr. Ahmed Ejaz Nadeem and his family with whom very pleasant time was spent at Maguire Village apartments. Mr. Kaiss Al-Ahmady and Mr. Haiquan Dai are thanked for sharing not only moments of joys but also sharing difficult times. Mr. Louis Iselin is acknowledged for helping me to keep the NQR lab computer in operating condition. Last but not the least, Mr. Sergio Gavazza and his family deserve special recognition for their friendship, hospitality, and Brazilian barbecue parties.

All my family members including my wife, Farhat Fatma, my son Ashar, and daughter Anam are greatly acknowledged for their endurance and patience to spare me so long to complete this dissertation.

TABLE OF CONTENTS

ACKNOWLEDGEMENTS iii

ABSTRACT viii

CHAPTERS

1 INTRODUCTION 1

General Introduction 1
Literature Review 2
Objectives and Goals 9
Layout of the Dissertation 10

2 NQR SPECTROSCOPY: BACKGROUND THEORY AND METHODS . 13

Background Theory 13
    Classical Concept of Quadrupole Moments . . . 13
    Nuclear Quadrupole Interactions 19
        Static quadrupole interaction 19
        Dynamic magnetic interaction 34
    Nuclear Spin Relaxation Theory 36
Method of NQR Spectroscopy 40
    General Principle of NQR Measurements 40

3 EXPERIMENTAL PROCEDURES AND METHODS 45

Procedures and Methods of NQR Experiments 46
  Pulsed NQR Spectrometer 46
  System Description 51
  Exposure of Urea and Thiourea at CVP of the UFTR 52
Procedures and Methods of Supporting Experiments . . 53
    In Core Gamma Dose Measurement 53
        TLD calibration curve for gamma dose . . 54
        Gamma dose rate at CVP of the UFTR . . . 56
    Out Core Gamma Exposure of Urea and Thiourea . 58
    Temperature Determination of Urea and Thiourea at CVP of the UFTR . . 62
    Out Core Heating of Urea and Thiourea 64
    X-ray Diffraction of Neutrons Irradiated Samples 64

4 EXPERIMENTAL RESULTS 66

Results of the NQR Experiments 67
NQR Raw Data 67
NQR Data Analysis 67
Programs for NQR parameter extraction . 70
Error Analysis of the NQR Parameters 77
Results of Urea and Thiourea Exposed at CVP of the UFTR 85
Results of Supporting Experiments 88
In Core Gamma Dose Rate Measurement 88
Gamma dose at CVP of the UFTR 88
Out Core Gamma Exposure of Urea and Thiourea . 88
Out Core Temperature Effects on Urea and Thiourea . . . 100
X-ray Diffraction of Neutrons Irradiated Samples 100

5 DISCUSSION 111

Effects of Gamma Photons on Urea and Thiourea . . 112
Monte Carlo Simulation of NQR Experiments at CVP of the UFTR . . . 115
Neutron Energy Spectrum at CVP of the UFTR Core 116
Neutrons Dose in Urea and Thiourea 119
Effects of Reactor Neutrons on Urea and Thiourea 123
Effects on the NQR Signal Amplitude . . 123
Effects on Inverse Linewidth 130
Mathematical Model 135
Development of Mathematical Model 138

6 CONCLUSIONS 149

APPENDICES

A A SPIN-ECHO OF THIOUREA 152

B RAW DATA FILE OF A NQR SPECTRUM 153

C COMPUTER PROGRAMS LISTINGS: NQR PARAMETER EXTRACTION 156

Computer Program DFCPN 156
Computer Program COPROC 157
Nonlinear Fitting (NOLFIT) Program 161

D MONTE CARLO NEUTRON PHOTON TRANSPORT CODE (MCNP) . 168

An Example of MCNP Input for the UFTR 168

Explanations of Input Cards 169
Abridged Sample Output of MCNP 174

REFERENCES 191

BIOGRAPHICAL SKETCH 197

Abstract of Dissertation Presented to the Graduate School
of the University of Florida in Partial Fulfillment of the
Requirements for the Degree of Doctor of Philosophy

EFFECTS OF IONIZING RADIATION ON THE ENVIRONMENT OF ^{14}N IN ORGANIC COMPOUNDS BY NUCLEAR QUADRUPOLE SPECTROSCOPY

By

KHALID JAMIL

December 1993

Chairperson: Dr. D. E. Hintenlang
Major Department: Nuclear Engineering Sciences

This research is an innovative application of the noninvasive state-of-the-art NQR spectroscopy in studying the effects of mixed radiation fields of gamma and neutron from a nuclear reactor on two dry polycrystalline organic materials: urea, $OC(NH_2)_2$, and thiourea, $SC(NH_2)_2$. These tissue equivalent compounds have simple structures, known NQR transition frequencies and strong signals.

The out-core gamma doses up to 622 kGy, much higher than in-core gamma dose determined at the center vertical port (CVP) of the University of Florida Training Reactor (UFTR), have shown no significant effects on these compounds observed by the NQR parameters. Similarly, no significant effects of elevated temperatures similar to observed at CVP of the UFTR on fresh samples of urea and thiourea have been observed on these compounds by the NQR parameters.

Thus, the neutron fluence $\geq 1.0 \times 10^{15}$ cm^{-2} at the CVP of the UFTR has shown effects on the NQR signal amplitude and the inverse linewidth, for both materials studied in this work. The experimentally measured inverse linewidths determined the relative dispersions in intermolecular distances, $(\Delta r_m)_r$, after four-hour-neutron irradiations, as $2.1(\Delta r_m)_u$ and $1.5(\Delta r_m)_u$ for thiourea and urea, respectively where $(\Delta r_m)_u$ is the intermolecular distances for unirradiated samples.

The NQR spectroscopy results using inverse linewidths find that the effects of neutron irradiation on urea and thiourea are dominantly due to lattice defects. The results have also been supported by X-ray spectroscopy and Monte Carlo simulations.

Using experimental data, the average number of secondary damages per primary damage, N_{sd}, has been determined as 2.2×10^6 and 2.8×10^5 for thiourea and urea, respectively. The experimentally determined value of N_{sd} is a useful parameter in the area of dose'calculation on cellular level.

CHAPTER 1
INTRODUCTION

This chapter presents the general introduction, literature review, objectives and goals of this research. Also the layout of this dissertation is outlined at the end of this chapter.

General Introduction

A body of mass exposed to ionizing radiation absorbs energy. The energy is deposited along the path of the radiation in microscopic volume elements within the material. The absorbed dose (energy/unit mass) from different ionizing radiations in a certain material may be the same but the resulting chemical and physical effects are entirely different [1]. Thus, it is not only sufficient to know the amount of energy deposited in a certain material by a particular type of ionizing radiation but also it is necessary to know how the energy has been deposited in the material especially on a microscopic level to understand the mechanism of chemical or physical changes produced by ionizing radiation.

In order to obtain information on the microscopic level concerning radiation induced changes in materials, a technique which can provide information from within the molecule using one of the nuclei as a detector must be used. Here nuclear quadrupole resonance (NQR) spectroscopy offers its applications.

In the NQR spectroscopic technique the nuclear quadrupole moments of the probe nuclei interact with their surrounding electric field gradient (efg) and furnish information about the environment of the probe nuclei embedded in spectrographic data. Any damage produced by ionizing radiation in the material changes the efg near the probe nuclei which can be observed by NQR spectrometry. Several other spectroscopic techniques such as Electron Spin Resonance (ESR), X-ray diffraction, and Raman spectroscopy can provide information concerning radiation defects itself and in the proximity of the probe nucleus but NQR spectroscopy is very promising to get response of the irradiated matrix for radiation defects in addition to providing information about localized radiation damage [2]. The background theory and method of NQR spectroscopy is explained in chapter two.

Literature Review

The changes in material properties aided the discovery of a new type of ionizing radiation, gamma, by Henri Becquerel in 1896 [3]. Prior to this discovery it was known that X-rays, one of the ionizing radiations, cause glass to fluoresce and blacken photographic film. Becquerel found blackening of photographic film that he left in his drawer near a uranium compound. He associated the change in material property, the blackness of photographic film, with the presence of ionizing radiation similar to X-rays but originating from uranium nuclei.

Subsequent experiments and research found the presence of many other types of ionizing radiations. Thus, the effects of ionizing radiation on materials enhanced human knowledge concerning the nature, properties, and types of these radiations. On the other hand, the subject of the effects of radiation on material became an interesting and rewarding area both for theoretical and experimental research.

Some ionizing-radiation effects are desirable and have applications in various branches of sciences and engineering. The applications of these radiations range from food preservation to medical sciences, from polymer science to biochemistry and from quality control to smoke detectors. In spite of the wide range of applications of these radiations in science and engineering, the detrimental aspects of these radiations cannot be neglected [1].

The growing industry of radiation applications demands the use of more radiation sources especially gamma and neutrons. These radiations not only have many useful applications but also have deleterious effects on many objects or devices in and around radiation sources, and on personnel dealing with radiation.

These radiations, gamma and neutron, interact with the medium through which they pass in a variety of ways. In general gamma photons primarily interact with matter in three popular modes, Photoelectric Effect (PEE), Compton Scattering (CS), and Pair Production (PP) [4]. In PEE, the gamma photons interact with the bound electrons of the atom and transfer full energy to the electron and the ionized atom recoils to conserve momentum. In CS, the gamma photons interact with the free electrons and excite or ionize the atoms of the medium and the interacting photons are scattered with reduced energy. In the case when gamma energy is more than 1.02 MeV, the gamma photon interacts with the coulomb fields of either the electrons or nuclei. Consequently, the photon disappears by leaving an electron-positron pair that may further interact with the medium in secondary interactions. In the case when gamma photons interact with the organic material, the chemical bonds are either broken or new electronic configurations take place.

However, neutrons interact with the atoms rather than with the electrons of the medium either by colliding elastically or inelastically or through nuclear reactions [5]. In elastic or inelastic collisions, energy is imparted to the atoms of the medium. If the energy of the neutron is more than the energy required to irreversibly displace an atom from a normal site in the crystal lattice, then a vacancy is created at the lattice point. A displaced atom residing at positions other than normal lattice site is called an interstitial substitution. If the energy of the displaced atom is sufficient, it further collides with the electrons of the medium to excite and ionize the atoms, or it displaces other atoms to interstitial positions. In this way a cascade of displacements is initiated and the damage is extended over several molecular distances [6]. Sometimes, neutrons interact with the nuclei in the medium through nuclear reaction and change the constituents in the material which is tantamount to adding impurity atoms, called substitutional impurities, in the medium.

A computer search of existing literature under the rubric of radiation damage or radiation induced defects or changes by NQR methods has been carried out. Only a very limited work has been done on the study of radiation effects by NQR spectroscopy. The little work that has been done is confined to moslty chlorine compounds while using gamma and X-ray photons [2,7,8,9].

Research by Vargas et al. shows that irradiation defects in chlorates ($NaClO_3$, $KClO_3$, and $Ba(ClO_3)_2$) compounds modifies the electric field gradients. The NQR signal intensity and the inverse linewidth decrease with gamma radiation in these compounds [2]. Recently, Hintenlang and Higgins have published a paper on the effects of gamma photons on hydrated urea using ^{14}N as probe nuclei [10]. In their paper changes in inverse linewidth have been measured and correlated with the subtle changes in the electronic distribution without major structural changes in urea.

The limited work that has been done shows that the NQR spectroscopy has potential to provide information regarding radiation effects near the environments of probe nuclei, with spin $I \geq 1$, embedded in a host medium. Since NQR studies have not been carried out to investigate radiation induced changes in most compounds, this research employs the NQR spectroscopy to organic compounds especially nitrogenous organic compounds because of their biological significance. Two organic compounds urea and thiourea have been selected to employ this spectroscopy technique especially in mixed radiation fields of gammas and neutrons. These compounds have simple structure, known NQR frequencies, and strong signals.

Urea, NH_2CONH_2, is an organic compound which is produced in biological systems through the metabolism of amino acids in the citric acid cycle [11]. The molecular structure of urea is planar; i.e., all atoms are in the same plane as shown in the figure 1-1 [12]. All the molecules are linked to each other through hydrogen bonding forming an infinite plane. All the planes containing urea molecules are mutually perpendicular to each other through hydrogen bonding [13].

Thiourea, NH_2CSNH_2, also known as thiocarbamide is an organic compound. The thiourea molecule has a plane structure as shown in figure 1-2(a). It is interesting that thiourea forms a molecular crystal in which molecules are not linked

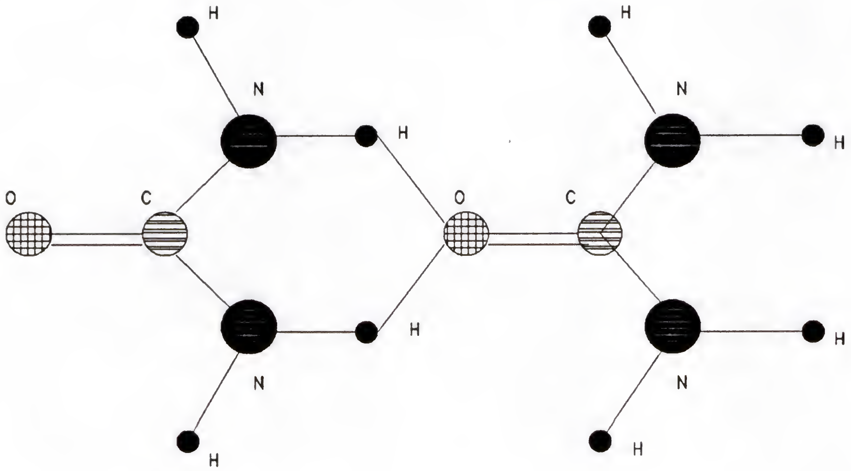

Figure 1-1: The two urea molecules are shown linking through hydrogen bonding.

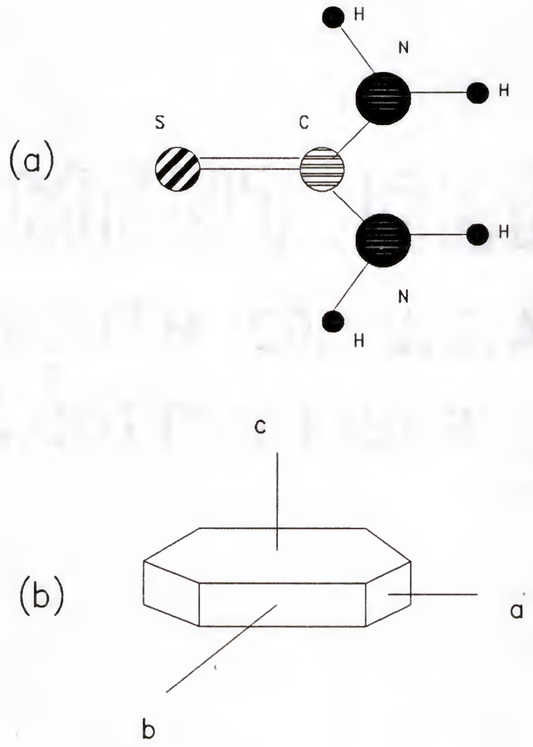

Figure 1-2: (a) The planar molecule of thiourea and (b) the orthorhombic six-sided crystalline structure for thiourea a-, b-, and c- are the orthogonal crystal axes.

with each other through hydrogen bonding [14]. Thiourea, a ferroelectric material, has five phases. All phases have an orthorhombic structure having six-sided prisms as depicted in figure 1-2(b) and have four molecules per unit cell. In Phase I (at low temperature) there is incomplete cancellation of the dipole moment projection along the crystalline b axis. Two of the molecular planes in the unit cell make an angle of 29.5° while the other two make an angle of 19.6° with respect to the b-axis. The latter is called a type-1 molecule (site-1) and the former a type-2 molecule (site-2) [15]. That is why two peaks appear in thiourea NQR spectrum corresponding to site-1 and site-2, respectively. All thiourea spectra are fitted with the "two site model" explained in chapter four.

Objectives and Goals

The study of nitrogenous organic compounds for radiation effects by gamma photons and neutrons are of prime importance in the area of radiation effects. Two simple organic compounds--urea, a biologically significant compound, along with thiourea, a close relative of urea--are chosen. These nitrogenous compounds (1) are tissue equivalent for gamma and neutron doses, (2) are relatively simple in structure, and (3) have known NQR frequencies and strong signals.

The present work reports the first application of the NQR spectroscopy for measuring the effects of, gammas and reactor neutrons on the NQR parameters to obtain, type of damage i.e.

chemical and/or physical (lattice damage), the relative intensity of the damage in urea and thiourea, the prominent locations of damages in urea and thiourea molecules, and size (volume) of damage in urea and thiourea. All of those objectives could be achieved by the NQR spectroscopy but a determination of the damage locations in urea and thiourea molecules required application of Monte Carlo simulations. However, X-ray diffractometry of irradiated samples and the Monte Carlo simulations of the experiments, conducted at center vertical port (CVP) of the University of Florida Training Reactor (UFTR), were employed to support and strengthen the NQR results.

Layout of the Dissertation

Chapter two of this dissertation enunciates the theory of the NQR spectroscopy starting from a very rudimentary knowledge of physics. After building up the necessary concepts to understand the work done in this dissertation, chapter two describes the method of the NQR spectroscopy.

Chapter three deals with the procedures and methods of the NQR experiments carried out at CVP of the UFTR in mixed fields of gammas and neutrons. The procedural details of all supporting experiments are given. The supporting experiments were performed to independently determine the gamma dose rate and the temperature of the samples at CVP of the UFTR. The procedures and methods are explained that how to observe the effects of out core gamma doses (but equivalent to in core gamma doses) on the NQR parameters for urea and thiourea. Similarly, the procedures and methods are given how to observe the effects of out core temperature (but for equivalent temperature observed at CVP of the UFTR) on the NQR parameters of urea and thiourea. Finally, procedures of X-ray analyses on samples of urea and thiourea are given.

Chapter four describes the results of the NQR experiments conducted at CVP of the UFTR. The raw data, resulting from the experiments, are converted into physically meaningful parameters for presentation and discussion. Thus, data analyses techniques are given and then the results of the NQR experiments are given along with a determination of the errors in each parameter. The results of supporting experiments are given in the same order as described in chapter three.

Chapter five discusses the results given in chapter four. The effects of gamma doses on urea and thiourea are discussed. Then, the results of the Monte Carlo simulation experiments conducted at CVP of the UFTR are discussed. Moreover, the experimental results demonstrating the effects of reactor neutrons on urea and thiourea by the NQR spectroscopy are discussed. The relationship to various NQR parameters is subsequently described. Then, using the support of the Monte Carlo calculations and X-ray spectrometry, the results of NQR spectroscopy are explained and related to the objectives of this dissertation. The significant conclusions are summarized in chapter six from the results obtained in this study.

CHAPTER 2
NQR SPECTROSCOPY: BACKGROUND THEORY AND METHODS

Background Theory

Classical Concept of Quadrupole Moments

The theory of nuclear quadrupole moments is developed using classical concepts. The classical treatments help one to understand the physical concepts of the multi-pole moments and their origin. The applicable quantum mechanical ideas as required by the very nature of the problem will be given later in this chapter.

One can start the development of the concepts of moments from Coulomb's law which finds the force between two point charges q_1 and q_2 separated by a distance r and is given by

$$\vec{F} = k\frac{q_1 q_2}{r^2}\hat{e} \qquad (2\text{-}1)$$

where k is a constant and $\hat{e}$ is the unit vector in the direction of force chosen by convention [16].

Associated with each static charge in space, there is an electric field surrounding the charge. The field strength can be found at a distance r from a charge q if a small test charge q_{test} is brought to the point of interest. Thus, the electric field strength can be expressed using Coulomb's law as given in equation (2-2)

$$\vec{E} = Lim_{q_{test} \to 0} \frac{\vec{F}}{q_{test}} \qquad (2-2)$$

where $\vec{F}$ is the Coulombic force between the charge q and the test charge q_{test}.

A static electric field formed by a charge or group of charges is a conservative field; thus, the electric field must satisfy the following relationship as

$$\nabla \times \vec{E} = 0 \qquad (2-3)$$

The potential theory demands that if the curl of a vector is zero then there must exist a scalar function, V, such that

$$\vec{E} = -\nabla V \qquad (2-4)$$

where V is the electric potential for a charge q at a distance r and is given by

$$V = k\frac{q}{r} \qquad (2-5)$$

Hence, if V is measured at a known distance from a point charge, the electric field can be found. Let there be a charge q_1 in space and an orthogonal coordinate system is set up as shown in figure 2-1 such that the distance of charge q_1 from the origin is R. If a small test charge q is placed along the z-axis at a distance Z from the origin, then equation (2-5) gives the potential as

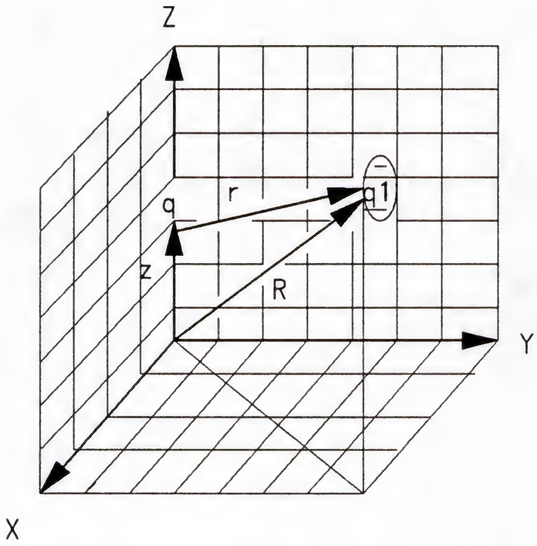

Figure 2-1: Moments formation due to the charge q1 observed by a test charge q on z-axis.

$$dV = k\frac{q_1}{r} \tag{2-6}$$

One can find r in terms of R, Z and θ. It is convenient to use spherical polar coordinates. Using the law of cosines one gets

$$r^2 = Z^2+R^2-2ZR\cos\theta \tag{2-7}$$

or

$$\frac{1}{r} = \frac{1}{Z}(1-[\frac{2R}{Z}\cos\theta-\frac{R^2}{Z^2}])^{-\frac{1}{2}} \tag{2-8}$$

Solving equation (2-6) with the binomial expansion of equation (2-8) yields

$$dV=kq_1\ [\frac{1}{Z}+\frac{R}{Z^2}\cos\theta+\frac{R^2}{Z^3}(\frac{3}{2}\cos^2\theta-\frac{1}{2})+...] \tag{2-9}$$

To generalize, the charge q_1 may be replaced by a group of charges with a distributed density function $\rho(R,\theta,\phi)$, where ϕ is the azimuthal angle. The above expression can be written in a compact form using Legendre's polynomial series, independent of ϕ, as

$$V=k\sum_{l=0}^{\infty}\frac{1}{Z^{(l+1)}}\int_{\nu}\rho(R,\theta)R^{l}P_{l}(\cos\theta)\,d\nu \tag{2-10}$$

where $d\nu=2\pi\sin\theta\, d\theta\, dR$.

or

$$V = k\sum_{l=0}^{\infty}\frac{1}{Z^{(l+1)}}Q_l \tag{2-11}$$

where

$$Q_l = \int_{\nu}\rho(R,\theta)R^{l}P_{l}(\cos\theta)\,d\nu \tag{2-12}$$

Here Q_l is called the Z-component of the electrostatic 2^l-pole moment [17]. For l=0, Q_0 is simply a monopole. For l=1, Q_1 is referred to as the dipole moment and for l=2 the Q_2 is called the quadrupole moment.

Physically, the quadrupole moment is a measure of the sphericity of a charge distribution about a point in space. If the charge distribution is spherical about a point then the quadrupole moment will be zero, otherwise the quadrupole moment may be positive or negative depending on whether the charge distribution is prolate or oblate. Figure 2-2 depicts the prolate, spherical, and oblate charge distributions, respectively. The classical description provides the picture of how the charge distribution about a point results in different moments. However, the classical definition of quadrupole moment differs from the quantum mechanical definition [18]. The difference will be quite clear in the next section where the quantum mechanical definition of quadrupole moment is developed.

Once the idea of quadrupole moment is formed, the theory for interactions of the quadrupole moment with the surrounding electric and magnetic fields can be developed based on a formal quantum mechanical foundation.

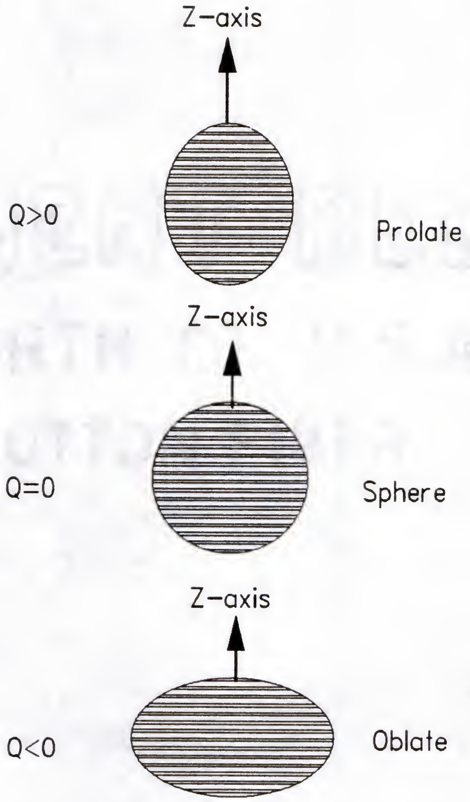

Figure 2-2: The prolate, sphere, and oblate charge distributions shown with quadrupole moment, Q.

Nuclear Quadrupole Interactions

Static quadrupole interaction

The nonspherical distribution of protons in a nucleus creates a nonzero nuclear quadrupole moment. The nuclear quadrupole moment interacts with the strong electric field gradient (efg) which exists inside condensed matter due to the nonsymmetric distribution of neighboring nuclei and the nonspherical distribution of bonding electrons [19]. The value of the efg in solids is of the order of 10^{21} $\mathrm{Vm^{-2}}$ [20] which cannot be produced in the laboratory. As an example, consider that the efg due to a single electronic charge at a distance of 1Å is

$$\mathrm{efg}=2ke/r^3=2.8\mathrm{x}10^{21}\ \mathrm{Vm^{-2}}.$$

The nuclear quadrupole moment of the probe nucleus interacts with this large efg at the site of interest. In order to investigate how the nuclear quadrupole interacts with its surrounding efg, one needs to solve the Schrodinger's equation in matrix form.

$$H|\psi\rangle = E|\psi\rangle \tag{2-13}$$

where $|\psi\rangle$ is the eigenket and E the energy eigenvalues of the Hamiltonian operator, H. The Hamiltonian operator describes the conservation of total energy and is given by the sum of two operators corresponding to the kinetic energy (KE) operator and potential energy (PE) operator, respectively. Thus, H is defined by the following expression

$$H = KE+PE \tag{2-14}$$

Further development of the theory needs to assume a nucleus with spin I having a nonzero quadrupole moment in a host medium surrounded by other nuclei and electronic clouds. It is further assumed that the electronic clouds are stationary surrounding the probe nucleus. Then the kinetic energy (KE) operator will be equal to zero. Thus, only the potential energy (PE) operator is needed which is equivalent to the Hamiltonian operator H. The mathematical expression of the operator H is developed from classical electrostatic potential energy, W, of a probe nucleus which is given by

$$W = \int_{v} V(r)\,\rho(r)\,dv \tag{2-15}$$

where $\rho(r)$ is the charge density of the nucleus and V(r) is the electric potential due to charges external to the nucleus. The integration is taken over a small volume v. Since the nuclear size is ~10^{-12} cm, much smaller than the atomic size, the electric potential can be expanded in a Maclaurin's series taking the center of mass of the nucleus as the origin of a Cartesian coordinate system, then

$$\begin{aligned} W=&(V(r))_{r=0}\int\rho(r)\,dv+\sum_{i=1}^{N}\left(\frac{\partial V(r)}{\partial X_i}\right)_{r=0}\int X_i\rho(r)\,dv \\ &+\frac{1}{2}\sum_{i=1}^{N}\sum_{j=1}^{N}\left(\frac{\partial^2 V(r)}{\partial X_i\partial X_j}\right)_{r=0}\int X_iX_j\rho(r)\,dv+\ldots \end{aligned} \tag{2-16}$$

where i and j vary from 1 to 3 representing x-, y-, and z-axes. The number of subscripts in each term indicate the rank of the tensor. The number of components in each term is given by N^l where N is the dimension of space and l is the rank of the tensor. The first term is of no use since it is a monopole and does not depend on the orientation of the charge. The second term, the dipole moment, is zero which is theoretically proven and experimentally observed as zero. The third term, a tensor of rank 2, having nine components is called the quadrupole moment.

Higher moments than quadrupole may exist but are difficult to observe experimentally and can be neglected [21]. All the odd electric multipole moments are zero as required by the condition of parity and no multipole moment of order 2^l can be observed for $l>2I$ where I is the nuclear spin [22]. Thus, the classical quadrupole electrostatic potential energy, W_Q, can be written as

$$W_Q=\frac{1}{2}\sum_{i=1}^{3}\sum_{j=1}^{3} V_{ij}\int X_i X_j \rho(r)\,dv \qquad (2\text{-}17)$$

where $V_{ij}=\dfrac{\partial^2 V}{\partial X_i \partial X_j}$.

Since $\vec{E}=-\nabla V$, one can express the electric field gradient as

$$\begin{aligned}\nabla\cdot\vec{E}&=-\nabla\cdot\nabla V\\ \nabla\cdot\vec{E}&=-\nabla^2 V\end{aligned} \qquad (2\text{-}18)$$

Gauss' law of electrostatics which is one of Maxwell's equations shows that

$$\nabla\bullet\vec{E}=\sum_{i}\frac{Q_i}{\epsilon_0} \tag{2-19}$$

where ΣQ_i is the total charges enclosed within the Gaussian surface and ϵ_0 is the permeability of free space. Since the probe nucleus which experiences the quadrupole interaction is a test charge which satisfies the condition $\Sigma Q_i \rightarrow 0$, equation (2-19) becomes

$$\nabla^2 V=0 \tag{2-20}$$

which is Laplace's equation. Since part of the quadrupole energy W', which does not depend on the orientation of the nucleus in space, must be subtracted from the total quadrupole energy. The energy W' is given by

$$W'=\frac{1}{6}\sum_{i=1}^{3}\sum_{j=1}^{3} V_{ij}\delta_{ij}\int_{v} r^2\rho(r)\,dv \tag{2-21}$$

where $\delta_{ij}=0$ when $i\neq j$ otherwise $\delta_{ij}=1$.

The above equation is invariant under the rotation of coordinates and is actually zero as long as the electronic clouds do not penetrate the probe nucleus. Therefore, subtracting W' from W_Q (equation (2-17)) produces the net quadrupole electrostatic potential energy, W_Q^{net}, depending upon orientation as

$$W_Q^{net}=\frac{1}{6}\sum_{i=1}^{3}\sum_{j=1}^{3}V_{ij}\int_v(3X_iX_j-r^2\delta_{ij})\rho(r)\,dv \qquad (2\text{-}22)$$

It is customary to define the classical quadrupole moment in Cartesian coordinates [23] as

$$Q_{ij}=\int_v(3X_iX_j-r^2\delta_{ij})\rho(r)\,dv \qquad (2\text{-}23)$$

Then the total potential energy, depending upon the orientation, for the quadrupole interaction is given by

$$W_Q^{net}=\frac{1}{6}\sum_{i=1}^{3}\sum_{j=1}^{3}V_{ij}Q_{ij} \qquad (2\text{-}24)$$

The classical expression for the quadrupole moment, equation (2-23), can be transformed into an operator by defining charge density $\rho(r)$ as an operator $\rho^{op}(r)$ [24],

$$\rho^{op}(r)=e\sum_k\delta(r-r_k) \qquad (2\text{-}25)$$

where e is the charge of a proton and $\delta(r-r_k)$ is the Dirac delta function. The summation $\sum_k$ is over all the number of protons in the nucleus.

Then one can write equation (2-23) in operator form as

$$Q_{ij}^{op}=\int_v(3X_iX_j-\delta_{ij}r^2)\rho^{op}(r)\,dv \qquad (2\text{-}26)$$

Solving equation (2-25) and (2-26) yields

$$Q_{ij}^{op}=e\sum_{i=1}^{3}\sum_{j=1}^{3}\sum_{k}(3X_{ik}X_{jk}-\delta_{ij}r_k^2) \qquad (2\text{-}27)$$

Thus, the net quadrupole electrostatic potential energy, W_Q^{net} (equation (2-24)), can be written into an operator, PE, as

$$PE = \frac{1}{6}\sum_{i=1}^{3}\sum_{j=1}^{3}V_{ij}Q_{ij}^{op} \qquad (2\text{-}28)$$

The quadrupole Hamiltonian, H_Q, which is simply equal to PE, becomes

$$H_Q=\frac{1}{6}\sum_{i=1}^{3}\sum_{j=1}^{3}V_{ij}Q_{ij}^{op} \qquad (2\text{-}29)$$

A nucleus with spin I has m energy states where m is the magnetic quantum number, having 2I+1 possible values, and varies from -I to I in step of one. In order to find the m energy states, a matrix can be formed using operator Q_{ij}^{op}. The operator Q_{ij}^{op} is symmetric and has nine components but only five are independent. The operator Q_{ij}^{op} is given in terms of space coordinates although one needs to find a representation of the operator in terms of known and measurable parameters of the spin vector I and its components. This can be achieved by applying the Wigner-Eckart theorem [25] to the matrix element of the quadrupole operator using the simultaneous eigenket notation [26] as

$$\langle Im\,|Q_{ij}^{op}|\,Im'\rangle = A\langle Im\,|\frac{3}{2}(I_iI_j+I_jI_i)-\delta_{ij}I^2|\,Im'\rangle \tag{2-30}$$

The constant A, the Clebsch-Gordan coefficient, is independent of m and m′. If one selects i=j=z the z-axis as axis of quantization and for m=m′=I which is the maximum projection on the z-axis, equations (2-30) and (2-27) become

$$\langle Im\,|Q_{ij}^{op}|\,Im'\rangle = A\langle II\,|3I_z^2-I^2|\,II\rangle \tag{2-31}$$

and

$$Q_{ij}^{op}=e\sum_k(3Z_k^2-r_k^2) \tag{2-32}$$

Solving equations (2-31) and (2-32) yields

$$\begin{aligned}\langle II\,|e\sum_k(3Z_k^2-r_k^2)|\,II\rangle &= A\langle II\,|3I_z^2-I^2|\,II\rangle\\ &= AI(2I-1)\end{aligned} \tag{2-33}$$

Letting eQ be the quantum mechanical definition of the electric quadrupole moment [24], then

$$\begin{aligned}eQ &= \langle II\,|e\sum_k(3Z_k^2-r_k^2)|\,II\rangle\\ &= e\langle II\,|3I_z^2-I^2|\,II\rangle\end{aligned} \tag{2-34}$$

The above quantum mechanical definition of a quadrupole moment is obviously different from the classical definition given by equation (2-12).

Then, the Clebsch-Gordan coefficient, A is given by solving equations (2-33) and (2-34) as

$$A=\frac{eQ}{I(2I-1)} \tag{2-35}$$

Equation (2-30) can be written as

$$\langle Im\ |Q_{ij}^{op}|\ Im'\rangle=\frac{eQ}{I(2I-1)}\langle Im\ |\frac{3}{2}(I_iI_j+I_jI_i)-\delta_{ij}I^2|\ Im'\rangle \tag{2-36}$$

or the operator Q_{ij}^{op} can be found as

$$Q_{ij}^{op}=\frac{eQ}{I(2I-1)}(\frac{3}{2}(I_iI_j+I_jI_i)-\delta_{ij}I^2) \tag{2-37}$$

Substituting equation (2-37) into equation (2-29) gives,

$$H_Q=\frac{eQ}{6I(2I-1)}\sum_{i=1}^{3}\sum_{j=1}^{3}V_{ij}[\frac{3}{2}(I_iI_j+I_jI_i)-\delta_{ij}I^2] \tag{2-38}$$

In the above equation, the efg is given by a tensor V_{ij} having nine components as

$$V_{ij}=\begin{bmatrix} V_{xx} & V_{xy} & V_{xz} \\ V_{yx} & V_{yy} & V_{yz} \\ V_{zx} & V_{zy} & V_{zz} \end{bmatrix} \tag{2-39}$$

The components of the efg matrix depend upon the choice of the coordinate axes. Since there are infinite coordinate axes possible in space, the uniqueness of the efg components is lost. Thus, it is imperative to choose a unique coordinate system. This can be achieved by choosing a coordinate system, the principal-axis system, in which all the off-diagonal components in the efg matrix become zero. In the principal axis system, the efg matrix becomes

$$V_{ij} = \begin{bmatrix} V_{xx} & 0 & 0 \\ 0 & V_{yy} & 0 \\ 0 & 0 & V_{zz} \end{bmatrix} \tag{2-40}$$

The sum of the diagonal elements of a square matrix is always invariant under the rotation of coordinates and is called the trace. The V_{ij} matrix is traceless because the efg is only due to the charges external to the nucleus which is also evident by equation (2-20). In order to make the operator H_Q practically useful, it becomes more convenient to minimize the number of degrees of freedom. It is customary to define a parameter η in terms of the efg components in the principal axis system as

$$\eta = \frac{(V_{xx} - V_{yy})}{V_{zz}} \tag{2-41}$$

with the constraints that

$$| V_{xx} | \leq | V_{yy} | \leq | V_{zz} | \tag{2-42a}$$

and

$$V_{xx} + V_{yy} + V_{zz} = 0 \tag{2-42b}$$

where η is called the asymmetry parameter and it measures the deviation of the efg from axial symmetry and is normalized such that

$$0 \leq \eta \leq 1 \tag{2-43}$$

Then, only two parameters, η, and the maximum component of the efg, V_{zz}, are needed to describe the quadrupole interaction. Using parameters η and V_{zz} in the principal axis system, the Hamiltonian (equation (2-38)) can be written as

$$H_Q=\nu_Q\,h[(3I_z^2-I^2)+\eta(I_x^2-I_y^2)] \qquad (2\text{-}44)$$

where $\nu_Q=eQV_{zz}/4I(2I-1)h$ is the quadrupole frequency [27] and h is Planck's constant. The quadrupole frequency measures the strength of the nuclear quadrupole interaction. It can be observed that for the cases I=0 and I=1/2 the quadrupole frequency, and consequently the Hamiltonian is not defined, consistent with the quadrupole interaction not being observed for spin I<1.

Once the operator H_Q is known one can apply the Schrodinger equation to find the energy eigenvalues of a nucleus with quadrupole moment eQ and subjected to high efg. The different projections of spin I on the axis of quantization can produce m energy states which can be determined as

$$H_Q\,|Im\rangle=E\,|Im\rangle \qquad (2\text{-}45)$$

or matrix elements can be written as

$$\langle Im'\,|\,H_Q\,|\,Im\rangle=E\,\langle Im'\,|\,Im\rangle \qquad (2\text{-}46)$$

Solving equation (2-44) with equation (2-46), using ladder operators of quantum mechanics, and performing a little involved but straightforward algebra, one can find the expression for the matrix element [28] as

$$\langle Im' \mid H_Q \mid Im\rangle = \nu_Q\, h\Big([3m^2 - I(I+1)]\,\delta_{mm'} + \frac{1}{2}\eta\,[(I\mp m)(I\mp m-1)(I\pm m+1)(I\pm m+2)]^{\frac{1}{2}}\,\delta_{m\pm 2,m'}\Big) \qquad (2\text{-}47)$$

For spin I=1 equation (2-47) can be written as

$$\nu_Q\, h \begin{bmatrix} 1 & 0 & \eta \\ 0 & -2 & 0 \\ \eta & 0 & 1 \end{bmatrix} = E \begin{bmatrix} 1 & 0 & 0 \\ 0 & 1 & 0 \\ 0 & 0 & 1 \end{bmatrix} \qquad (2\text{-}48)$$

The above matrix equation gives three distinct roots representing the eigenstates of the nucleus by the following equations

$$E_1 = \nu_Q\, h\ (1+\eta) \qquad (2\text{-}49)$$

$$E_2 = \nu_Q\, h\ (1-\eta) \qquad (2\text{-}50)$$

$$E_3 = -2\nu_Q\, h \qquad (2\text{-}51)$$

The nuclear quadrupole energy splitting is, therefore, not uniform for spin I=1. The energy splittings vary linearly with η as shown in figure 2-3. For the case of axial symmetry (η=0) the energy levels have twofold degeneracy; i.e, energy levels for m=±1 are the same but the m=0 energy level is still nondegenerate.

In the absence of external fields, there is no preferred direction in space. The m energy states associated with spin I are degenerate; i.e, they have the same energy. If one

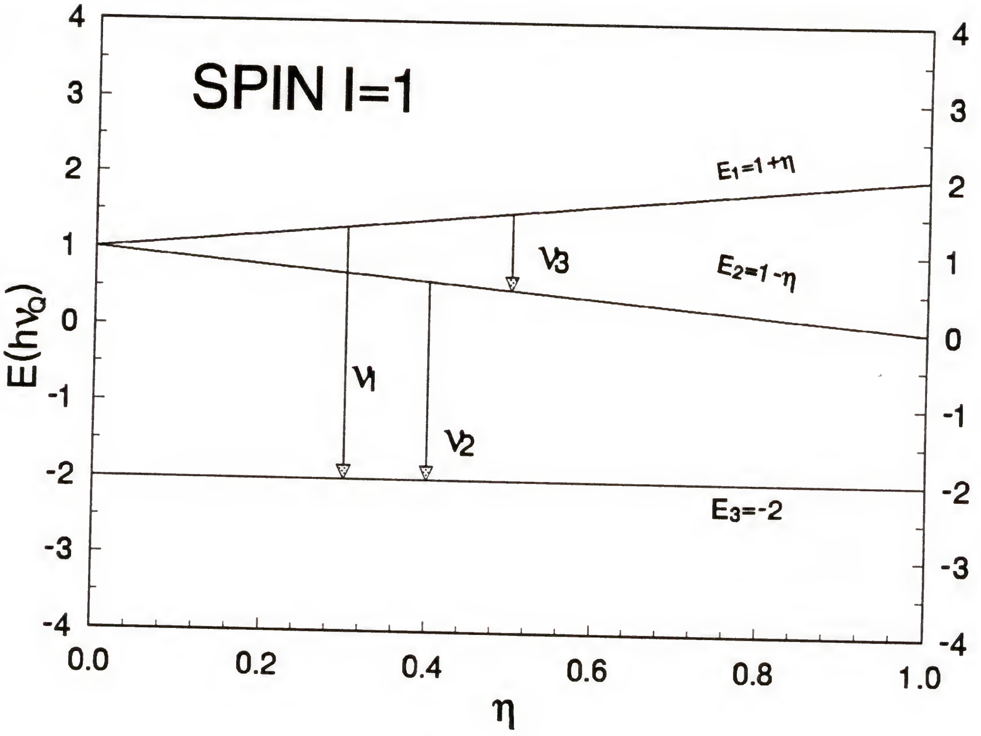

Figure 2-3: Variation of energy splittings with η parameter for spin I=1.

defines the direction of the efg in a crystal as the axis of quantization, then the m projections of spin I on the axis of quantization will be nondegenerate. Any quantum states can be measured experimentally if the system is excited into one of the eigenstates. The process of exciting a system into one of the eigenstates, i.e inducing transitions from a lower energy state of a system to the higher energy state, is called resonance. Using the resonance condition,

$$\Delta E = h\nu \tag{2-52}$$

where ΔE is the energy difference between any two energy levels and h is Planck's constant. Energy in the form of an appropriate electromagnetic frequency, ν, is supplied to the system to satisfy the resonance condition. Then, the energy absorbed by the transition of a spin to higher energy states is released which can be detected. Thus, resonance is important for the detection of the signals.

The branch of spectroscopy in which the nuclear quadrupole moment interacts with its ambient environment and resonance is achieved by application of radio frequency (rf) magnetic fields, H_f, is traditionally called Nuclear Quadrupole Resonance (NQR) spectroscopy.

For the case of ^{14}N (spin I=1) the quadrupole interaction frequencies fall in the region of radio frequencies and are given by the following equations

$$\nu_1 = |E_1 - E_3| = \nu_Q(3+\eta) \tag{2-53}$$

$$\nu_2 = | E_2 - E_3 | = \nu_Q (3-\eta) \quad (2\text{-}54)$$

$$\nu_3 = | E_1 - E_2 | = \nu_Q \,(2\eta) \quad (2\text{-}55)$$

The transition frequencies are shown in figure 2-4 as a function of η. The frequency ν_3 is too low to be observed in most cases for nitrogenous compounds [29]. If one measures the frequencies ν_1 and ν_2, then ν_Q and η can readily be found as

$$\nu_Q = \frac{1}{6}(\nu_1 + \nu_2) \quad (2\text{-}56)$$

and

$$\eta = \frac{3(\nu_1 - \nu_2)}{(\nu_1 + \nu_2)} \quad (2\text{-}57)$$

These two parameters (ν_Q and η) are sensitive to the electronic distribution surrounding the ^{14}N nuclei in the host medium. Samples exposed to ionizing radiations may have a change in the bonding electronic distribution or may have dislocation/vacancies nearby a number of ^{14}N nuclei which can be reflected in the NQR parameters ν_Q and η.

So far, only the static quadrupole interaction was described. The transitions between energy levels are induced to detect the static NQR parameters experimentally. However, the excited system returns to the equilibrium state or relaxes through dynamic processes whenever the cause of excitation is removed.

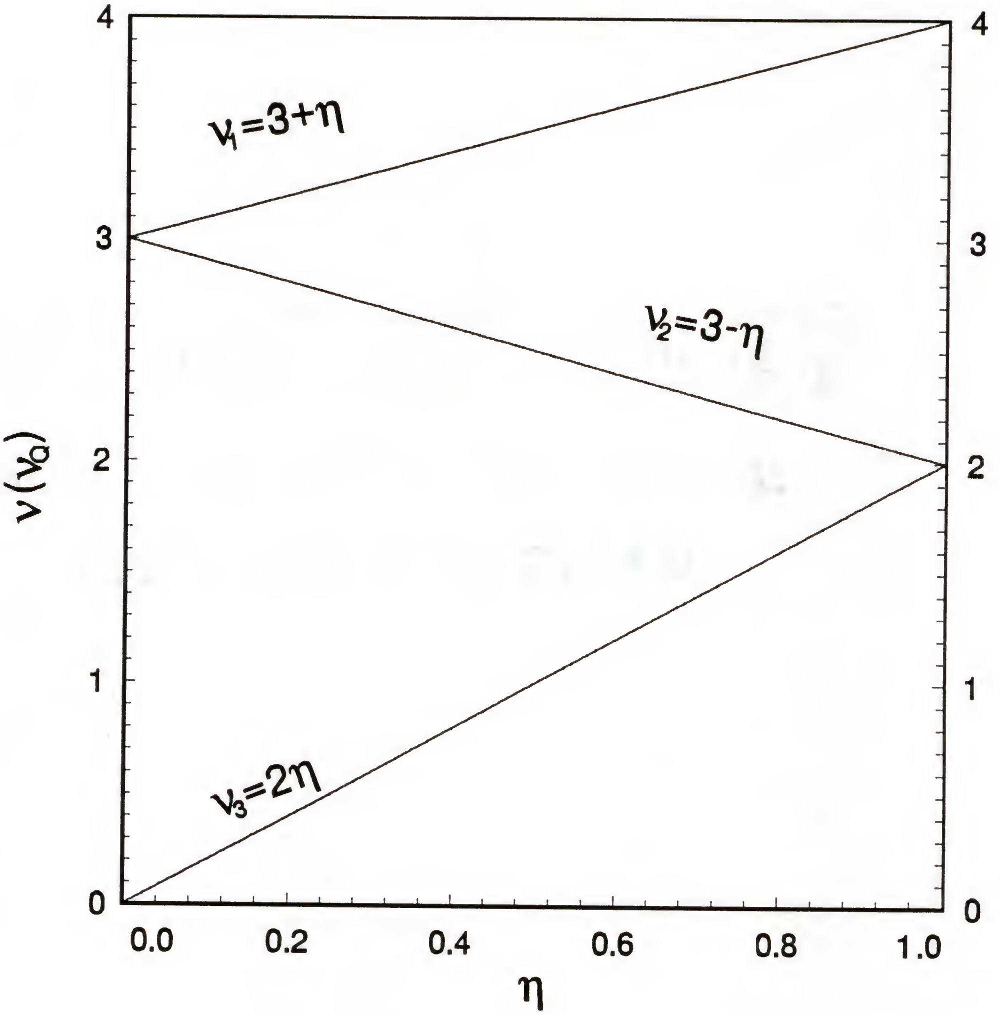

Figure 2-4: The transition frequencies variation as a function of η parameter for spin I=1.

Dynamic magnetic interaction

All nuclei have intrinsic spin although it may be zero. The orbital motions and of course the intrinsic spin of the nucleons within the nucleus provide the magnetic dipole moments μ (J/T). The magnetic dipole moment provides a measure of the strength and direction of the magnetic field surrounding the nucleus. All the nuclei in a polycrystalline sample have their magnetic dipole moments oriented in arbitrary directions in space. The sum of all magnetic moments (for one specific value of m) in a given volume gives a magnetization vector, $M=\Sigma\mu_i$. In NQR spectroscopy, there exists no magnetization vector M before applying the rf field. However, if one applies a sinusoidal rf magnetic field in the xy-plane, perpendicular to the axis of quantization, matching with one of the quadrupole transition frequencies to the system of nuclei then all magnetic dipole moments precessing with m corresponding transition frequencies will be in the xy-plane. When the rf magnetic field is no longer present, the individual components of the magnetization, μ_i, return to their equilibrium positions, the position they were in before applying the rf field, with a characteristic time called the longitudinal relaxation time, or T_1. When the magnetization vector M is in the xy-plane, precessing with one of the quadrupole transition frequencies, the individual components of the transverse magnetization dephase with another characteristic time, T_2^*, called the transverse relaxation time.

F. Bloch, in 1946, developed a set of equations describing the relaxation of magnetic moments for a system of nuclei after being disturbed from an equilibrium state [30]. Although Bloch equations were developed for nuclear magnetic resonance (NMR), similar equations are also used in NQR spectroscopy. Bloch equations are not valid under two conditions: (a) at very low temperature when Curie's law is not valid and (b) for certain solids when T_2^* is not exponentially decreasing. These are not the cases encountered in this research. Therefore, it is pertinent to examine Bloch's approach toward relaxation mechanisms. In essence, all other theories [31,32,33] explaining relaxation mechanism test their validity, in the range of their applicability, by converging to the Bloch equations.

The governing equation for T_1 is given as

$$M(t)=M_o(1-e^{-\frac{t}{T_1}}) \tag{2-58}$$

where M_o is the magnetization as $t\rightarrow\infty$.

This is a fundamental equation in the field of magnetic relaxation describing T_1. Modification to equation (2-58) to fit NQR experimental data has been suggested by Koukoulas and Whitehead [34]. The magnetization M, while precessing in the xy-plane follows the equation

$$M(t) = X(t)+iY(t) \tag{2-59}$$

where $i=\sqrt{-1}$. The functions X(t) and Y(t) are defined as

$$X(t)=M_0\cos(\omega_j t)\,e^{-\frac{t}{T_2^*}} \tag{2-60}$$

$$Y(t)=M_0\sin(\omega_j t)\,e^{-\frac{t}{T_2^*}} \tag{2-61}$$

where $\omega_j=2\pi\nu_j$ is the jth transition frequency.

A computer generated graph of equation (2-59) is shown in figure 2-5. The figure shows how the amplitude of magnetization M decreases with a characteristic time T_2^* in time. Also the type of the signal collected is shown onto the X-t plane in figure 2-5.

Nuclear Spin Relaxation Theory

This short review of the theory of NQR would be incomplete without mentioning the spin temperature concepts associated with magnetic relaxation.

A population of spins may be considered as 'hot' or having spin temperature. A nucleus with spin I may have 2I+1 spin energy levels. Bloembergen et al. [35] first developed a theory of magnetic relaxation based on the concepts of nuclear spin temperature. In their theory one may assume a system of nuclei having the population densities N_p and N_n in the energy levels E_p and E_n, respectively. If $W_{p\text{-}n}$ and $W_{n\text{-}p}$ are the transition probabilities per unit time from energy state E_p to E_n and vice versa due to the applied rf oscillating magnetic field, then rate equations can be written as

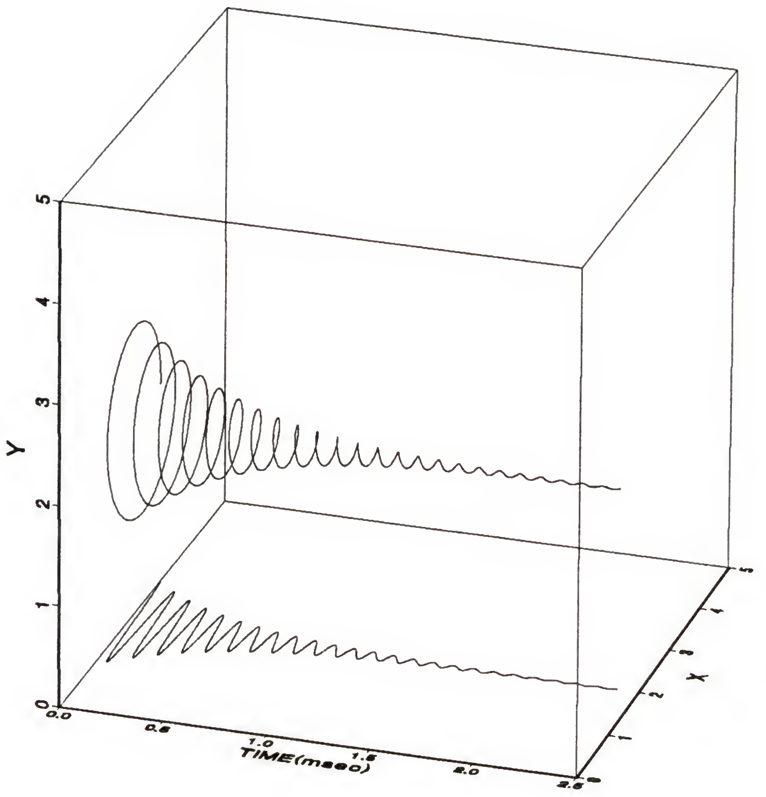

Figure 2-5: A computer generated graph shows decreasing amplitude of magnetization M in three dimensions. The projection onto X-t plane shows the type of spectrum observed on an oscilloscope.

$$\frac{dN_p}{dt} = -N_p(W_{p\to n}+P_{p\to n})+N_n(W_{n\to p}+P_{n\to p}) \tag{2-62}$$

and

$$\frac{dN_n}{dt} = -N_n(W_{n\to p}+P_{n\to p})+N_p(W_{p\to n}+P_{p\to n}) \tag{2-63}$$

where $P_{p\to n}$ and $P_{n\to p}$ are the lattice induced transition probabilities per unit time from energy state E_p to E_n and E_n to E_p, respectively. If the difference in the spin population densities is $n=N_p-N_n$, then from equations (2-62) and (2-63) one finds

$$\frac{dn}{dt} = -2nW-\frac{n-n_0}{T_1} \tag{2-64}$$

where

$$n_0 = N\frac{P_{n\to p}-P_{p\to n}}{P_{n\to p}+P_{p\to n}} \tag{2-65}$$

and

$$\frac{1}{T_1} = P_{p\to n}+P_{n\to p} \tag{2-66}$$

where N is the total spin population $N=N_p+N_n$ and $W=W_{p\to n}=W_{n\to p}$. When a system of nuclei attains a state of thermal equilibrium, the thermal populations are governed by Boltzmann's distribution as

$$\frac{N_n^0}{N_p^0} = e^{-\frac{(E_p-E_n)}{k_BT}} \tag{2-67}$$

where N_n^0 and N_p^0 are the thermal population of the spins in

Boltzmann's distribution, k_B is Boltzmann's constant and T is the temperature in degree Kelvin (K). The concept of low temperature thermometry of the above equation (2-67) has been exploited successfully for low temperature measurements at milli- and micro-kelvin [36].

In spin temperature theory, T_1 is the characteristic time with which the spin system gives off its spin temperature to the surrounding lattice to attain the equilibrium state following the excitation due to an rf field. That is why T_1 is often called the spin-lattice relaxation time. Since spin-lattice relaxation time represents communication time between spins and the lattice, it is, therefore, a function of the material properties such as conductivity, viscosity, specific heat, etc., and may contain significant information about radiation induced damage.

The time T_2^* is defined in the spin theory by a shape function g(ν) in the frequency domain such that

$$\int_0^{\infty} g(\nu)\,d\nu = 1 \qquad (2\text{-}68)$$

The shape function g(ν) can be found by taking the Fourier transform (FT) of the function in the time domain as

$$g(\nu) = c\mathcal{F}(f(t)) \qquad (2\text{-}69)$$

where c is a constant and can be found from equation (2-68). If the function in the time domain is exponential, as is equation (2-60), the FT will be given by equation (2-70).

$$\mathcal{F}(X(t)) = \frac{\frac{1}{T_2^*}}{(\nu_j-\nu)^2+(\frac{1}{T_2^*})^2} \tag{2-70}$$

This is a Lorentzian function. The full width at half maximum (FWHM) of the Lorentzian function is related to the shape function as

$$FWHM = g(\nu) = \frac{1}{\pi T_2^*} \tag{2-71}$$

Thus, T_2^* is proportional to the inverse of the linewidth of the FT of a NQR frequency spectrum [37]. Therefore, linewidth is another term frequently used in NQR and similar spectroscopic techniques. Even if the line shape is not Lorentzian (when T_2^* is not defined in Bloch theory), the shape function $g(\nu)$ can extract information regarding the linewidth by taking the Fourier transform of the NQR spectrum in the time domain and hence T_2^* can be determined. The inverse linewidth contains significant information about the nonuniformity of the efg existing in the material exposed to radiation [10].

Method of NQR Spectroscopy

General Principle of NQR Measurements

In NQR spectroscopy, transitions between energy levels of a probe nucleus incorporated in a host molecule are produced by applying an oscillating magnetic field perpendicular to the direction of the efg in the principal axis system which is the z direction as shown in figure 2-6. The rf magnetic field applied along y-axis brings the individual dipole moments of the probe nuclei onto xy-plane and forms a magnetization, M, which precesses with the transition frequency which matches the rf frequency. It is not the magnetization M which is measured experimentally. Rather, a time dependent voltage is induced in a coil surrounding the system of nuclei owing to a changing magnetic flux B_y associated with M. This time dependent voltage, varying with the transition frequency, is measured experimentally [38]. Since the free induction also decays, therefore it is called free induction decay (FID).

In order to estimate the magnitude of the induced voltage in the sample coil containing the material to be studied by NQR spectroscopy one can consider equation (2-61). The magnetic flux B_y along the y-axis is given by

$$B_y = \mu_0 Y(t) = \mu_0 M_0 \sin(\omega_j t)\, e^{-\frac{t}{T_2^*}} \tag{2-72}$$

where μ_0 represents the magnetic permeability of vacuum. Faraday's law of induction states that a voltage is induced in a coil having N turns and a cross sectional area, A, as

$$V = -NA\frac{dB_y}{dt} \tag{2-73}$$

Substituting equation (2-72) in equation (2-73) and simplifying yields

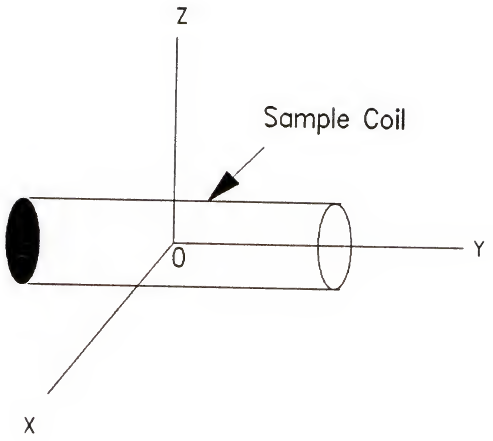

Figure 2-6: A principal axis system is shown in the sample coil. The y-axis is the cylindrical axis of the coil.

$$V = \mu_0 M_0 N A K_1 \cos(\omega_j t+\phi)\, e^{-\frac{t}{T_2^*}} \tag{2-74}$$

where $K_1=(\omega_j^2+(\frac{1}{T_2^*})^2)^{\frac{1}{2}}$ and $\phi=\arctan((-T_2^*\omega_j)^{-1})$.

In most cases $\omega_j \gg \frac{1}{(T_2^*)}$, and $(\omega_j T_2^*)^{-1} \approx 0$; therefore, one may assume the constants $k_1=\omega_j$ and $\phi=0$. Then equation (2-74) becomes

$$V = \mu_0 M_0 N A \omega_j \cos(\omega_j t)\, e^{-\frac{t}{T_2^*}} \tag{2-75}$$

In the above expression M_0 is related to the magnetic susceptibility, χ_0, by the Curie formula [30] as given in equation (2-76)

$$\chi_0 = \frac{I(I+1)}{3K_B T} n\gamma^2 h^2 \tag{2-76}$$

where

I= Spin of the probe nucleus

n= Number density of spin nuclei (m^{-3})

γ= Gyromagnetic ratio of the probe nucleus (Hz/T)

h= Plank's constant (J-sec)

T= Sample temperature in degree kelvin (K) and

k_B= Boltzmann's constant (J/K).

Assuming that at resonance the value of rf field $H=\omega_j/\gamma$. Then

$$M_0 = \chi_0 \frac{\omega_j}{\gamma} \tag{2-77}$$

Using equations (2-76) and (2-77) and solving with equation (2-75), one finds the expression for the induced voltage in the sample coil as

$$V = \mu_0 NA \frac{I(I+1)}{3k_B T} n\gamma\omega_j^2 h^2 \cos(\omega_j t)\, e^{-\frac{t}{T_2^*}} \tag{2-78}$$

For ^{14}N a value of 56μV is obtained for N=33, $A=\pi 10^{-4}\ m^2$, $\gamma=1.94x10^7 Hz/Tesla$, T=77 K, $n=10^{27}\ m^{-3}$ and $\omega_j=2\pi(2.9x10^6 Hz)$ at t=0.

Such a small time dependent voltage signals need to be amplified for detection. Thus, the amplification of the induction voltage and consequently its detection is achieved by using electronic devices as explained in chapter three under the title of pulsed NQR spectrometer.

CHAPTER 3
EXPERIMENTAL PROCEDURES AND METHODS

This chapter details the experimental procedures of the NQR experiments related to urea and thiourea irradiated at center vertical port (CVP) of the University of Florida Training Reactor (UFTR), along with the supporting experiments in sequence of their performance and necessity. Whenever, it was deemed necessary a concise explanation of the method has also been included.

In order to determine the contributions of reactor gamma and neutron fields separately, auxiliary experiments were carried out to independently determine the (a) gamma dose rate and (b) temperature of the samples at CVP of the UFTR.

After determining this information, experiments were performed to observe the possible effects of (a) out core gamma doses (but equivalent to in core gamma doses) on the NQR parameters of urea and thiourea and (b) out core temperature (but similar to observed at CVP of the UFTR) on the NQR parameters observed for urea and thiourea.

X-ray diffractometry was also performed on samples irradiated at CVP of the UFTR to observe any chemical and/or physical changes resulting from reactor neutrons.

Procedures and Methods of NQR Experiments

A sample enclosed in a sample coil when subjected to the rf magnetic field produces a time dependent voltage signal in the coil. These time dependent induce voltage signals are observed using electronic modules. There are two widely used methods for the detection of such a time dependent voltage, (a) the continuous wave (CW), and (b) the pulsed NQR methods [39]. In the continuous wave method, the rf field is continuously applied and the induction voltage gives information about transition frequencies. This method does not permit the measurement of the relaxation times T_1 and T_2^*. The CW method can have problems with rf saturation i.e, at high rf fields the spin populations are degenerate and no free induction decay is observed. In pulsed NQR method, pulses of rf magnetic fields are applied to the sample and induction voltage is observed in absence of rf magnetic field. The excited system of spins in absence of rf fields relaxes. Thus, the pulsed NQR method is an excellent technique for relaxation time measurements. This method also has superior signal-to-noise (S/N) ratios compared to CW methods. In the present work, pulsed NQR technique has been employed.

Pulsed NQR Spectrometer

The schematic block diagram of a conventional pulsed type NQR spectrometer is shown in figure 3-1. The block diagram is divided into two parts representing the transmitter and the

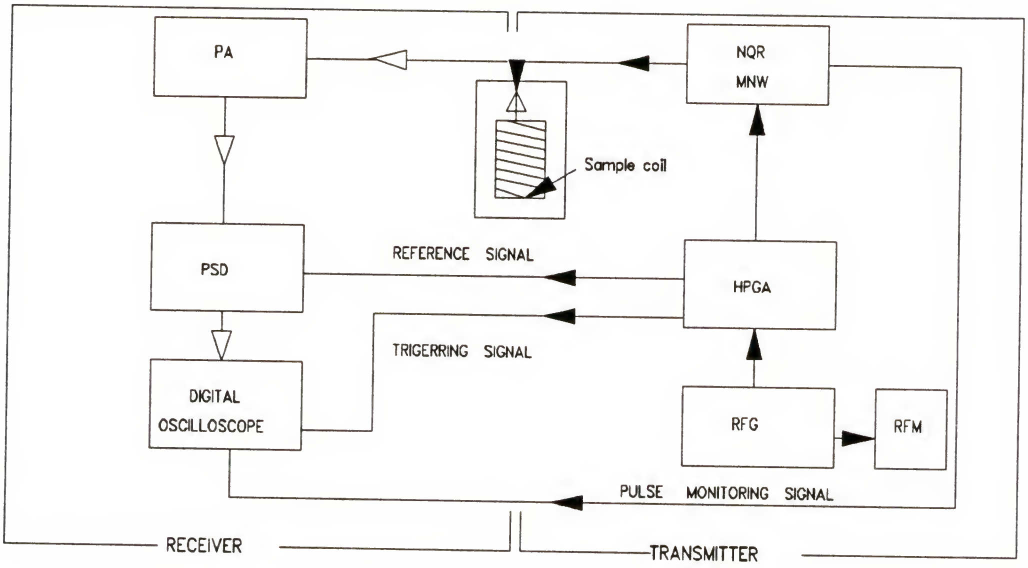

Figure 3-1: A schematic of a pulsed NQR spectrometer. The components are radio frequency generator (RFG), radio frequency meter (RFM), high power gated amplifier (HPGA), matching network (MNW), pre-amplifier (PA), and phase sensitive detector (PSD).

receiver. The sample coil works with both the transmitter and the receiver. The arrows show the routing of the signals.

Transmission of the radio frequency field to the sample coil requires a rf generator (RFG) which produces a continuous wave of rf. The Radio frequency meter (RFM) reads the value of radio frequency from RFG in digital form. From the RFG module, the required rf is fed to a high power gated amplifier (HPGA). The HPGA first converts the continuous rf into a pulse of desired length using electronic switches and gates. The duration between the rf pulses can also be controlled by programmed switching of the rf at desired time intervals. After gating, the pulses are amplified and applied to the transmitter containing the polycrystalline sample to be studied. The pulse from the HPGA is fed to the sample coil through a NQR matching network (MNW). The NQR matching network works just like a walkie-talkie in which while someone is talking (transmitting signals) one cannot listen (receive signals) and vice versa. When the NQR matching network transmits the rf signal to the sample coil no pulse goes toward the pre-amplifier and when the receiver pulse is routed toward the pre-amplifier the NQR matching network prevents any further pulse from reaching the sample coil from the transmitter. Thus, the sample coil works both with the transmitter and the receiver through the function of the NQR matching unit. The filled arrows shown in figure 3-1 indicate the path of the pulse from the transmitter and the open arrows guide the pulse path toward the receiver. The functioning of the NQR matching network based on the electronic components is well explained, for example, by Clark and Smith [39,40].

On the first stage of signal amplification, the receiver signal enters the high impedance pre-amplifier (PA). Since the pre-amplifier receives pulses from the coil in microvolts, it must be protected from the high voltage present during pulses from the HPGA. This is also accomplished by the NQR matching network. After amplification from the pre-amplifier, the signal enters the phase sensitive detector (PSD).

The main purpose of the phase sensitive detector is to amplify the signal linearly to the millivolt level and improve the S/N ratio. The phase sensitive detector detects the beat frequency which is the difference of the precessional frequency and the applied radio frequency ν_{rf} which is used as a reference signal. In doing so, the phase sensitive detector receives one signal from the HPGA as a reference signal and one from the PA. When both signals have exactly or nearly the same frequencies, the PSD gives a dc output as a function of cosines of the difference of the phase angle between the two signals. This signal is recorded by a digital oscilloscope for observation and analysis.

The S/N ratio has usually very poor response from a single pulse. However, each rf pulse generates a spectrum which can be summed with the previous spectra to cancel random noise. This process of signal averaging provides an averaged spectrum with an improved S/N ratio. The upper limit of S/N ratio depends upon the dynamic range of the analog to digital converter (ADC) and the computer where data are stored.

In the pulse method if only a $\pi/2$ pulse (a pulse which brings the magnetization M_0 onto xy-plane) is used, the signal furnished is called the free induction decay. However, in cases when the time T_2^* is very short, falling within the dead time limit of the spectrometer, the signal cannot be observed. The dead time is the time during which the spectrometer's electronics cannot detect any signal. In these cases a series of rf pulses can be used to observe the NQR transition frequencies. In such a case, for example, a $\pi/2$-pulse is applied to the sample coil and after a delay time τ a π-pulse is applied to the sample coil which reverse the direction of the spins by 180° and after a time 2τ an echo is observed. The first spin-echo was observed by Hahn [41]. Since the inverse linewidths involved in this work were long enough to observe the FID, the spin-echo method was not applied in general. However, the first ever observed spin-echo for thiourea is reported in Appendix A. Typical FIDs, collected by the above mentioned pulsed NQR spectrometer, are shown in chapter four.

System Description

The sample coil used in all NQR experiments was custom designed and constructed with No. 18 copper magnet wire having 33 turns. The length and diameter of the sample coil was 7.0 cm and 2.4 cm, respectively.

All other modules used in the NQR pulse spectrometer are commercially available. The RFG, from Matec Instruments (model 110), is capable of generating the rf from 0.5 to 50 MHz. It has a stability of 1 part in 10^7 but the RFM (HP universal 5314 A) gives an error of ±10 Hz in reading the radio frequency from the RFG. The HPGA, from Ritec Instruments, (model RX 1-2500c), gives a maximum power of 2.5 kW into a 50 Ω load. The pulse width is selectable from 0.5 μsec to 100 μsec. The receiver (Ritec Instruments, model BR-640) has the sensitivity of micro-volts and has built-in low and high pass filters which may be used to provide a window of frequencies ranging from 12 MHz to 1 MHz. The receiver gain is available up to 64 db. The NQR MNW was constructed by Ritec Instruments, following a design similar to given by Clark [39]. The digital oscilloscope (Nicolet 4180) consists of an ADC, an oscilloscope, model 4094C, for spectrum display and a disk recorder F43, for saving data on floppy diskettes. The digital oscilloscope is capable of storing data sets up to 16 thousand points in one spectrum.

Typical experimental settings for urea and thiourea are given as:

$\pi/2$ pulse width = 18-20 μsec,

Pulse height from Peak-to-Peak = ~ 2kV,

Delay time between pulses = 1-3 msec,

Radio frequency = 2-3 MHz, and

Receiver gain = 44-58 db.

Exposure of Urea and Thiourea at CVP of the UFTR

The urea and thiourea used in this research were obtained from Fisher Scientific in polycrystalline form. Two sets of samples were prepared for in core irradiations. In one set, all samples consisted of 16 grams (g) of urea and in the other set 10 g of thiourea constituted all the samples. All materials were sealed (air tight) in double plastic bags to avoid any leakage of radioactivity during irradiations in reactor and to make handling of post-irradiated samples safe. All thiourea samples were consisted of 10 g in order to transfer the irradiated thiourea in glass vials with sealed plastic bags. The amount of thiourea was reduced to 10 g to accomodate the volume taken by the plastic bags in glass vials. This practice was adopted, to be conservative, to avoid any spread of radioactive powder. However, the urea grains were large and it was found to be safe to transfer the irradiated urea into glass vials without the plastic bags. All samples were irradiated at CVP of the UFTR at 100 kW power for times ranging from 0.25 hour to 4.0 hours. The total integrated neutron flux at CVP was 1.2×10^{12} cm^{-2} sec^{-1}, determined by gold foil activation method.

After neutrons irradiations, the samples were held for four weeks, in the hot cell located at the UFTR facility area, to permit the decay of activated species. The total radioactivity of the collective samples of urea and thiourea was found less than 0.1 mr/h at the surface after four weeks. These samples were inserted into glass vials for NQR spectroscopy. The NQR spectroscopy was carried at 77 K using the previously described pulsed NQR spectrometer. The results are described in chapter four.

Procedures and Methods of Supporting Experiments

In Core Gamma Dose Measurement

Since gamma flux co-exists with the neutrons in the reactor core, the gamma dose rate was independently determined, using thermoluminescence detectors (TLD), in the reactor core at CVP of the UFTR where the samples were irradiated.

CaF2 TLD. Among the several commercially available TLDs, CaF_2 (TLD-200) was chosen for in core gamma dose measurement. The constituent materials of CaF_2 are Calcium (Ca) and Fluorine (F). Both have very low neutron absorption cross sections compared to LiF_2 TLDs. The CaF_2 TLD is thirteen times more sensitive to gamma radiation than the LiF_2 TLD.

The glow curve for CaF_2 TLD has peaks at 200°C and 240°C, respectively [42]. These glow peaks are much above the temperature recorded at CVP of the UFTR at the power levels (200 W to 600 W) this experiment was performed (see section in this chapter entitled "Temperature Determination of Urea and Thiourea at CVP of the UFTR"). Therefore, the CaF_2 TLD's temperature (25°C to 35°C) at CVP did not affect the energy stored by the reactor gammas in the TLDs. Although CaF_2 TLD shows higher sensitivity for gamma photon energies below ~200 keV, this low energy spectrum was cut off by the presence of a minimum of 11.0 cm of graphite between the CaF_2 TLDs at CVP and the fission gamma sources in the UFTR. Figure 3-2 depicts the exposure geometry of TLDs at CVP of the UFTR. However, Cadmium (Cd) filters were also used to eliminate low energy gamma photons besides eliminating low energy neutrons. Above ~200 keV energy of gamma photons, the CaF_2 TLD responds linearly with energy [42]. The upper absorbed dose for CaF_2 TLD is reported to be 10^3 Gy [42]. The detectors used in this work were obtained from the Harshaw Crystal and Electronic Products in sizes of 3.2x3.2x0.9 mm.

TLD calibration curve for gamma dose

Since TLDs are secondary type of dosimeters they need to be calibrated against the known gamma doses. A calibration curve was obtained using CaF_2 TLDs which were irradiated with known gamma doses from 12 kCi ^{60}Co source located at the

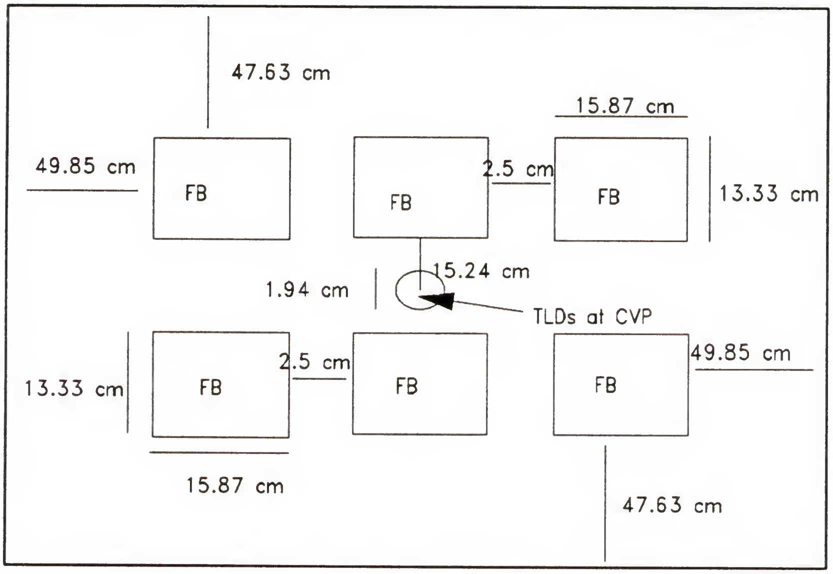

FBs ARE FUEL BOXES

NOTE THAT FIGURE IS NOT DRAWN TO SCALE

Figure 3-2: The exposure geometry of TLDs at CVP of the UFTR.

Shands Cancer Center, Gainesville Florida. The response of TLDs, in micro Coulombs (μC), versus gamma dose, Gy, is shown in figure 3-3. The x-axis shows the known gamma doses and the y-axis shows the response of CaF_2 TLD in μC. The solid curve, in figure 3-3, is the best fitted curve by linear regression method.

Gamma dose rate at CVP of the UFTR

A set of detectors ,consisting of five fresh CaF_2 TLDs, was lowered at CVP of the UFTR for gamma dose measurement. The reactor was operated at 200 W power level controlling the exposure time such that the total gamma dose was below the maximum gamma dose limit, 10^3 Gy, of CaF_2 TLDs. Similarly, two other sets of CaF_2 TLDs were exposed to gamma photons at CVP while operating the UFTR at 500 W and 600 W power levels, respectively. Since exposure time was controlled manually, short exposure times, at reactor power of a few watts, were introducing significant errors in results. Similarly, higher reactor power (~kW) needed extremely short exposure times while not exceeding the upper dose limit of CaF_2 (10^3 Gy). Therefore, a few attempts were made to optimize the time of exposure and reactor power in such a way that the upper dose limit of CaF_2 TLD, 10^3 Gy, was not exceeded. All three sets of TLDs were exposed for 20 minutes (min).

The response of the energy released from the TLDs was measured in μC using a Harshaw 2000 TLD reader. Figure 3-4

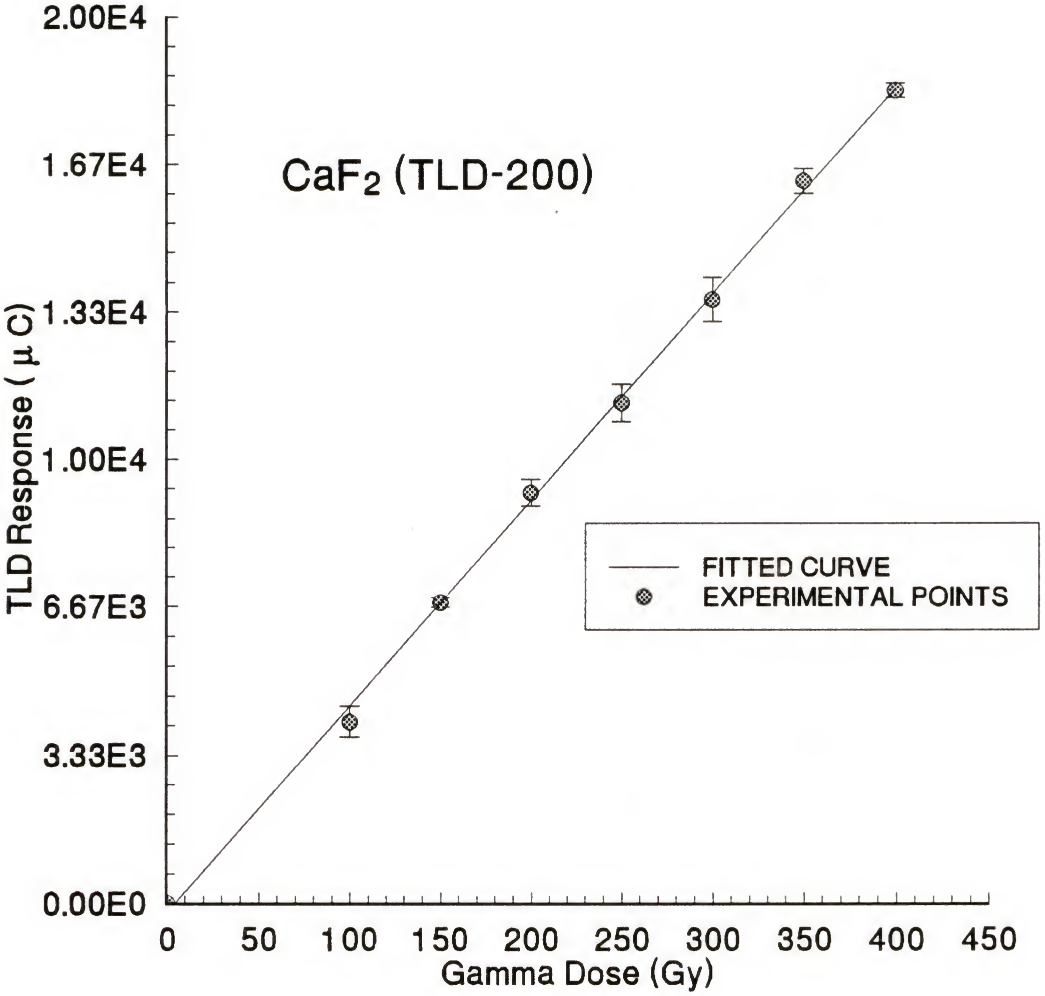

Figure 3-3: A gamma dose calibration curve for CaF_2 TLD.

shows a block diagram of the TLD reader. The nitrogen gas was used to heat the TLDs to emit the stored energy due to gamma irradiation. Fast heating of the TLDs showed a significant loss in photon counts owing to photomultiplier dead time. Therefore, the TLD's temperatures were raised slowly at the rate of ~20°C/min to the glow peaks so that photons emitted could be recorded by the photomultiplier tube.

An experimental relationship between in core gamma dose rate and the reactor power is given in chapter four and discussed in chapter five.

Out Core Gamma Exposure of Urea and Thiourea

In order to observe the effects of gamma photons alone (without neutrons) on the NQR parameters for urea and thiourea, external radiation sources of Cobalt-60 (^{60}Co) and Cesium-137 (^{137}Cs) were used. The samples were irradiated up to 620 kGy, a value which is about twice the gamma dose delivered at CVP for four hour operation of the UFTR at 100 kW power (see chapter five for discussion under the rubric of Effects of Gamma Photons on Urea and Thiourea).

Cobalt-60 source. A ^{60}CO source was available in the department of Nuclear Engineering Sciences. This source was installed on May 1, 1988, with a nominal source strength of 600 curies (Ci).

The dose rate from ^{60}Co was determined as a function of distance from the center of the source by using the CaF_2 TLD

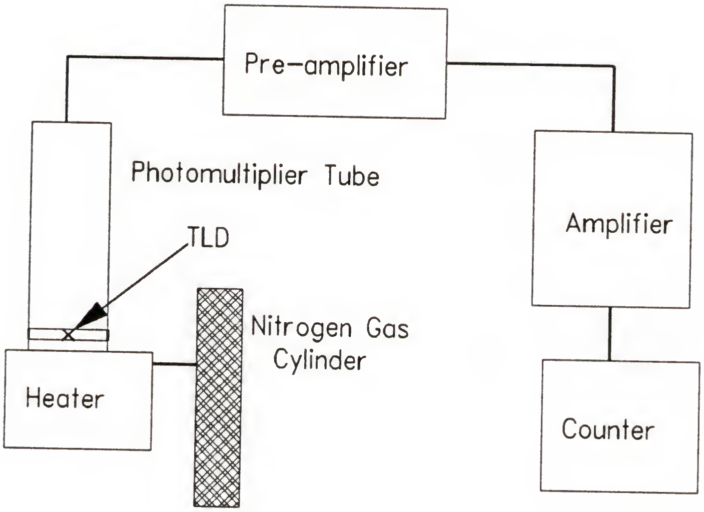

Figure 3-4: A schematic diagram of a TLD reader.

calibration curve (figure 3-3). Five sets, each consisting of five CaF_2 TLDs, were placed surrounding the ^{60}Co source at radii of 2.54 cm, 5.08 cm, 10.16 cm, 15.24 cm, and 20.32 cm, respectively. All samples were exposed for 63 minutes. The TLDs were read using the Harshaw 2000 reader system. The results of this experiment are shown in chapter four.

The gamma dose rate of ^{60}Co was also determined by other methods to verify the TLD results.

Radiochromic film detectors. These detectors are gamma sensitive imaging films for high gamma dose measurements [43]. These films are commercially available from GAF Chemical Corporation, 1361 Alps Road, Wayne, NJ. The trade name is Gafchromic detector. The Gafchromic detectors consist of materials of low atomic numbers so the films do not change the radiation fields. Also, these detectors are insensitive to room light. The detectors can measure gamma doses from 50 Gy to 40 kGy. The exposed detectors change their color (blue) when irradiated and the optical density provides a means to quantify gamma doses.

Two sets of Gafchromic detectors were used at 2.52 cm and 5.08 cm from the ^{60}Co source. The spectrophotometry analysis was performed at the 500 nm wavelength using the facility at the Florida Agricultural Commodities Irradiator, Gainesville. The calibration curve provided by the manufacturer was used and doses were determined at 2.54 cm and 5.08 cm from the ^{60}Co source.

Theoretical calculation. The dose rates were calculated at various distances from the ^{60}Co source using information provided by the manufacturer. The nominal source was 600 Ci on May 1,1988. The source was cylindrical in shape having a length of 2.54 cm and radius of 0.502 cm. The procedure for theoretical calculation was followed as given by Blizard et al., [44].

Experiments with the Co-60 source. Samples were prepared consisting of 16 g urea or thiourea in cylindrical glass vials having a volume of 126.3 cm^3. The length of the vial was 8.36 cm. The samples were placed surrounding the ^{60}Co source. The time of exposure was used to control the dose to urea and thiourea samples. Since the ^{60}Co source is a heavily used facility for gamma irradiations at the University of Florida, five consecutive days is the maximum time permitted to a single user. Therefore, the ^{60}Co source was used to deliver doses below 100 kGy to urea and thiourea. Alternatively, a ^{137}Cs source available for long irradiation times was used to reach the dose limit of about 600 kGy.

Experiments with the Cs-137 source. The ^{137}Cs source was used for irradiating the urea and thiourea samples. This 6.0 kCi source, manufactured by J. L. Shepherd and Associates, was installed on October 15, 1971. The gamma dose calibration was provided by the manufacturer within 10% error. The gamma dose rate, corrected by half-live of ^{137}Cs (30.17 years), was found to be 5.28±0.52 kGy/h at the position where all the samples were exposed. All samples were prepared as mentioned for ^{60}Co irradiations. The samples were rotated 90° after every one forth of the irradiation time. This practice was adopted to deliver the gamma dose uniformly to the samples. The samples were irradiated one by one for the gamma dose from 100 kGy to 620 kGy using ^{137}Cs.

Experiments were carried out to observe the effect of ^{60}Co and ^{137}Cs sources on the NQR parameters. The results are described in chapter four and discussed in chapter five.

Temperature Determination of Urea and Thiourea at CVP of the UFTR

Before observing the possible effects of temperatures on the NQR parameters of urea and thiourea, the temperature at CVP of the UFTR in samples of urea and thiourea must be determined. Therefore, temperatures of urea and thiourea samples were measured using copper-constantan (type T) thermocouples from Omega Engineering, Inc. Two thermocouple probes, one inserted in urea and the other in thiourea samples, were lowered into CVP of the UFTR. The experimental situation is shown in figure 3-5. The thermocouple wires were routed to the reactor control room for analog measurement of the temperature. The reactor power was increased to 100 kW and the temperature rise was monitored with time for about 3.5 hours. The result is given in chapter four. The maximum observed temperature of urea and thiourea reached 85.6°C and

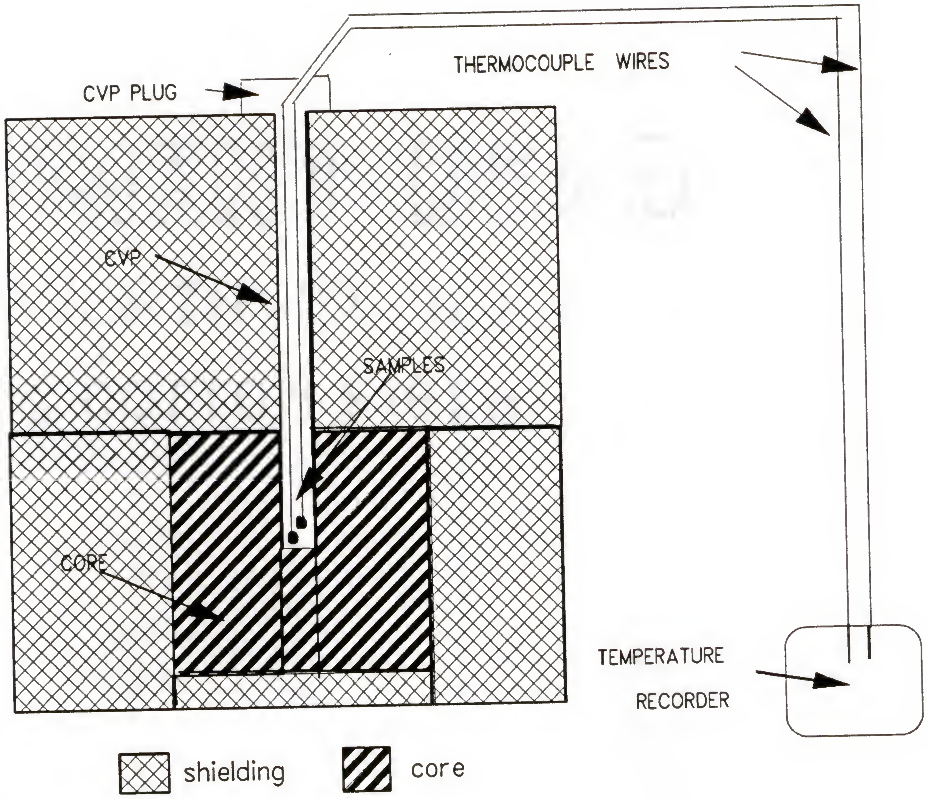

Figure 3-5: The diagram showing the temperature measurement of urea and thiourea samples at CVP of the UFTR.

86.5°C, respectively. This information was helpful to design the following experiment.

Out Core Heating of Urea and Thiourea

To observe effects of temperature on the NQR parameters of urea and thiourea, fresh samples of urea and thiourea (heated up to maximum temperature measured at CVP of the UFTR) were used. Fresh samples of urea and thiourea were enclosed in plastic bags and were heated to 40°C, 60°C, 80°C, and 100°C using a Napco (Model 620) air heating furnace. The furnace temperature was stable within an error of ±5°C for four hours. The copper-constantan thermocouple and Micromite reader, calibrated in degree Celsius, were used for temperature measurements. All samples were heated for the time as samples were at CVP of the UFTR and then cooled in air at room temperature. The plastic bags used in the experiment started melting at ~100°C. NQR spectroscopy of these samples was carried out at 77 K and results are given in chapter four.

X-ray Diffraction of Neutrons Irradiated Samples

Powder X-ray diffractometry was carried out for some of the samples of urea and thiourea which were irradiated in the UFTR to observe any chemical or physical changes in these materials. For this purpose automated powder diffractometer system (APD1700), available at the Major Analytical Instrumentation center (MAIC), the University of Florida was used. All analyses were made using Cu K-α doublet (wavelengths 1.54060 Å and 1.54439 Å). Since large grains of urea were not producing the standard X-ray diffraction pattern because of self absorption, the urea samples were ground using ceramic mortar and pestle. The thiourea samples were not ground as the grain sizes were already small enough to reproduce the standard X-ray diffraction pattern. The results are given in chapter four and discussed in chapter five.

CHAPTER 4
EXPERIMENTAL RESULTS

This chapter describes (a) the results of the NQR experiments on urea and thiourea samples exposed at CVP of the UFTR and (b) the results of the supporting experiments.

Before presenting the results, this chapter explains the need, development, and applications of several computer programs to convert the spectrometric raw data into physically meaningful NQR parameters. After determining the error associated with each NQR parameter, the salient features of each set of NQR experimental results are presented in terms of physically meaningful NQR parameters.

Since urea and thiourea samples were irradiated at CVP of the UFTR, the results of supporting experiments are described to quantify independently the in-core-gamma dose rate and temperature of the samples at CVP of the UFTR. Then, results of the NQR experiments are presented on samples of urea and thiourea (1) exposed with external gamma sources (but equivalent to the in-core-gamma doses) and (2) heated externally at equivalent temperatures to those observed at CVP of the UFTR. The main features of the results are highlighted. The physical explanation and interpretation of the results are discussed in chapter five.

Results of the NQR Experiments

NQR Raw Data

All results of NQR spectroscopy are in digital form exportable to an IBM compatible personal computer (PC). Appendix B shows an example of a digital data file exported to an IBM compatible computer from the spectrometer. The data give values of voltage in eight columns and a value of dwell time which is the time interval between two consecutive data points. There are 16 thousand data points in each spectrum. Figures 4-1 and 4-2 illustrate examples of urea and thiourea spectra generated by the raw data.

NQR Data Analysis

Two of the basic NQR parameters, (1) transition frequency or frequencies, and (2) inverse linewidth, cannot be determined from the NQR spectra as viewed on oscilloscope. Although the NQR signal amplitude, the third basic NQR parameter, can be determined from the raw data directly, the other two parameters essentially require applications of computer programs to extract these parameters from the raw NQR data. For this purpose, the raw data consisting of a set of voltage values and a value of dwell time, are transferred to an IBM compatible personal computer where systematic data analysis methodologies are implemented as explained below.

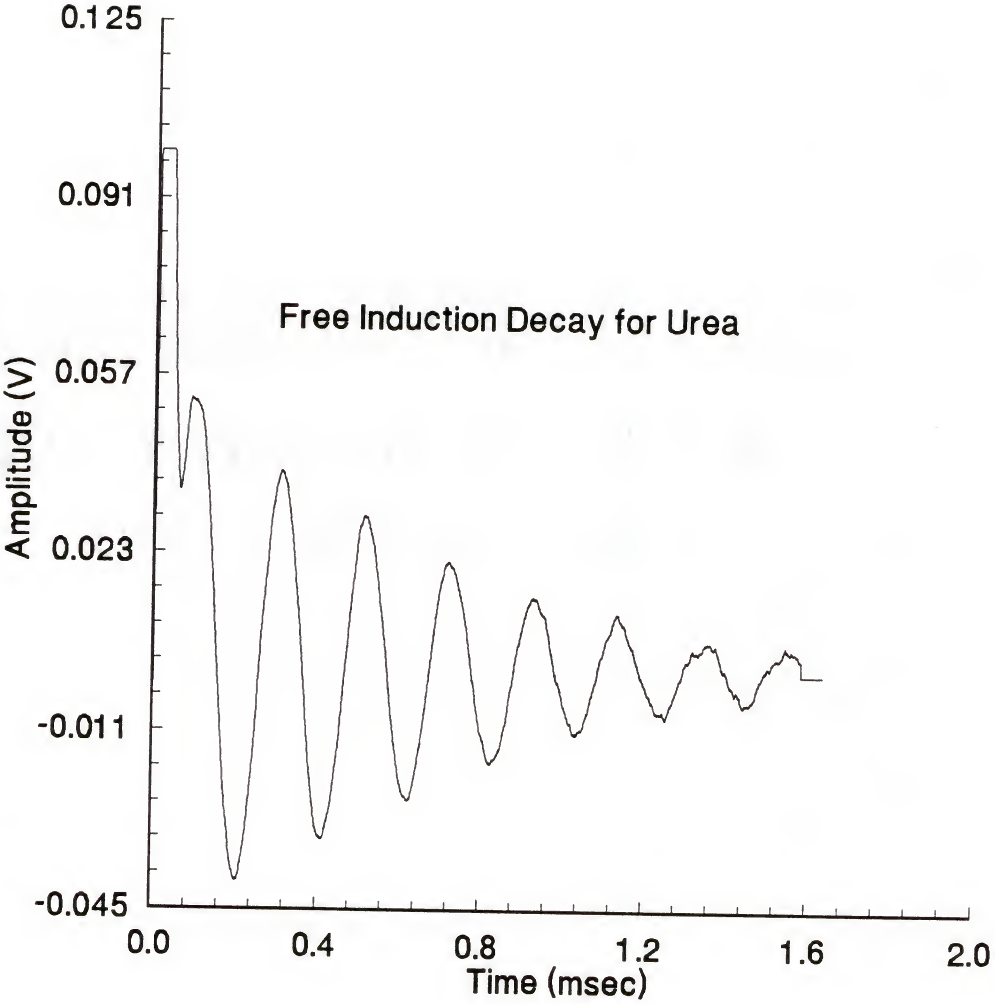

Figure 4-1: The Free Induction Decay (FID) for a standard urea sample generated by raw data collected by an IBM compatible computer.

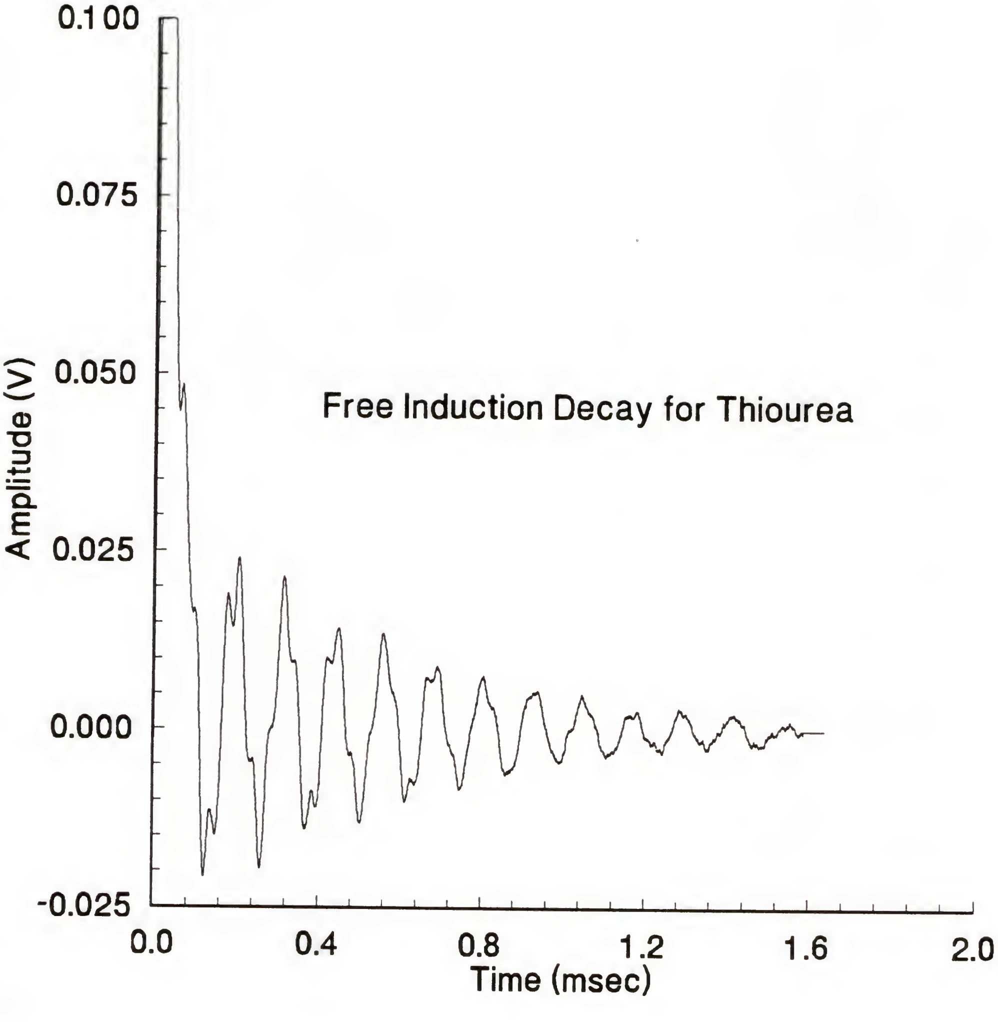

Figure 4-2: The Free Induction Decay (FID) for standard thiourea sample.

Programs for NQR parameter extraction

DFCPN computer program. A computer program for Data-Formatting-Compressing-Plotting-and-Noise elimination, DFCPN in FORTRAN 77, has been developed. The program formats the data transferred to PC from the digital oscilloscope and constructs an array of time and corresponding signal voltage values. There are provisions in the program to delete any number of corrupted data points, (x_1,y_1), (x_2,y_2), $(x_3,y_3)\ldots,(x_n,y_n)$, where n is determined by human judgement. The corrupted data points appear in the beginning of the NQR spectra as shown in figures 4-1 and 4-2. These corrupted points are due to pulse breakthrough. In this phenomenon, the transmitter coil still radiates energy when the first data sample is taken. This phenomenon lasts a few microseconds and results in only corrupting the first few hundred points which must be removed before further data analysis. DFCPN can control the number of data points by skipping any number of alternative data points. The program DFCPN also shifts the origin of the spectrum at (x_n,y_n), the beginning or starting point of an analyzable spectrum. The output file of DFCPN is used to plot the spectrum and as an input file for other computer programs. Figures 4-1 and 4-2 have been constructed by using DFCPN. The complete listing of the program is given in Appendix C.

COPROC computer program. A FORTRAN 77 program, Coarse-Parameters (NQR) and Routine-Operational Check-up of spectrometer (COPROC), has been developed. The program COPROC can find the transition frequency or frequencies from NQR spectra. Finding transition frequency quickly is also very often required for routine calibration and check up of the NQR spectrometer by observing a known transition frequency from a standard sample.

The program COPROC is based conceptually upon the discrete Fast Fourier Transform (FFT). The Fourier transform (FT) provides a mathematical method to convert the time domain function into the frequency domain and vice versa [45]. The subroutines, used in the program COPROC, are taken from Press et al. [46]. COPROC accepts input values from the DFCPN output file and gives the square of the magnitude versus frequency as the output file. The program listing, in Appendix C, shows various options offered in COPROC.

The first option in COPROC is the autocorrelation function. The autocorrelation function, Corr(f(t),f(t)), of a real time dependent function f(t) is defined as

$$Corr(f(t),f(t))=\int_{-\infty}^{\infty}f^{*}(\tau)\,f(t+\tau)\,d\tau \qquad (4\text{-}1)$$

where τ is the lag time and $f(\tau)^{*}$ represents the complex conjugate of the function. Physically, autocorrelation is a measure of the correlation of a function with itself. Of course, a function always correlates itself. However, the random noises added from the spectrometer's electronics in the time domain function are not correlated. The use of autocorrelation helps to separate the random noises from the function representing experimental data. On the other hand, information about the phase angle is lost while using autocorrelation. For this reason the program provides an option to Fourier transform (FT) the function without using autocorrelation.

The other options address the use of various windows. Mathematically, the FT is defined for a continuous function in infinite time domain while in real practice the data are digitized and finite. Thus, the FT of a digitized and finite function is like a continuous function which is multiplied by a step function. This step function, a window, lasts only during the period the real data is available otherwise it is zero. Thus a finite digitized function, equal to the product of a continuous function with a step function, is converted to a Sinc function after its Fourier transform. The Sinc function is of the form given below

$$Sinc(2\pi\nu t) = \frac{\sin(2\pi\nu t)}{2\pi\nu t} \qquad (4\text{-}2)$$

and has a main peak corresponding to ν and many side peaks called side lobes. COPROC uses a square window (step function). However, functions other than step function can be used which may help to minimize the side lobes. Two optional windows are given in the program. Although the use of windows in the program can mitigate the side lobes, it is at the expense of frequency resolution. The frequency resolution is the ability to discern the spectral response of two or more frequencies.

The fast Fourier transform is computationally efficient, even on PCs, and produces preliminary information about the NQR parameters. In addition, it provides a quick way to calibrate the NQR spectrometer. However, there are two inherent limitations of the FFT. The first prominent limitation is the frequency resolution which is poor because of the short interval (~msec) during which the data are available. The second limitation is due to implicit windowing of data that occurs when dealing with the digitized finite FFT. Windowing leaks energy from the main peak of the spectrum into side lobes which obscures, masks, and distorts the other frequencies in the vicinity of side lobes. These limitations of FFT restrict its usefulness in this research so other methods are required for further data analysis.

NOLFIT computer program. A program, Nonlinear Fitting (NOLFIT), based upon nonlinear least squares fitting, has been developed to find the optimum values for each of the NQR parameters. The program listing is given in Appendix C. The NOLFIT accepts input data from the output of DFCPN. The required initial values of some of the parameters are supplied from the output of the COPROC.

The method of least squares has been used to find a set of 'best values' of the fundamental constants in physics [47]. This method is not only limited to linear functions but may also be applied to nonlinear functions. Therefore, nonlinear least squares fitting method has been employed to find the optimum values of the NQR parameters. In this method, χ^2, a measure of goodness (optimization) of fit, is defined as

$$\chi^2 = \sum_{i=1}^{N} \frac{1}{\sigma_i^2} [y_i - y(t_i, a_k)]^2 \qquad (4\text{-}3)$$

where y_i is the ith experimental data point out of the total N data points and σ_i^2 is the instrument uncertainty in the ith data point. The function $y(t_i, a_k)$ is the theoretical model with a_k (k=1,2,...,m) parameters to be determined.

A theoretical model, based upon the understanding of the NQR theory, has been chosen to fit experimental data. In this work a theoretical model fitted to the experimental data is defined by adding a constant a_0, the dc shift in the spectrum, in equation (2-60) and is given by

$$y(t_i, a_k) = a_0 + \sum_{j=1}^{n} a_{(4j-3)} \cos[2\pi(a_{(4j-2)} - \nu_{rf}) t_i + a_{(4j-1)}]\, e^{-t_i/a_{(4j)}} \qquad (4\text{-}4)$$

where $a_{(4j-3)}$ represents the amplitude and $a_{(4j-2)}$ is the transition frequency. The coefficients $a_{(4j)}$ and $a_{(4j-1)}$ are the inverse linewidth and the phase shift, respectively. Note that these constants are not related. The radio frequency ν_{rf} is known experimentally. The number n, taken to be one for urea and two for thiourea, is the number of ^{14}N sites in the compound used.

The program NOLFIT minimizes χ^2 with respect to each parameter in function $y(t_i, a_k)$. For m parameters there are m hypersurfaces in the m dimensional space having parabola of minima curves. Each parabola has a coarse minima and has many local minimas. The program NOLFIT calls the subroutine GRIDLS which is based on the grid search method [48]. The subroutine GRIDLS is capable of finding the coarse minima with the initial values far off from the parabola of minima curve. The GRIDLS is fast in locating coarse minima but is very slow in reaching the local minima. Hence, once the coarse minima is reached (when the difference of the two adjacent computed chi-squares is less than 10^{-2}) the program calls another subroutine called CURFIT to find the local minima [48]. The subroutine CURFIT is based on the Marquardt method [49]. The Marquardt method (and hence the CURFIT) cannot converge if the initial values are outside the parabolic minima curve. But the method converges and finds the local minima much faster than the grid search method if the initial values are within the parabolic curve of the minima. Hence the subroutine GRIDLS finds the coarse minima for each parameter, then the subroutine CURFIT finds the local minima. Although the subroutines GRIDLS and CURFIT have been taken from Bevington [48], their cascade applications in NOLFIT remarkably reduce the computational time.

Since the σ_i^2 for the individual points in the NQR experiments are not known, a constant value of an instrument error can be assumed to be associated with each point in the data. The parametric values are then independent of the errors in the individual points. An error of about 2% of the highest y-value is assumed as the initial value and the program iterates until all of the parametric values finally converge to a desired level (when the difference of the two adjacent computed chi-squares is less than 10^{-4}) defined in the program. This condition can be changed to any desired value from the main program.

After finding the best parametric values, the chi-squares is assumed equal to one and then the average instrument error in each parameter is found by using a subroutine, POLISH, specially developed for this purpose. These average instrument errors in the NQR parameters are of less importance because of the presence of other significant errors. However, the other possible sources of error in NQR experiments are discussed in detail in the next section.

In order to ensure the proper convergence of the parametric values, the program NOLFIT is run for at least two slightly different sets of initial values as suggested by Gallant [50]. The NQR parametric values computed by NOLFIT program for some of the NQR spectra were also compared with the values produced by the state space singular value decomposition (HSVD) algorithm [51]. The values were found to be in good agreement.

The program NOLFIT furnishes the numerical values for the amplitudes, the transition frequencies, the inverse linewidth, and the dc noise level, along with the instrument average error in each parameter.

Figures 4-3 and 4-4 show experimental data for urea and thiourea along with fitted curves using NOLFIT for one (n=1) and two (n=2) site models, respectively. Using DFCPN, several hundred redundant data points from the beginning of the spectrum were removed. In order to show the data points clearly in the figures, fewer than the actual number of data points fitted are shown.

While presenting results, all amplitudes were measured directly from the original spectra. However, all other NQR parameters as shown in the results were extracted using NOLFIT. The method of determining the total estimated errors in NQR parameters is explained in the following section.

Error Analysis of the NQR Parameters

Error in any measurable variable is the difference of the experimentally measured value and the absolute or true value. In the case, when the absolute value of a physical parameter is not known the average of many values is taken as the absolute value and the standard deviation about the mean value can be taken as an error. In the NQR spectroscopy, any

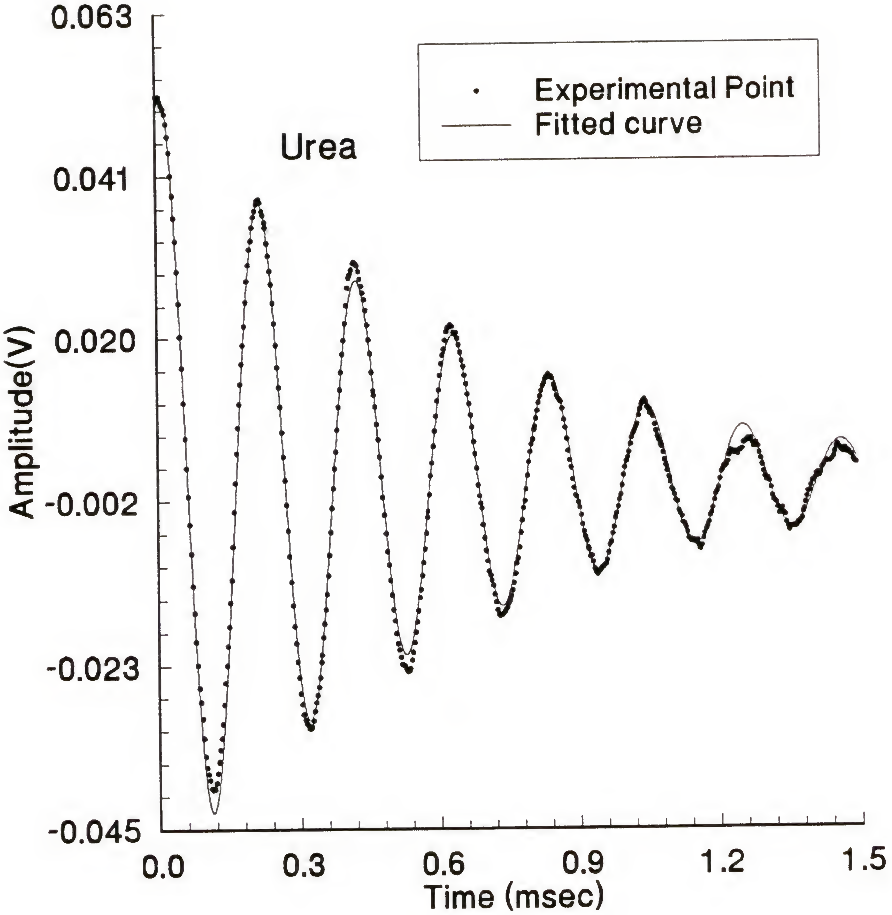

Figure 4-3: One site model, equation (4-4) with n=1, fitted to the raw data of a standard urea sample spectrum using NOLFIT.

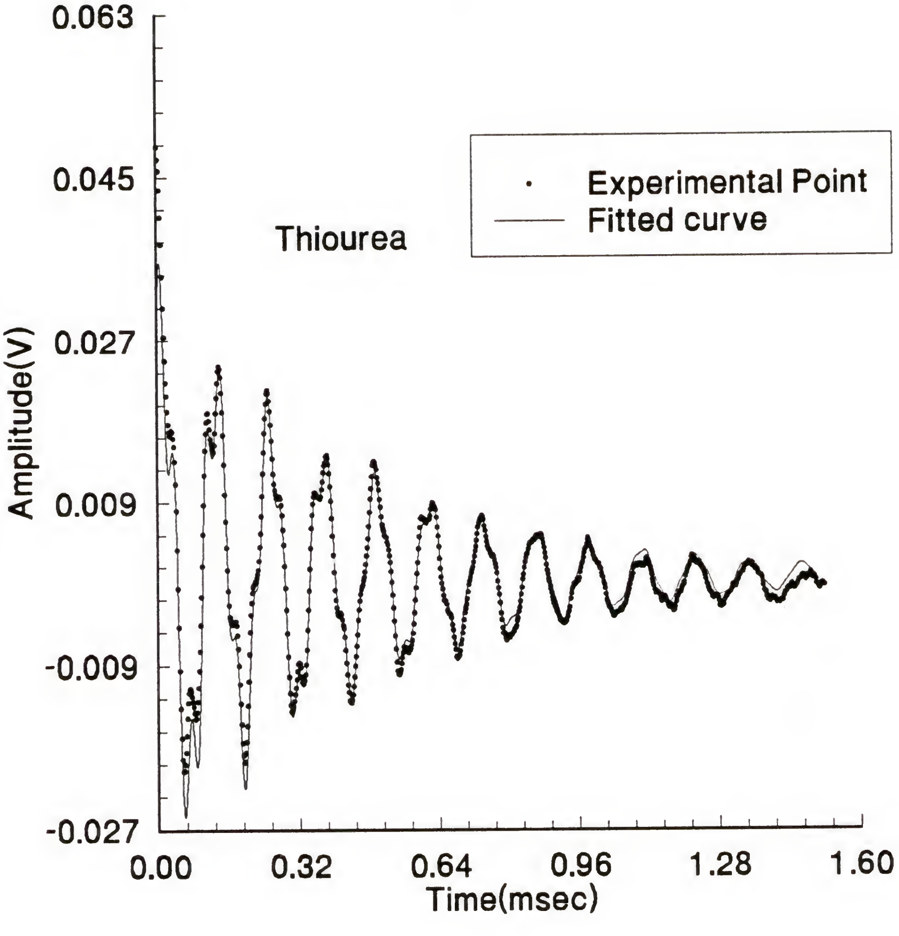

Figure 4-4: Two site model, equation (4-4) with n=2, fitted to the standard thiourea spectrum using NOLFIT.

analyzable spectrum is the average of spectra resulting from the process of signal averaging. If an experiment is repeated, some dispersion or scattering in NQR parametric values are observed.

In the NQR spectroscopy one can measure each NQR parameter several times using a standard sample of that compound and the dispersion, in term of standard deviations, in the value of that parameter can be estimated. The determined dispersion in the respective NQR parameters has a width, or limit, in which the experimental values are reproducible. This dispersion, within 95% confidence level, is assumed to be the error in that parameter and any measured value of that parameter out of the dispersion limit is considered to be significant. Consequently, the dispersion width in the parametric value not only contains the statistical error but also errors from other sources.

There are three primary sources of error in the determination of NQR parameters. First, some error is due to the statistical fluctuations in the formation of the magnetization vector, which varies slightly from experiment to experiment for the same sample. Second, errors in the NQR parameters are contributed by the NQR spectrometer's electronics. Third, errors are introduced from the data analysis methodology in determining the NQR parameters. All of these sources of error affect each of the NQR parameters, therefore, each source of error is discussed in detail.

Error in NQR signal amplitude. There are two sources of error in the NQR signal amplitude. One source is due to statistical fluctuation in the formation of magnetization vector which varies from experiment to experiment for the same sample and the other results from the NQR spectrometer's electronics. Error contributions from the data analysis methodology in NQR signal amplitude can be avoided by measuring this parameter directly from the spectrometric data. In order to estimate the possible error in the NQR signal amplitude the standard samples of urea and thiourea were measured ten times for each compound and dispersions in signal amplitudes were determined. In the case of urea the signal amplitude was found to be reproducible within an error of 5% about the mean amplitude. The fluctuations of amplitude more than 5% were considered to be a significant change for urea.

In the case of thiourea, the dispersion in signal amplitude has been found to be 7% about the mean amplitude. This error is higher than the error in the signal amplitude of urea because the signal amplitude of thiourea is the sum of two amplitudes from two sites. Figure 4-5 shows the radio frequency bandwidth as the full width at half maximum (FWHM) of the frequency peak of the Fourier transform of a typical radio frequency pulse applied in this research for thiourea NQR spectroscopy. Although molecules at site-1 are primarily excited, due to a finite bandwidth (637 kHz) of radio frequency applied in the experiment, site-2 molecules are

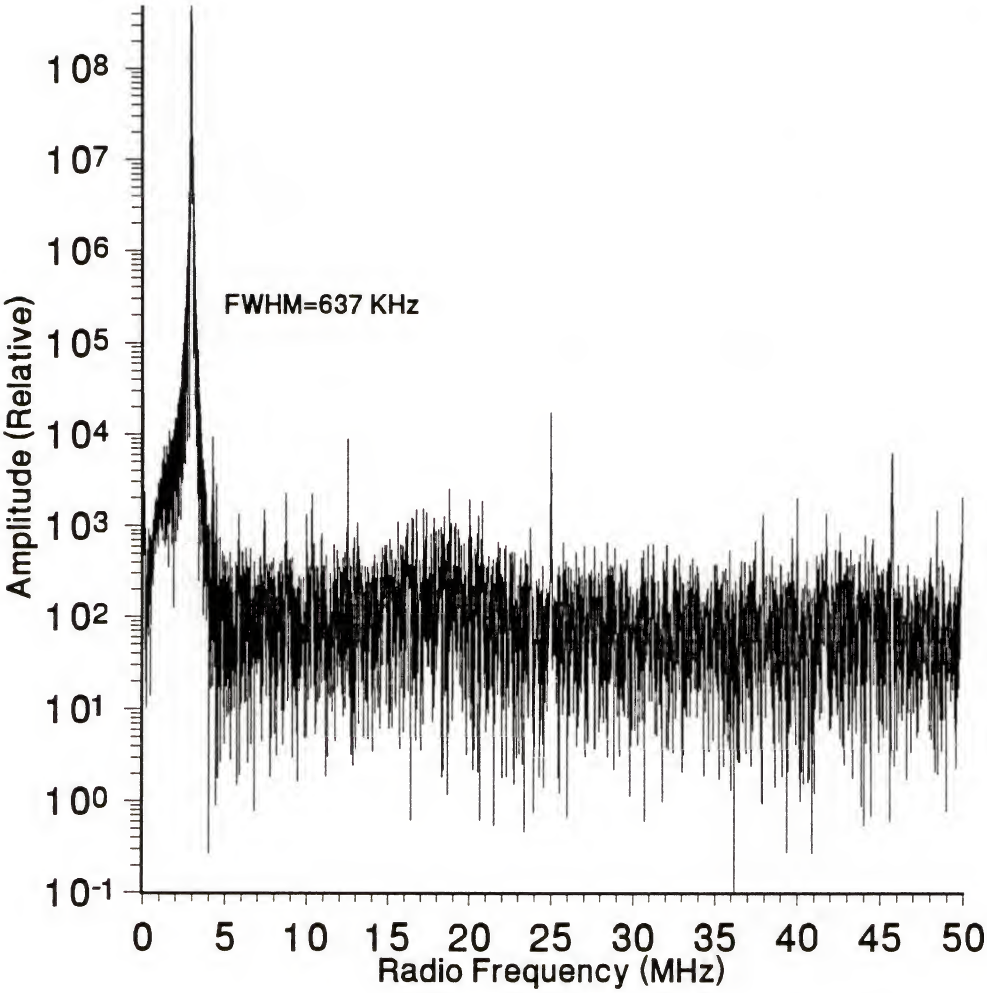

Figure 4-5: The Fourier transform of a pulse of radio frequency applied for thiourea studies using NQR spectroscopy.

simultaneously excited which contribute to the total signal amplitude. The contribution of signal amplitudes from site-1 and site-2 of thiourea in the total amplitude are found to be 70% and 30%, respectively. A small phase change induced by the spectrometer's electronics in signals from site-1 and site-2 in thiourea introduces errors in total signal amplitude. Therefore, the dispersion in the signal amplitude of thiourea was found to be 7% and changes greater than this value were considered to be significant for thiourea.

Error in transition frequency. The main sources of error in the transition frequency, or frequencies, are from the data analysis. The first cause, the statistical fluctuation in the formation of magnetization vector, has little effect on this parameter. The instrument errors are estimated from the data analysis NOLFIT program as discussed in the previous section of this chapter. Using ten spectra each from urea and thiourea standard samples, the instrument error in transition frequency from the NOLFIT program has been found to be ~6 Hz both for urea and thiourea.

The data analysis methodology itself, however, introduces significant errors in the evaluation of the transition frequency. The transition frequency has been found to be sensitive to the starting point of the spectrum. The human judgement in deleting the initial corrupted data points introduces some error because of the selection of starting point of the spectrum. The value of the transition frequency is also sensitive to the length of the spectrum and the total number of data points considered for the data analysis. Therefore, the effects of, (1) the starting point of the spectrum, (2) length of the spectrum, and (3) the total number of data points considered for the data analysis, were examined by using NOLFIT program on ten spectra each from urea and thiourea standards samples. The dispersion in transition frequency about ν_1 for both urea and thiourea (site-1) has been found to be ±80 Hz. Thus, any change in transition frequency of urea and thiourea more than ~80 Hz is considered to be significant for the analysis of all other samples of urea and thiourea.

Error in inverse linewidth. All sources of error mentioned for data analysis of transition frequency are also responsible for introducing errors in inverse linewidth, T_2^*. Analysis of ten individual spectra from urea and thiourea standard samples, corresponding to the transition frequency ν_1 for urea and thiourea (site-1), determined dispersions of 5% and 10% in mean values of inverse linewidths of urea and thiourea, respectively. Thus, any change more than 5% and 10% in inverse linewidth of urea and thiourea, respectively, is considered to be a significant change.

The errors applied to NQR parameters in this chapter are the total estimated errors from all possible sources.

Results of Urea and Thiourea Exposed at CVP of the UFTR

Samples of urea and thiourea were exposed to mixed radiation fields of neutrons and gammas from a nuclear reactor. Since the neutron flux at CVP was constant, only exposure time was varied in these experiments. Thus, the neutron fluence, the product of neutron flux and the exposure time, is found to be a convenient variable in this work for data presentation. Later, it is shown that this variable is also helpful in mathematical modelling of the results as given in chapter five.

The NQR parameters for urea and thiourea are presented as a function of neutron fluence. Subsequently, the dependence of NQR parameters on out core gamma dose and out core temperature are presented under the title of supporting experiments.

Figure 4-6 shows a plot of the NQR signal amplitude, normalized to the amplitude of standard urea sample A_0, as a function of neutron fluence for urea. The plot shows that the normalized amplitude of urea has a trend of decreasing amplitude at higher neutron fluence. The variation of the NQR signal amplitude, normalized to the amplitude of standard thiourea sample A_0, in thiourea (site-1) with the neutron fluence is shown in figure 4-7. The plot shows a rapid decrease in the normalized NQR signal amplitude with neutron fluence up to ~4.32×10^{15} cm^{-2} then shows a relatively slow decrease.

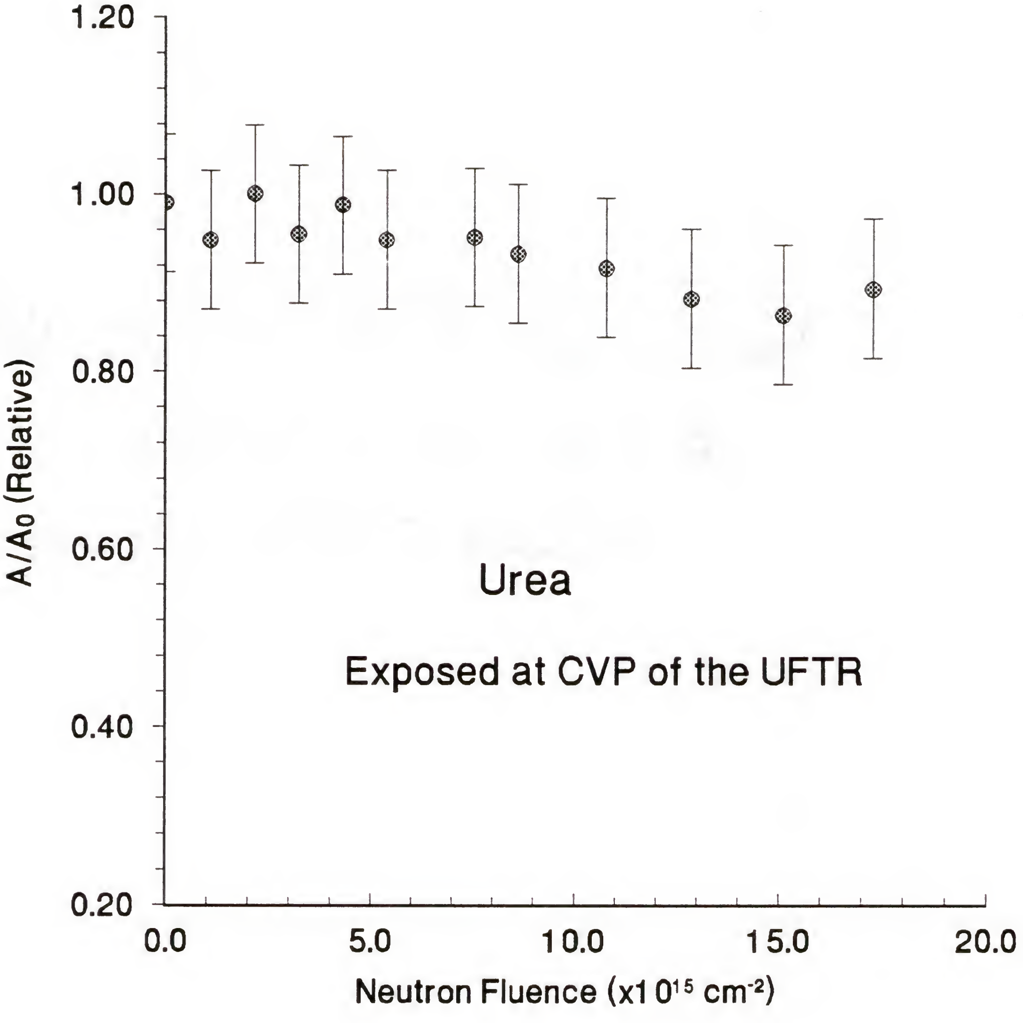

Figure 4-6: Variation of NQR signal amplitude for urea with neutron fluence at CVP of the UFTR.

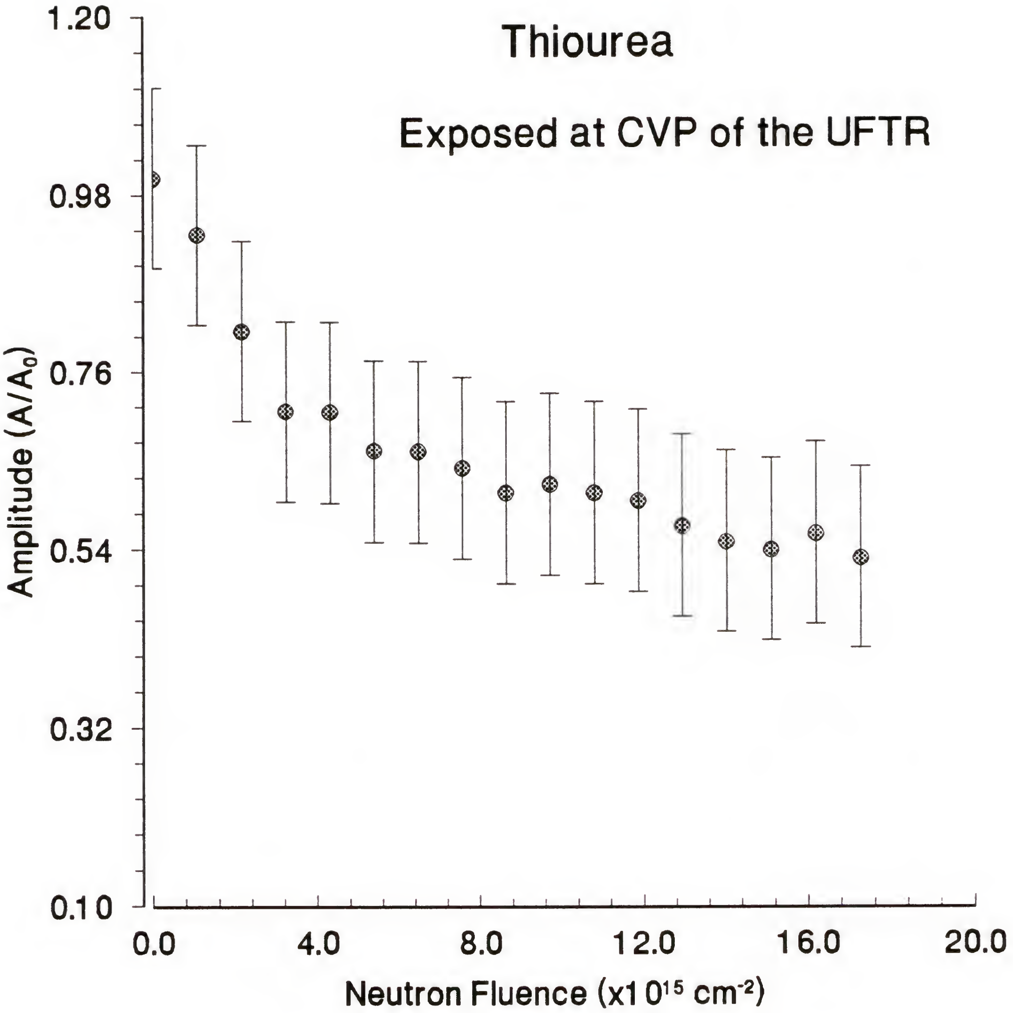

Figure 4-7: Variation of NQR signal amplitude for thiourea with neutron fluence at CVP of the UFTR.

The inverse linewidths vary with neutron fluence for urea and thiourea as depicted in figures 4-8 and 4-9, respectively. Note that the change in inverse linewidths with neutron fluence is observed for both urea and thiourea compounds.

Results of Supporting Experiments

In Core Gamma Dose Rate Measurement

Gamma dose at CVP of the UFTR

A relationship between in core gamma dose rate, determined by thermoluminescence detectors (TLD-200), and the reactor power is shown in figure 4-10. The errors shown in the graph are the statistical error of one standard deviation. The slope of the curve is 0.66±0.09 Gy/h-W. The gamma dose rate, extrapolated to 100 kW of reactor power, is determined to be 66±9 kGy/h. Using gamma dose rate of 75 kGy/h, the maximum gamma dose received by either urea or thiourea samples was found to be 300 kGy for four hour irradiations at CVP of the UFTR. The results are discussed in chapter five under the title of Effects of Gamma Photons on Urea and Thiourea.

Out Core Gamma Exposure of Urea and Thiourea

After knowing the gamma dose rate at CVP of the UFTR, external gamma sources were used to expose the samples of urea and thiourea up to 600 kGy, a value which is twice the gamma

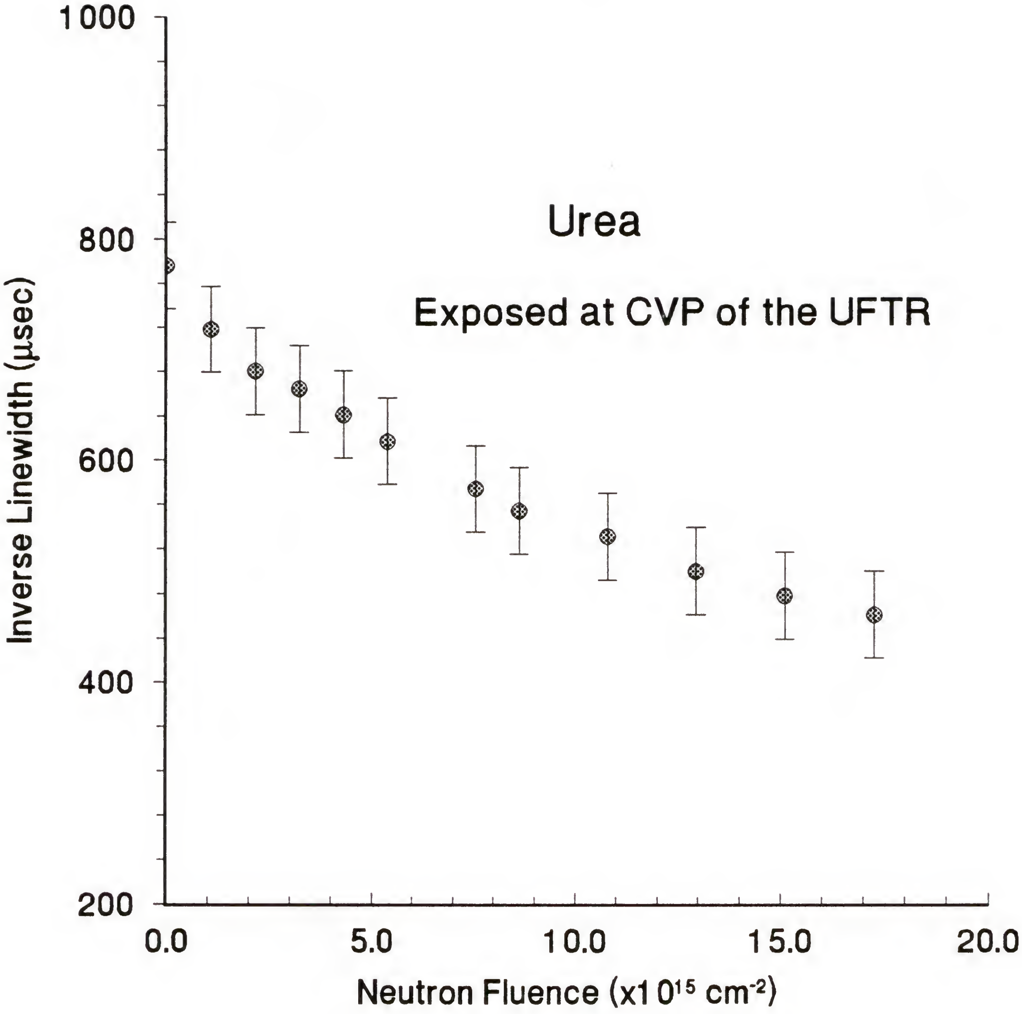

Figure 4-8: The dependence of inverse linewidth as a function of neutron fluence for urea irradiated at CVP of the UFTR.

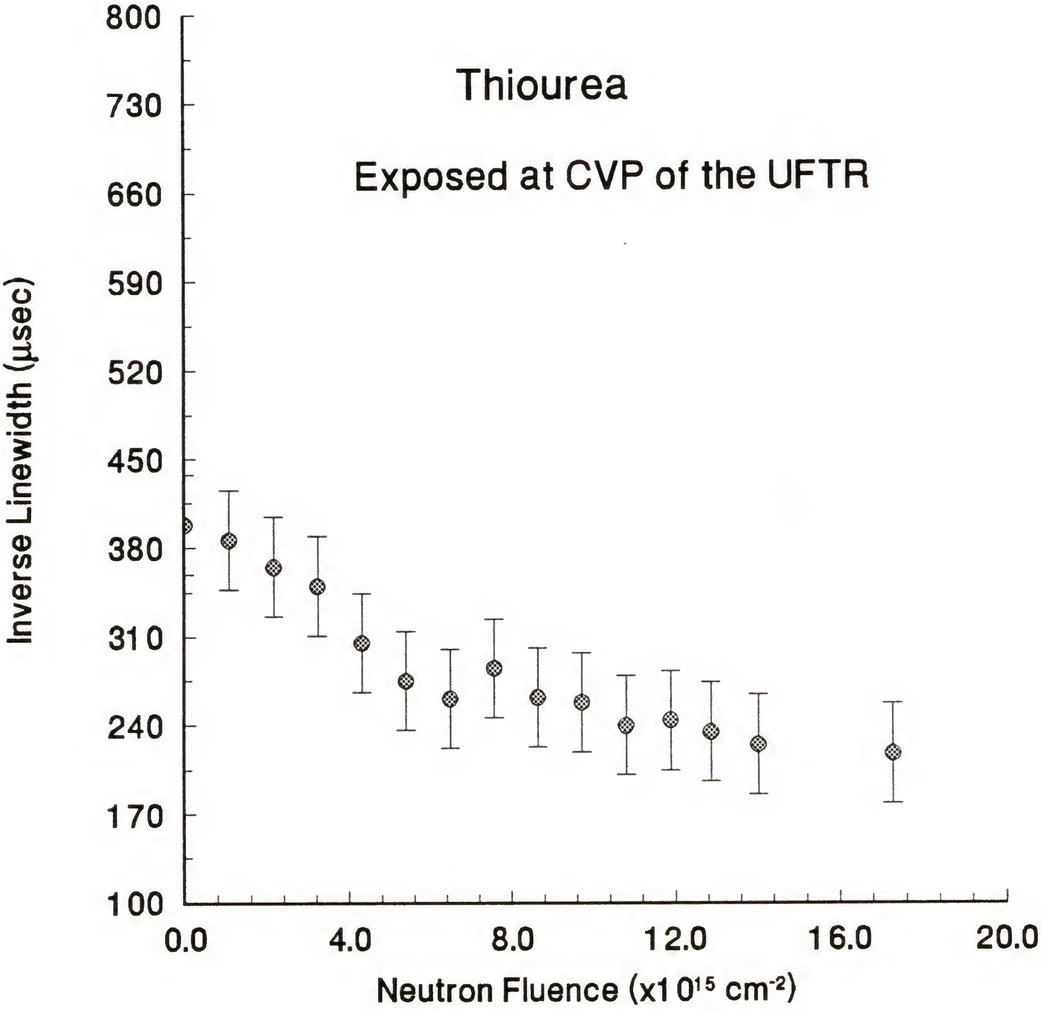

Figure 4-9: Change in inverse linewidth, for site-1, with neutron fluence for thiourea samples irradiated at CVP of the UFTR.

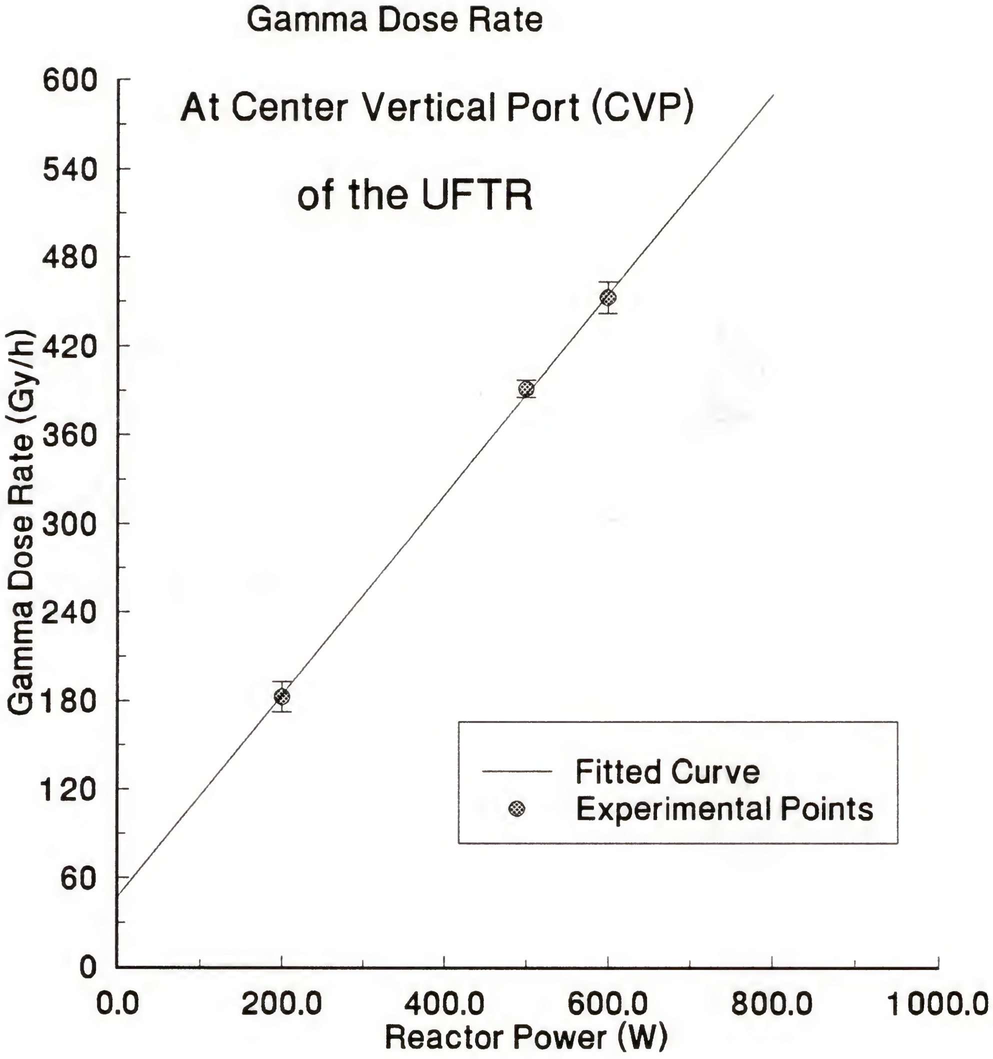

Figure 4-10: An experimental curve showing relationship between reactor power and in core gamma dose rate at CVP of the UFTR.

dose received by either urea or thiourea at CVP. The gamma dose rate from a ^{60}Co source was determined as described in chapter three. The gamma dose rate versus the distance from the center of the ^{60}Co source is plotted in figure 4-11.

In figures 4-12 to 4-17, the filled and empty circles represent samples exposed to ^{60}Co and ^{137}Cs gamma sources, respectively. Total estimated errors are shown in all figures.

Figures 4-12 and 4-13 show the effect of gamma radiation on the NQR signal amplitude for urea and thiourea, respectively. The NQR signal amplitudes for different gamma doses are all within the dispersion limits of 5% and 7% for urea and thiourea samples, respectively. Therefore, no effects of gamma radiation on urea or thiourea signal amplitudes have been found either from ^{60}Co or ^{137}Cs gamma photons.

Figures 4-14 and 4-15 show the effects of gamma dose from ^{60}Co and ^{137}Cs gamma photons on inverse linewidths, T_2^*, corresponding to ν_1, the highest transition frequencies, for urea and thiourea (site-1), respectively. Since the changes in T_2^* are less than 5% and 10% for urea or thiourea, respectively, the gamma photons do not produce any observable effect on inverse linewidths of these compounds.

The highest transition frequencies (ν_1) as a function of gamma dose from ^{60}Co and ^{137}Cs gamma sources for urea and thiourea are shown in figures 4-16 and 4-17. The dispersions

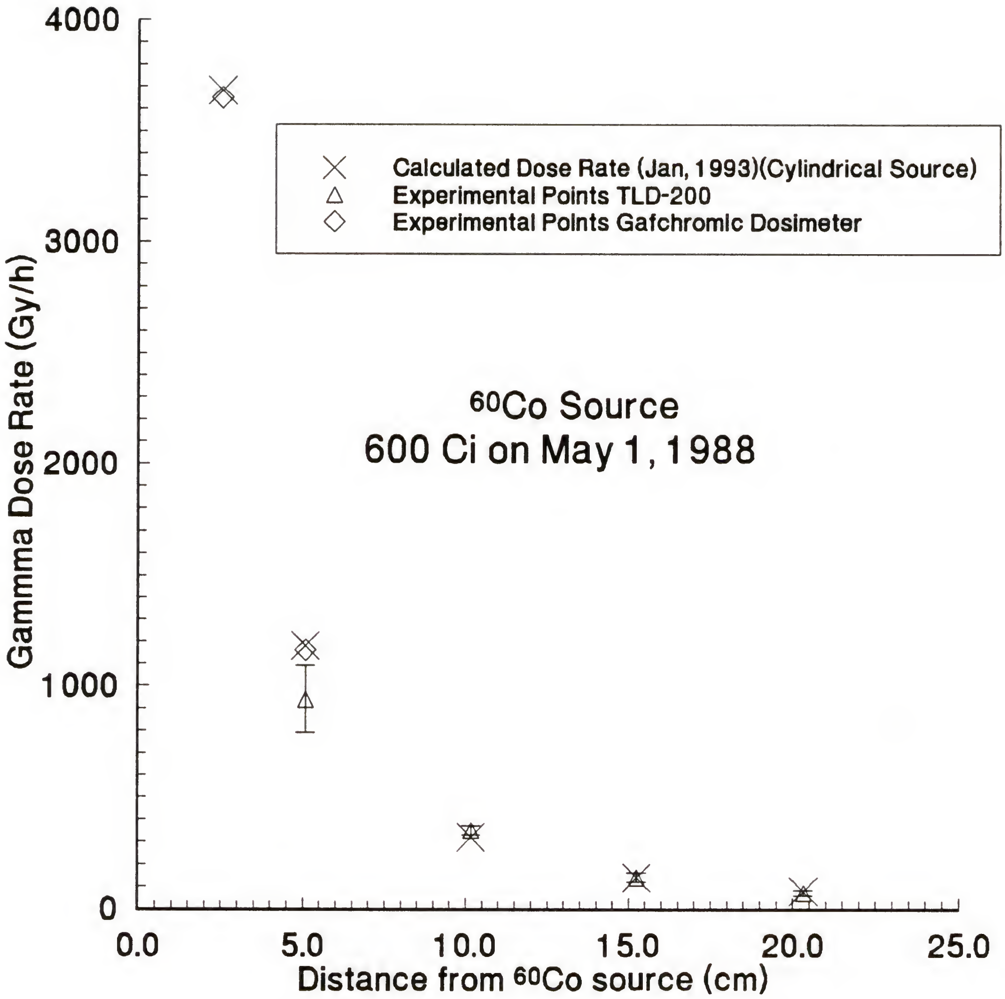

Figure 4-11: A dose-rate-distance relationship for ^{60}Co gamma source determined by various experimental methods. This source was used to irradiate urea and thiourea samples as explained in chapter three.

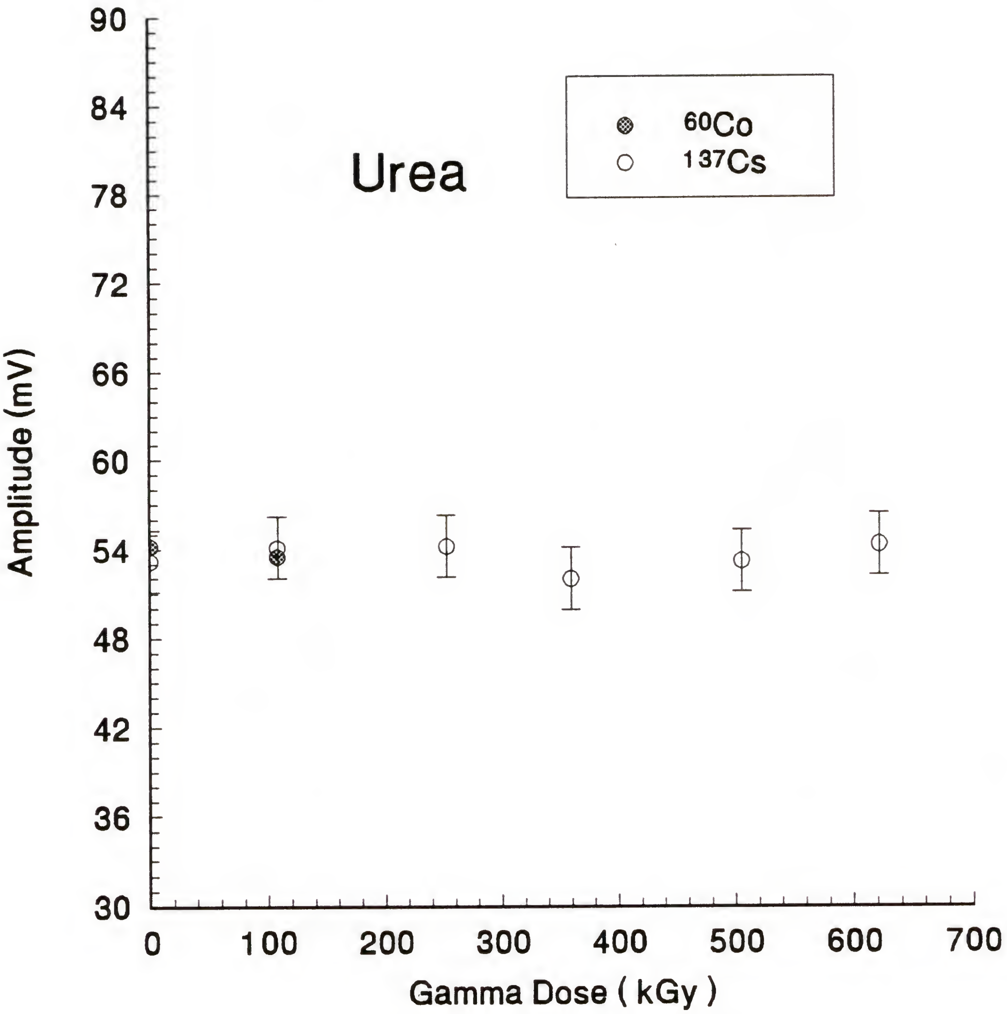

Figure 4-12: Effect of gamma dose on the NQR signal amplitude for urea.

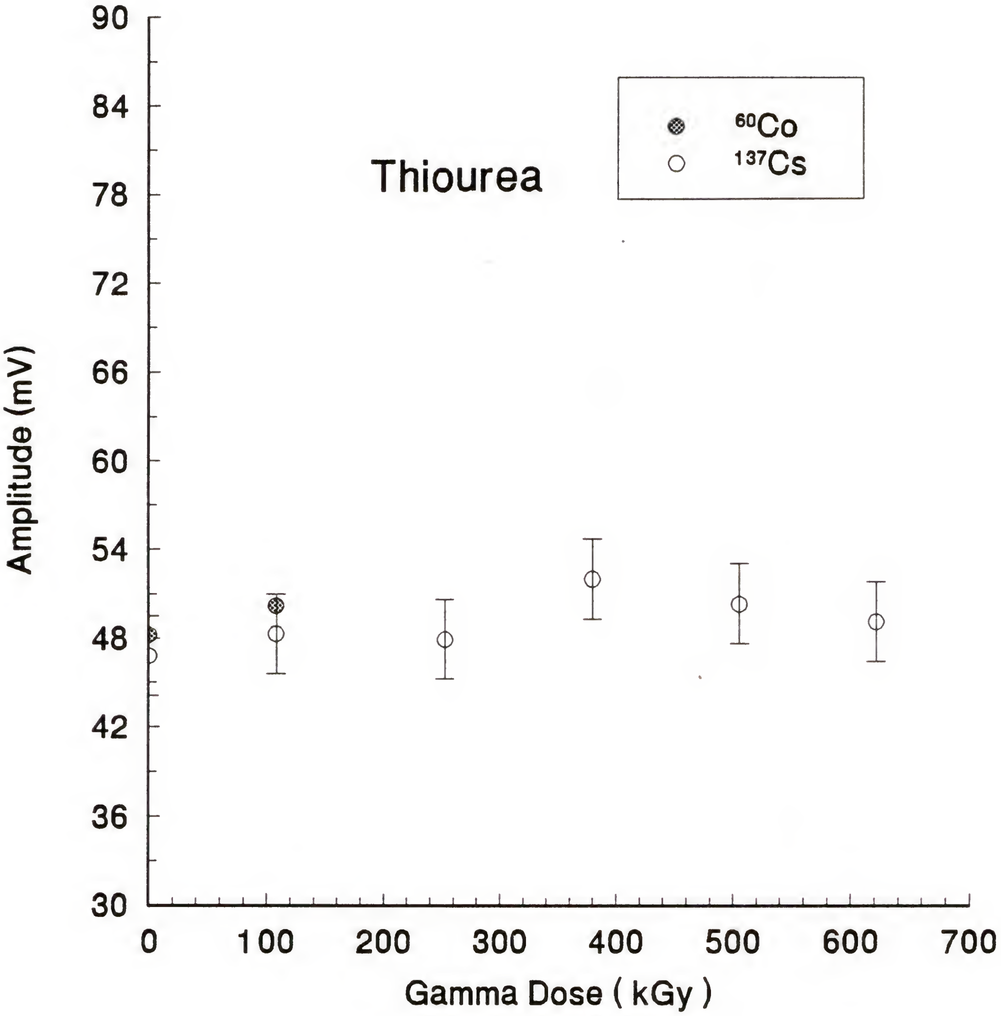

Figure 4-13: Plot of NQR signal amplitude with gamma dose for thiourea.

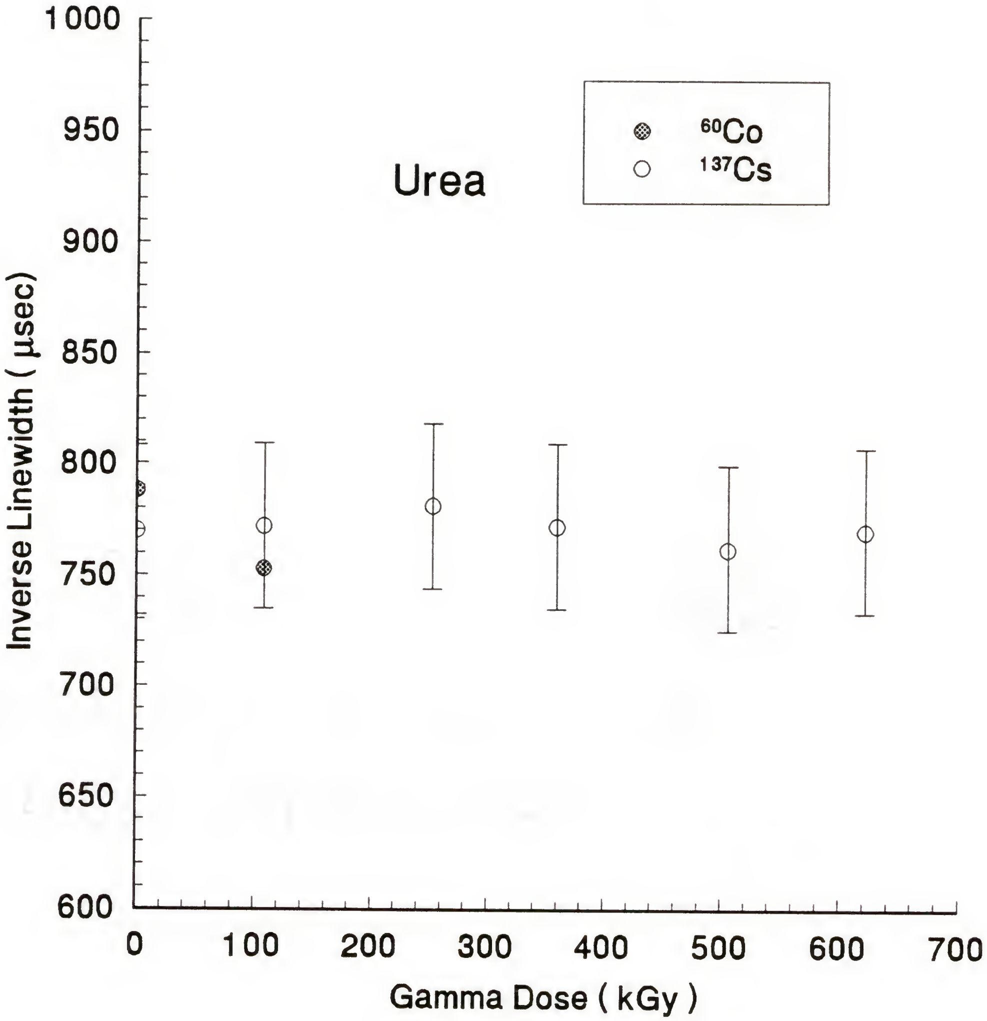

Figure 4-14: Inverse linewidth as a function of gamma dose for urea.

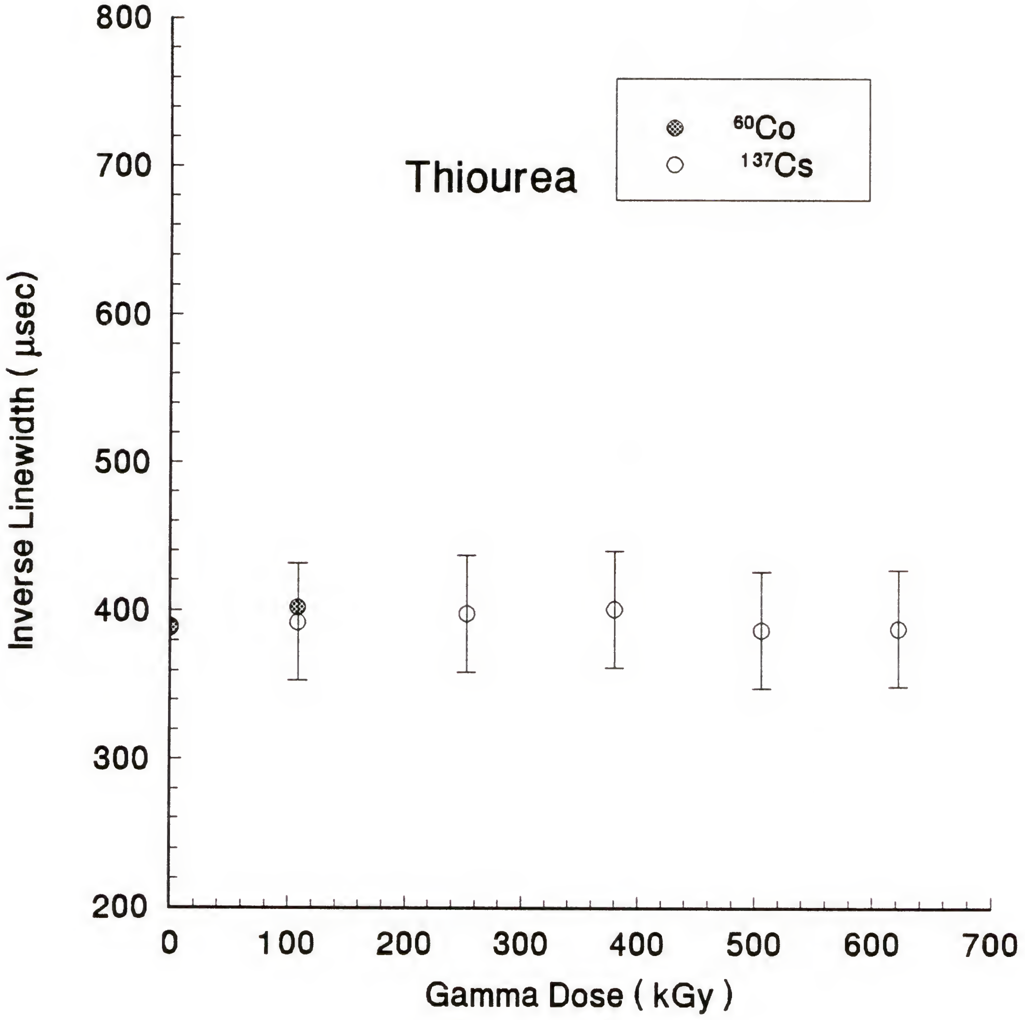

Figure 4-15: The inverse linewidth, for site-1, is depicted as a function of gamma dose for thiourea.

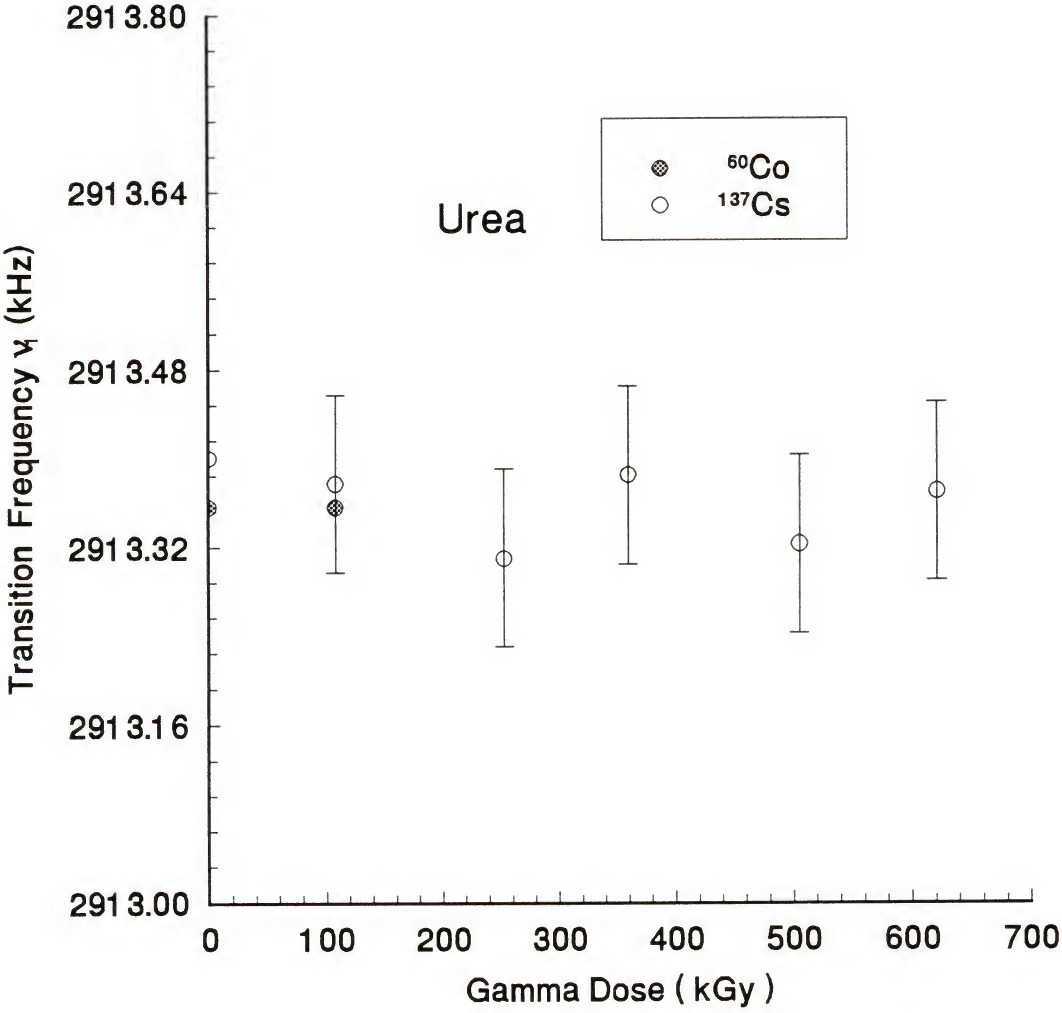

Figure 4-16: The transition frequency is plotted against gamma dose for urea.

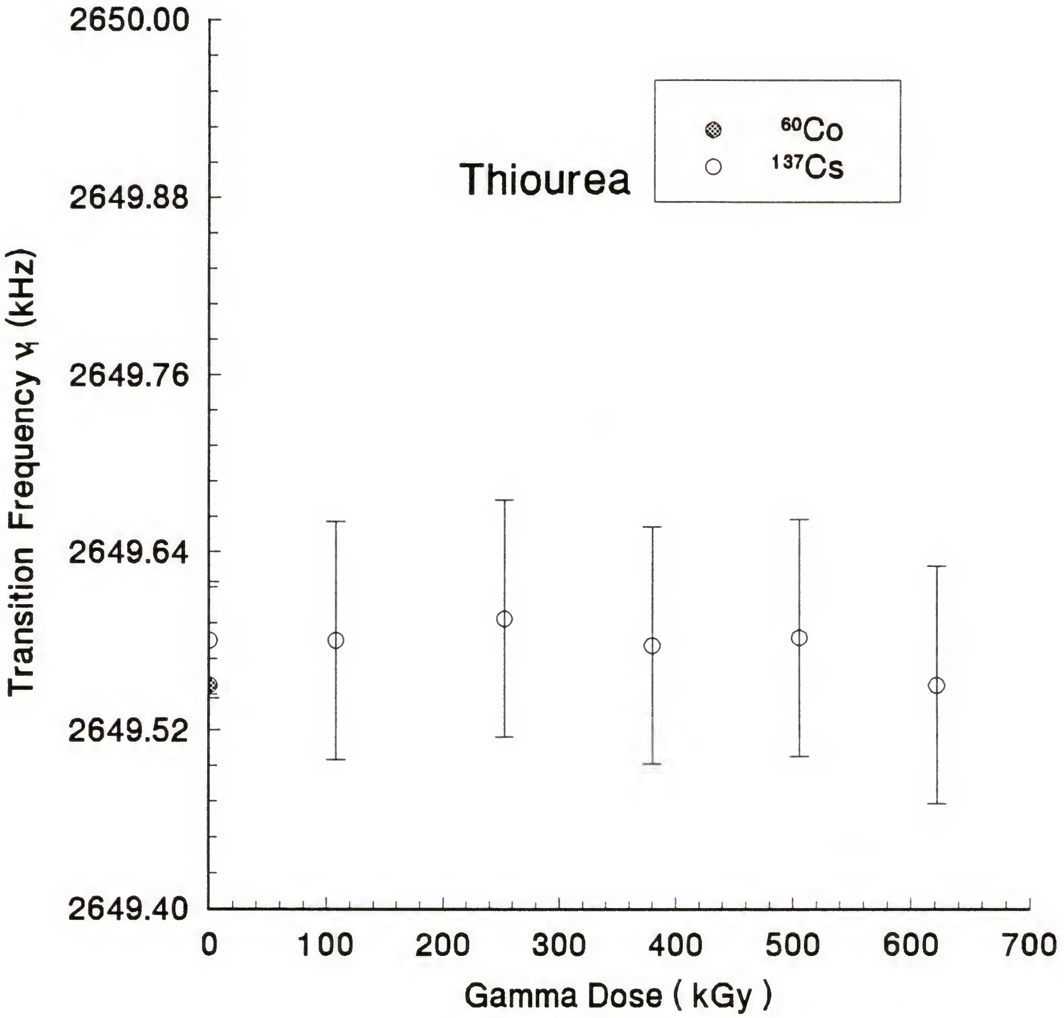

Figure 4-17: Effect of gamma dose on the transition frequency, for site-1, is shown varying with gamma dose.

in transition frequencies for urea and thiourea (site-1) are within ±80 Hz. Thus, this NQR parameter has not shown effects of gamma irradiations in urea or thiourea.

To summarize, the gamma doses from ^{60}Co and ^{137}Cs sources do not produce significant effects on neither urea nor thiourea observed through (1), NQR signal amplitude, (2) inverse linewidths, and (3) transition frequencies.

Out Core Temperature Effects on Urea and Thiourea

Figure 4-18 shows the temperature increase in samples of urea and thiourea with time. The results of NQR spectroscopy on samples of urea and thiourea heated out side the reactor core are shown in figures 4-19 to 4-24. The samples of urea and thiourea were heated in oven up to temperatures measured at CVP and then cooled at room temperature for NQR spectroscopy. However, enhanced temperatures of urea and thiourea samples do not show significant effects both in urea and thiourea samples observed through NQR parameters.

X-ray Diffraction of Neutrons Irradiated Samples

The X-ray diffractometry of urea and thiourea samples exposed for one and four hours at CVP of the UFTR are presented in figures 4-25 and 4-26, respectively. The figures compare the X-ray diffraction pattern of standard samples of urea and thiourea with diffraction pattern of samples irradiated at CVP of the UFTR. Figure 4-25 shows that no

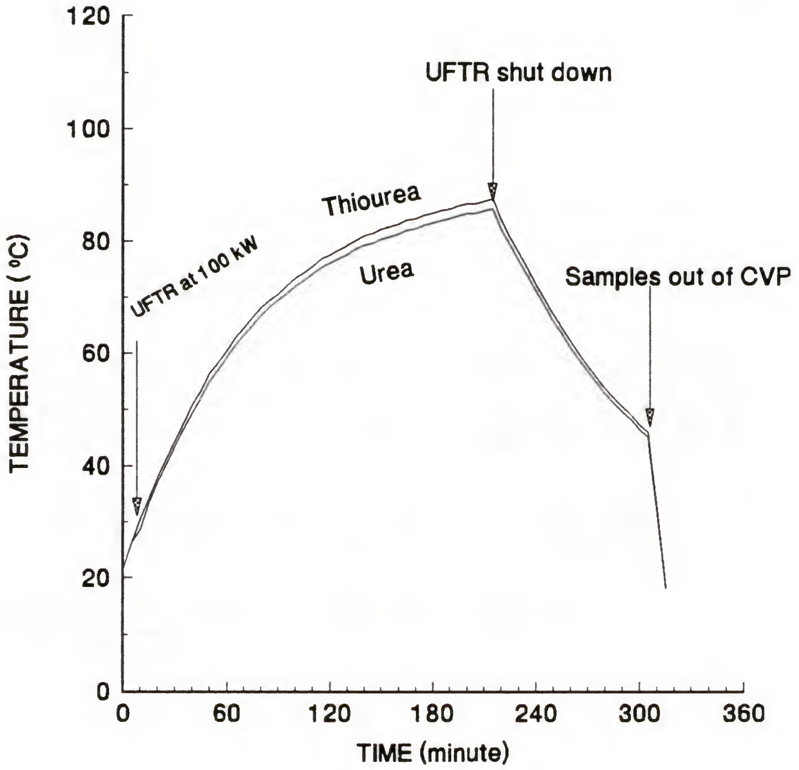

Figure 4-18: The temperature increase in samples of urea and thiourea at CVP of the UFTR measured with thermocouple.

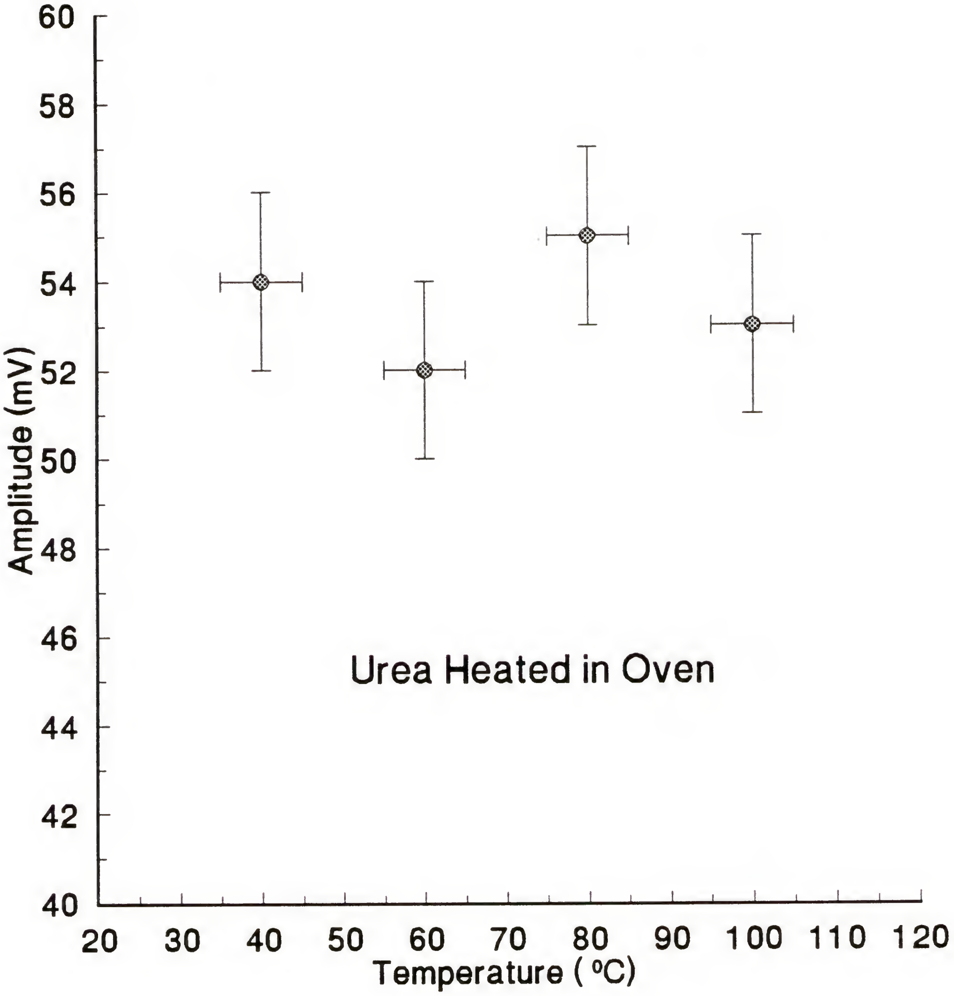

Figure 4-19: The NQR signal amplitude of urea plotted as a function of urea sample temperature.

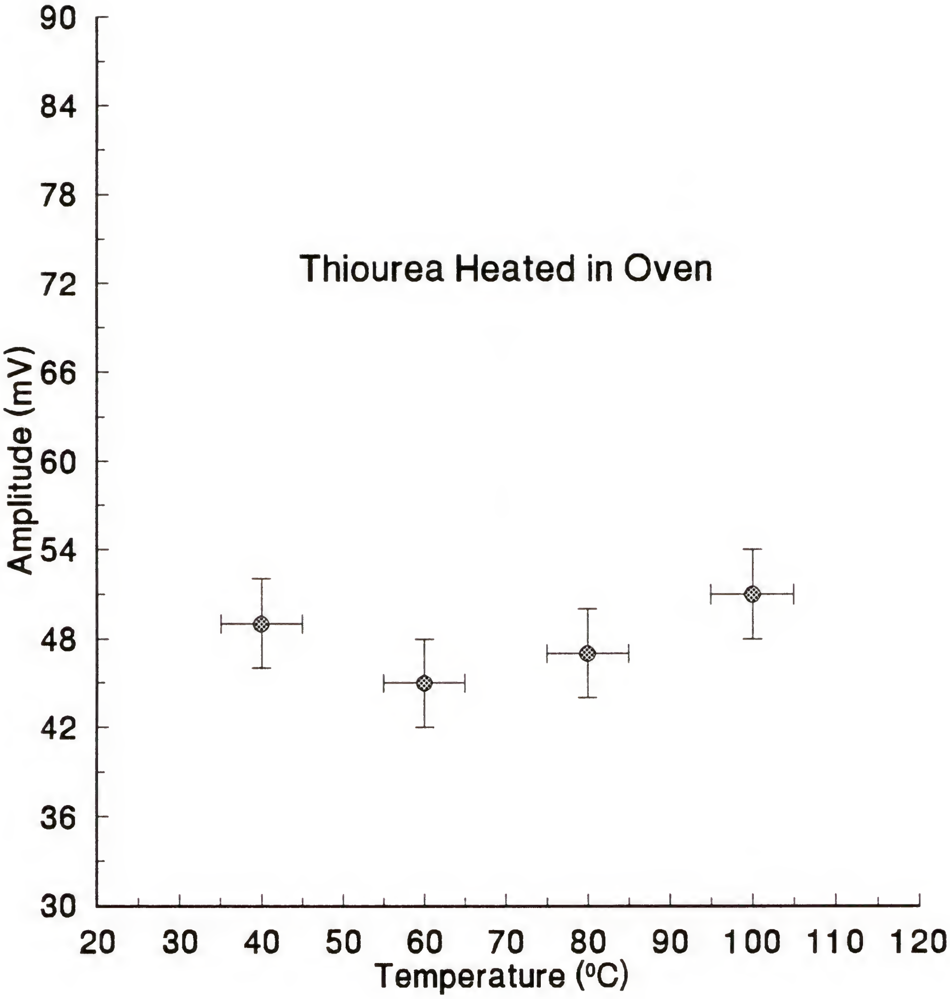

Figure 4-20: A plot between NQR signal amplitude of thiourea and temperature of thiourea.

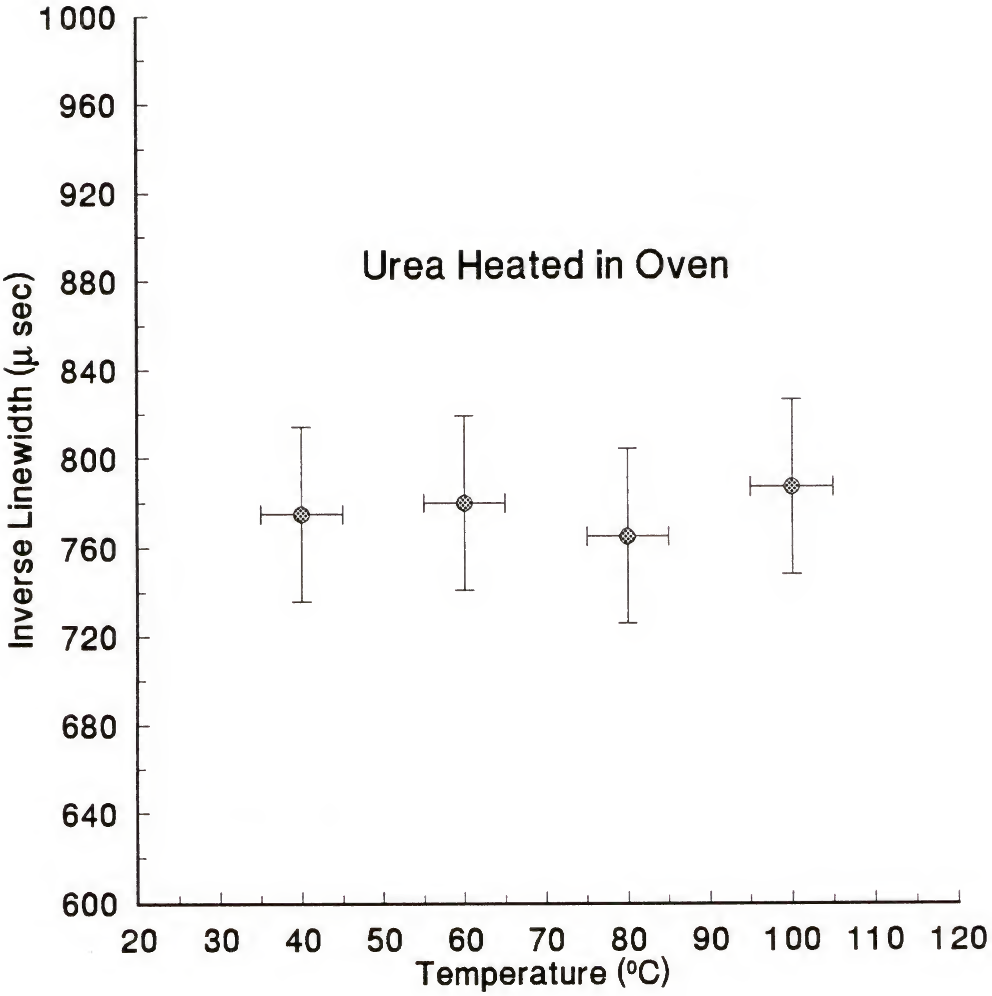

Figure 4-21: A graph of inverse linewidth of urea samples versus temperature of urea samples.

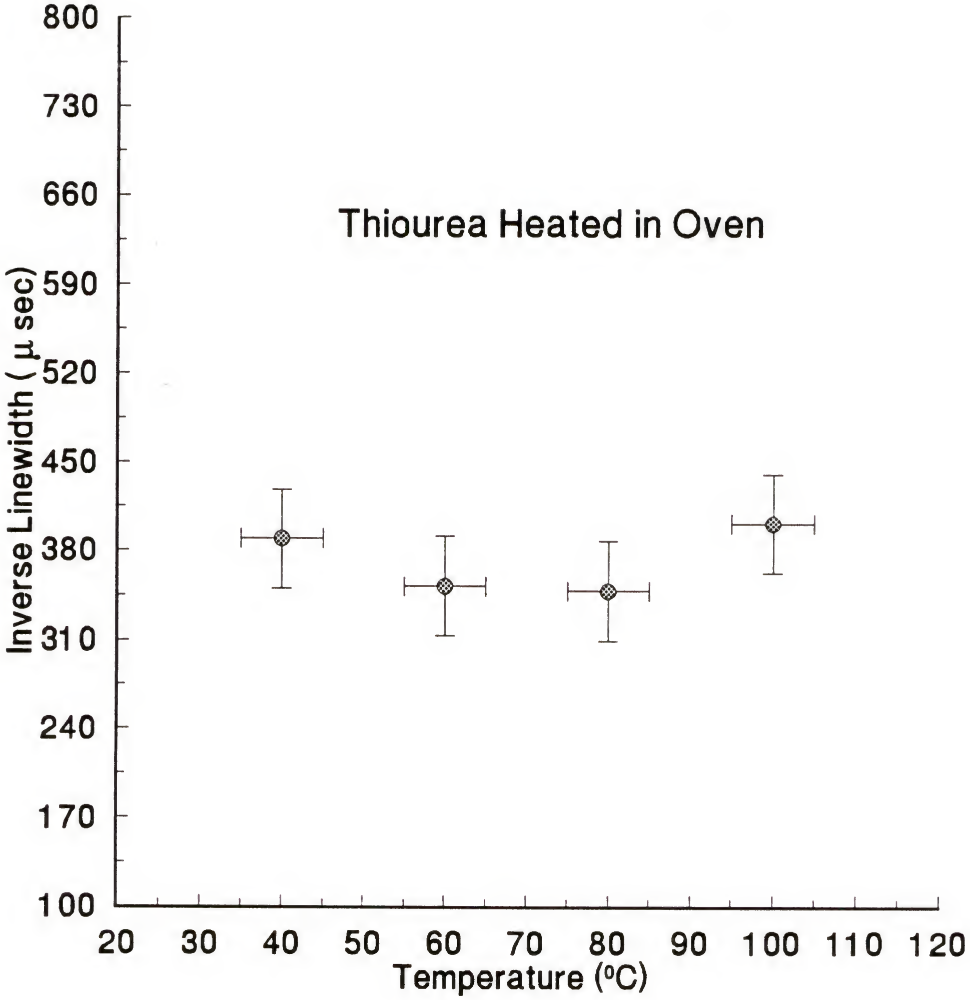

Figure 4-22: The inverse linewidth of thiourea as a function of thiourea sample temperature.

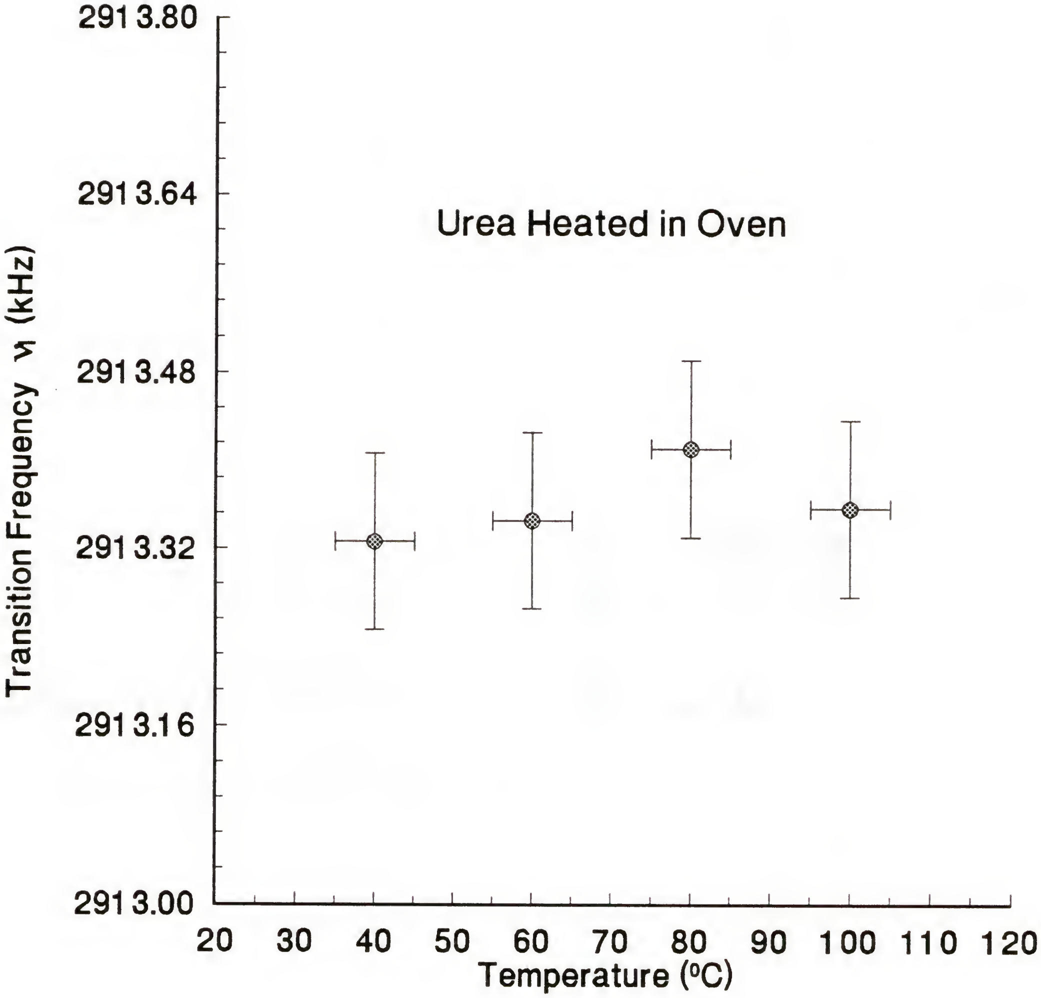

Figure 4-23: The transition frequency of urea as a function of urea temperature.

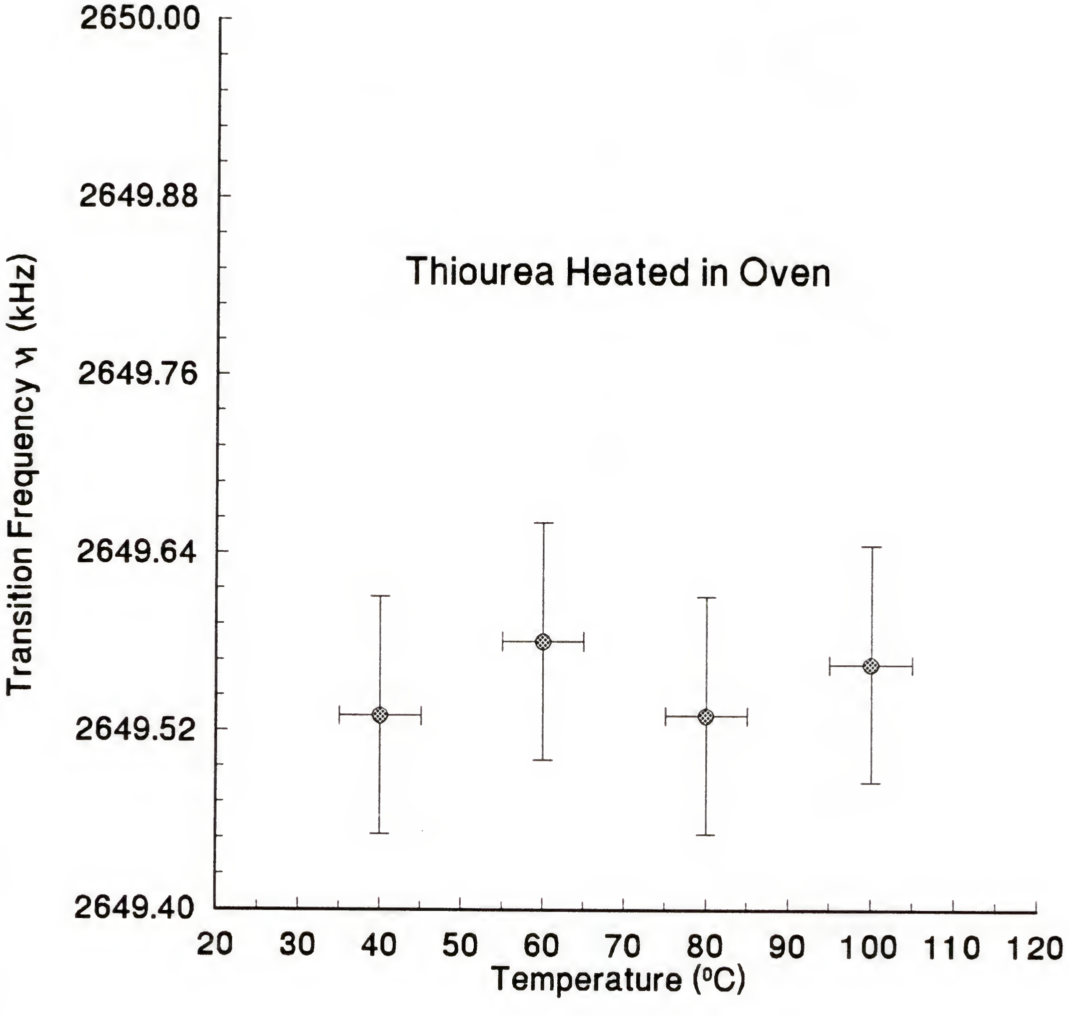

Figure 4-24: The transition frequency, for site-1, plotted as a function of thiourea sample temperatures.

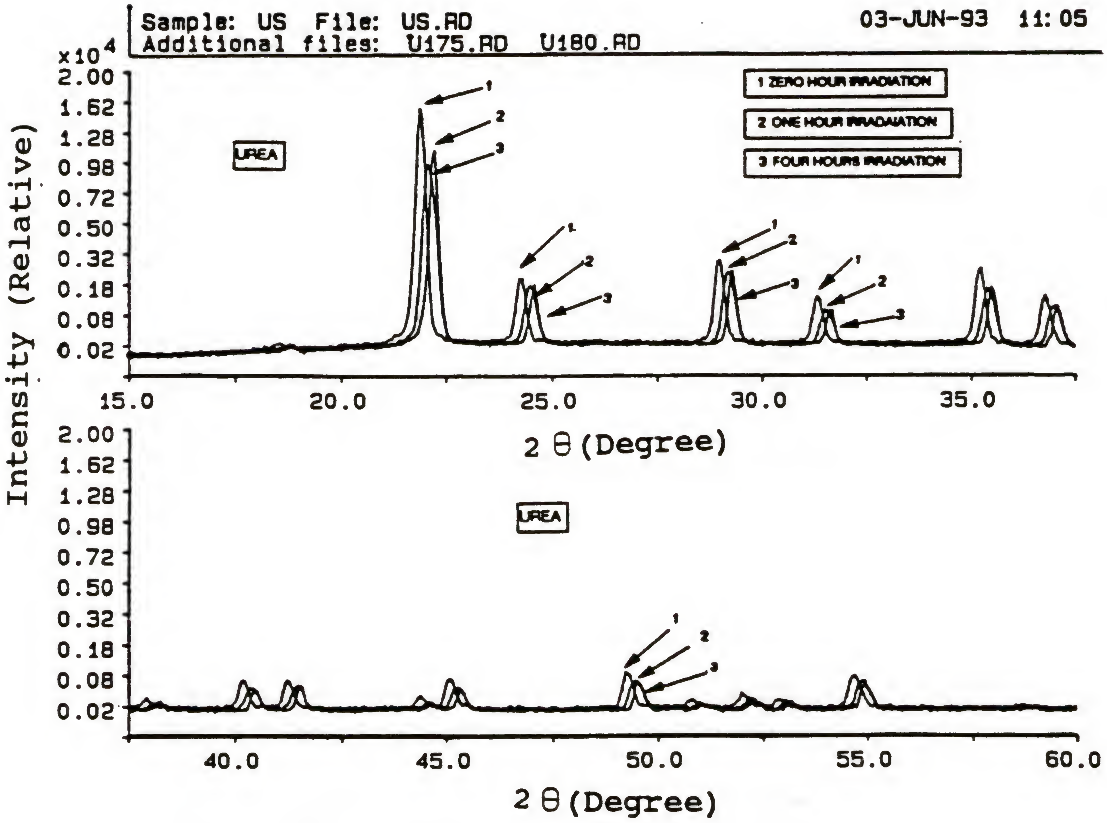

Figure 4-25: The X-ray diffraction of standard urea (unirradiated) along with one and four hours in core irradiated samples.

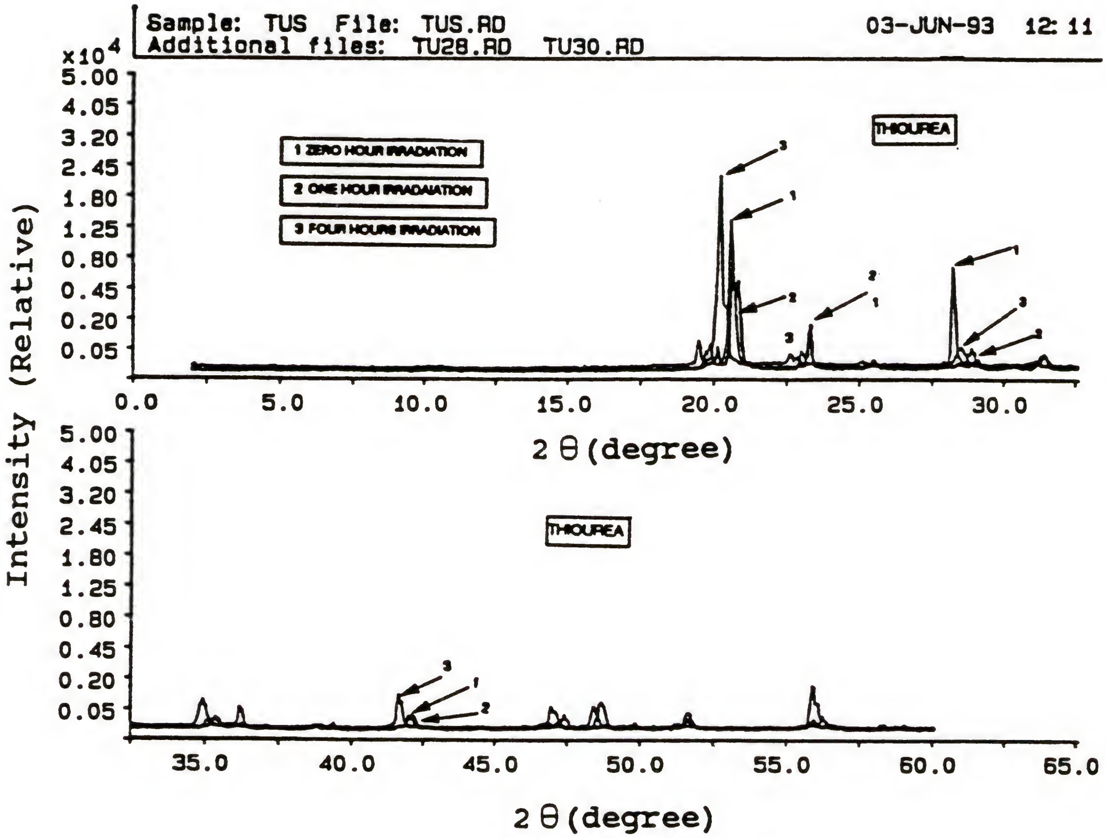

Figure 4-26: The X-ray analysis of thiourea samples irradiated for one and four hours at CVP of UFTR along with a standard (unirradiated) sample.

drastic changes in irradiated samples took place compared to standard urea sample. However, systematic shift in the peak positions are observed. Figure 4-26 shows that there are drastic changes in the irradiated thiourea X-ray diffractograph compared to one from the standard thiourea. The intensity of some of the peaks decreased after irradiations. The numbers 1, 2, and 3, in figures 4-25 and 4-26 represent, zero (standard or unirradiated), one, and four hours irradiated samples both for urea and thiourea compounds. Note that there is a change in scale in upper and lower parts of the figures 4-25 and 4-26. All results are discussed in chapter five and integrated to give a complete physical picture of irradiation effects in urea and thiourea.

CHAPTER 5
DISCUSSION

This chapter discusses the following in the order as stated here: (1) the effects of pure, but equivalent to in-core-gamma field on the NQR parameters, (2) the out-core temperature effects on the NQR parameters, and (3) the NQR parameters derived from experiments performed on samples of urea and thiourea exposed at CVP of the UFTR.

Since this research is the first application of NQR spectroscopy to the study of the effects of mixed radiation fields of gamma and neutron from a nuclear reactor on urea and thiourea, no experimental data exist for comparison with the present results. Therefore, X-ray diffraction which is an independent technique was employed to verify the findings of NQR spectroscopy.

The Monte Carlo simulation of the experiment was considered necessary to produce calculated values of, (1) the neutron energy spectrum at CVP of the UFTR, (2) the energy dependent neutron absorbed dose in urea and thiourea, and (3) the neutron reaction rates with individual nuclei in molecules of urea and thiourea.

Finally, a mathematical model is presented to quantitatively determine the lattice damage sites produced in thiourea and urea by neutrons at CVP of the UFTR.

Effects of Gamma Photons on Urea and Thiourea

Figures 4-12 to 4-17 show the effects of gamma photons on the following NQR parameters, (1) the NQR signal amplitudes, (2) the inverse linewidth, T_2^*, and (3) the transition frequencies.

It was experimentally observed that all of the NQR parameters examined were linear and parallel to the x-axis within the experimental error i.e. gamma doses did not produce observable effects in urea or thiourea.

In order to examine whether gammas contribute to the observed response of the NQR parameters, the gamma dose rate was measured in the core of the UFTR. In the reactor core there are three sources of gamma photons, (a) prompt gamma photons that accompany the fission reaction, (b) capture gamma photons from the structural materials, and (c) the gamma photons from fission fragments [44]. The contributions in gamma dose become significant from the prompt and the capture gamma photons in a research reactor like the UFTR, while it is operating at power levels above a few watts. Since the gamma dose (due to prompt and capture gamma) increases linearly with reactor power and the reactor power increases linearly with the fission rate therefore, an extrapolation of gamma dose to higher reactor power is reasonably justified above a few hundred watt power levels. Thus, the gamma dose rate, extrapolated to 100 kW of reactor power, was determined to be 66.0±9.0 kGy/h. Taking an upper value of the dose rate (66.0+9.0) kGy/h, the maximum dose deposited in urea and thiourea, for four hours of reactor operation at 100 kW, is found to be 300 kGy. To be conservative, a gamma dose of ~600 kGy, twice the extrapolated gamma dose at CVP of the UFTR, was used to expose urea and thiourea samples from out core gamma sources of ^{60}Co and ^{137}Cs, as described in chapter four.

Since the calibration curve of figure 3-3 is valid only for soft tissue, the question of whether the gamma doses in urea and thiourea are tissue equivalent arises. To answer the question, theoretical calculations were made to compare the gamma dose in urea, thiourea, and tissue. The gamma dose is the product of gamma energy flux, $\phi_\gamma(E)$, and mass absorption coefficient, (μ/ρ), under the condition of charge particle equilibrium. For a constant gamma energy flux one only needs to find the mass absorption coefficient which can be determined as

$$(\mu/\rho)_{urea/thiourea}=\sum_i \omega_i(\mu/\rho)_i \qquad (5\text{-}1)$$

where $(\mu/\rho)_i$ and ω_i are the energy dependent mass absorption coefficient and fractional abundance for the ith constituent in the molecule under consideration, respectively. The computed doses in thiourea were found to vary less than 13%

from the dose in tissue, within the energy interval 0.5 MeV to 5.0 MeV. However, the dose in urea is tissue equivalent within an error of 3% in the energy interval of 0.5 MeV to 5.0 MeV. Note that 98% of reactor gammas are in the energy interval of 0.5 to 5.0 MeV [44]. Thus, thiourea and urea perform as tissue equivalent materials for gamma radiations in this research.

The response observed for measured NQR parameters, i.e., (1) amplitude, (2) transition frequency, and (3) inverse linewidths, were independent of gamma doses as shown in figures 4-12 to 4-17 for ^{60}Co and ^{137}Cs sources. This is consistent with an experiment conducted by Ueda et al., on a single crystal of thiourea which was exposed to ^{60}Co gamma photons up to 500 kGy at 77 K subsequently, without changing the temperature, electron spin spectroscopy (ESR) was carried out [52]. The experiment was performed under two sets of conditions. First, the experiment was conducted at 77 K from the beginning of exposure and until the ESR spectroscopy had been completed. Second, a high gamma dose (500 kGy) was used. At such low temperatures (77 K), there is insufficient thermal energy available to the atomic electrons of the thiourea molecules to enable them to recombine. In the present experiment, the exposure was carried out at room temperature where sufficient kinetic energy is provided for electrons to recombine with atoms which are lacking on number of electrons.

Therefore, the NQR parameters were found to be independent of gamma doses in urea and thiourea.

Independent effects of in-core temperatures on urea and thiourea were also studied. Figure 4-18 shows analog temperature measurement in the reactor core for urea and thiourea. The maximum temperatures for the two compounds urea were found to be 85.6°C and 86.5°C, respectively. Figures 4-19 to 4-24 show the effect of temperature on the NQR parameters on of urea and thiourea. No significant effects were found in any of the NQR parameters in samples of urea and thiourea which were heated in an oven at temperatures up to 100±5°C for four hours.

After determining that there were no observable reactor gamma and temperature effects on the NQR parameters for dry polycrystalline samples of urea and thiourea, the effects of neutrons on the NQR parameters for dry polycrystalline samples of urea and thiourea are to be discussed.

Monte Carlo Simulation of NQR Experiments at CVP of the UFTR

Monte Carlo is a computational simulation technique which solves mathematical or physical problems through the use of random numbers in random sampling [53,54].

In this research, the Monte Carlo neutron photon transport code (MCNP) [55] was employed to find the neutron energy spectrum at CVP of the UFTR since no experimental data nor theoretical calculations were really available.

MCNP is a general purpose Monte Carlo code. It solves problems in three dimensional space and in user defined geometries of any shape. In addition to dealing with the neutron-photon coupled transport, MCNP can deal with the transport of only neutrons or photons in a nuclear reactor.

One of the subroutines, k-code, is available in MCNP which is used for criticality calculations for nuclear reactors. In k-code, neutron sources are introduced into the fuel assembly. The source neutrons interact with the nuclei present in fuel boxes or leave the fuel region and interact with the nuclei in other regions. All regions including fuel boxes are called cells. If a neutron is absorbed by a nucleus of ^{235}U, fission neutrons are generated following the fission watt spectrum. The selection procedures for, type of interactions, scattering angles, and the neutron energy descriptions are well explained by Cashwell et al.,[53]. MCNP keeps track of each neutron, history, until it is either absorbed or it leaves the cell. MCNP stops following the neutron, if it enters a cell of no interest. The program also picks random numbers to decide the types of several possible interactions based upon the libraries of the cross sections stored in the program. The program determines the type of interactions and registers those events into respective counters, called tallies, for each history. Using the k-code subroutine of MCNP, the neutron energy spectrum was obtained as follows.

Neutron Energy Spectrum at CVP of the UFTR Core

The neutron energy spectrum was generated at CVP of the UFTR by using the MCNP code. Figure 5-1 shows different views of the UFTR core, neglecting the shielding. Note that the figure is not drawn to the scale. The numbers in the figure are the surface numbers used in the program and the numbers in circles are the cell numbers i.e; the region with different material compositions. Samples of urea and thiourea were placed at cell #1 at the CVP of the UFTR. The fuel was considered as a homogenized mixture of 93% enriched ^{235}U, Al, and H_2O. The core composition, arrangement of the fuel boxes in the core of the UFTR, and their dimensions have been taken from the safety analysis report of the UFTR [56]. The amount of ^{235}U in the fuel mixture was reduced equally from all fuel boxes to adjust for the presence of two dummy fuel boxes in the reactor core.

The listing of the input cards for MCNP is given in Appendix D. The input listing has three sections. Each section is separated by a blank card. The first section defines the cell number, material density, and the surfaces bounding the cells. The second section contains the surface equations representing the geometry of the cells. The last section contains information for the k-code, i.e; the locations of the initial neutron sources, number of histories required, and the initial guess of the effective multiplication number , k_{eff}, which is the ratio between two

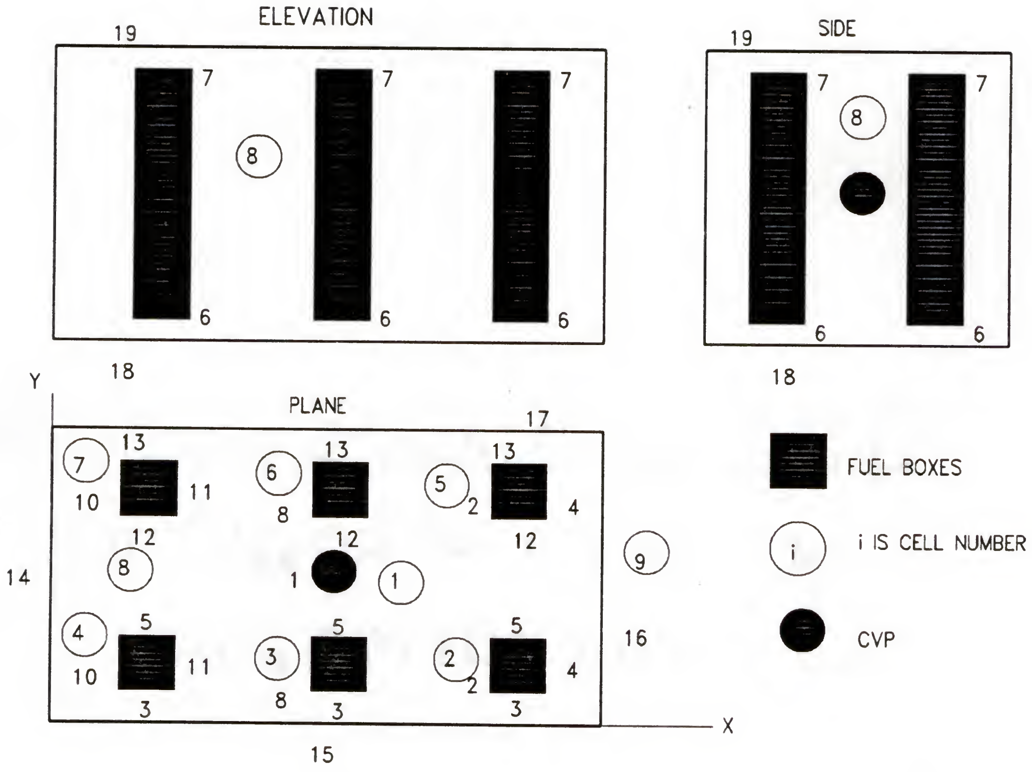

Figure 5-1: The front, side, and the planar views of the UFTR core. The z-axis is perpendicular to the plane of the paper.

successive fission generations. The material compositions in different cells along with the different tallies are also given in the third section. The program does the calculations while performing about two hundred different checks on the correctness of the input. The detailed explanations of the input cards for MCNP can be found in the users' manual of MCNP [55]. However, some necessary explanations of input cards have been included in Appendix D.

MCNP determines the neutron fluence, the product of neutron flux and time, either by counting the number of neutrons crossing a surface of a region defined in the program or by counting the length of neutron tracks in the cell of interest.

MCNP was run on an IBM compatible personal computer available in the NQR laboratory. The computer time in running MCNP was 1072.7 minutes for 6×10^4 histories. The calculated fluence was converted to flux using a conversion factor of 3.1×10^{10} fission/sec-watt of reactor power. Figure 5-2 depicts energy dependent flux observed at CVP of the UFTR as determined by MCNP for 100 kW of reactor power.

Neutron Dose in Urea and Thiourea

The energy deposition rate by neutrons, $\dot{D}_n$, in the unit mass of urea and thiourea was calculated by using MCNP at CVP of the UFTR. The calculations were done using the following equation (5-2)

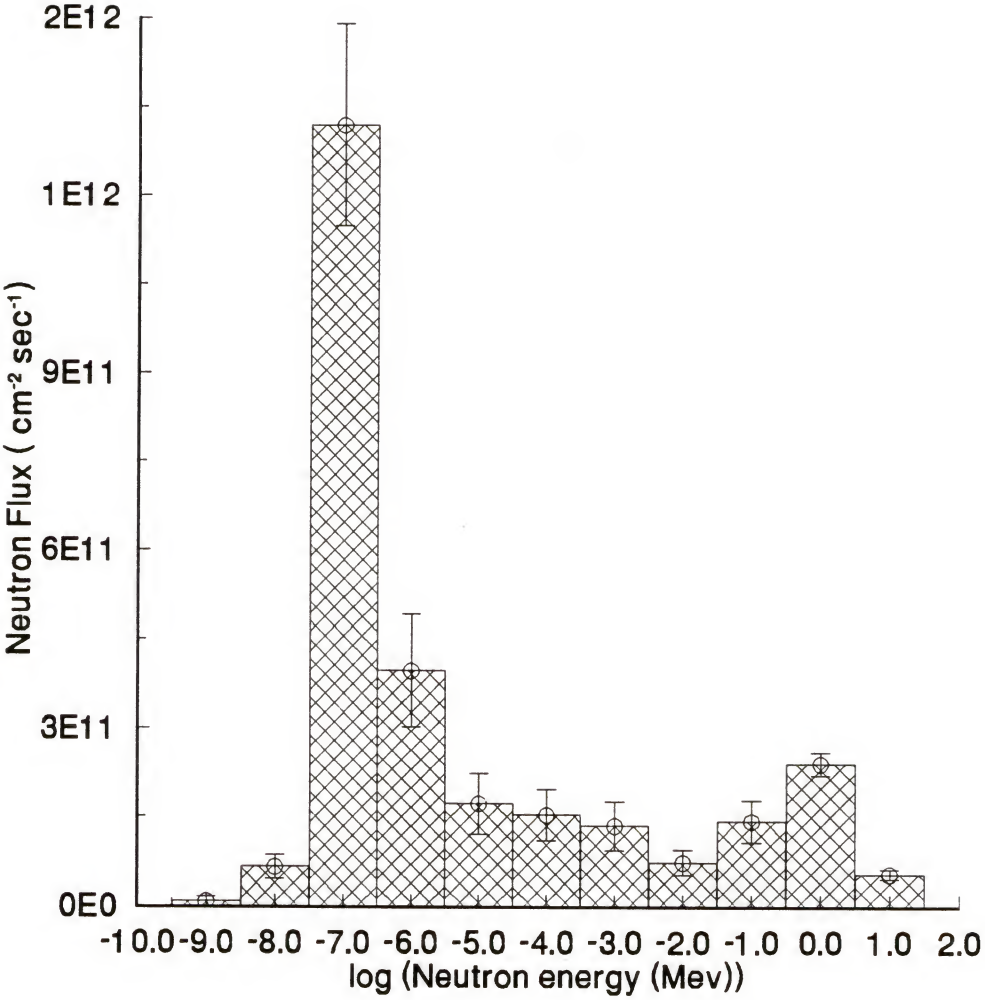

Figure 5-2: The energy dependent neutron flux at CVP of the UFTR. Note that the x-axis is the log of the neutron energy in Mev.

$$\dot{D}_n=C\int_{-1}^{1}\int_{t_{m-1}}^{t_m}\int_{E_{n-1}}^{E_n}\phi(E_i,t,\mu)H(E)\,dE\;dt\;d\mu \qquad (5\text{-}2)$$

where C= atoms/gram of material. $\phi(E,t,\mu)$ is the energy and time dependent angular flux and μ is the $\cos\theta$, where θ is the scattering angle of neutron with its initial direction of travel. The function H(E) is defined as

$$H(E)=\sigma_{tot}(E)\,H_{avg}(E) \qquad (5\text{-}3)$$

where $\sigma_{tot}(E)$ is the total neutron cross section. $H_{avg}(E)$ is the average energy (MeV) lost per collision in the energy interval $\Delta E=E_n-E_{n-1}$ provided in the input of MCNP. $H_{avg}(E)$ is available in the MCNP cross section libraries [55].

MCNP determines the neutron dose rate assuming that, (a) all nuclei are free i.e; there is no binding energy between atoms, and (b) all energy lost by neutrons is absorbed in the material. Figure 5-3 shows the neutron dose rate in urea and thiourea varying with the neutron energy at CVP of the UFTR. The total neutron dose rate integrated over all neutron energies, as determined by MCNP at 100 kW of reactor power, are 11.9±1.2 Gy/sec and 15.9±1.6 Gy/sec for urea and thiourea, respectively. The errors shown in neutron dose rate are of one standard deviation. The neutron doses calculated by MCNP in urea and thiourea are comparable within two standard deviations. Figure 5-3 shows a slight difference of neutron doses of urea and thiourea at energy of 0.1 eV. The errors in neutron doses at 0.1 eV are more than 20%.

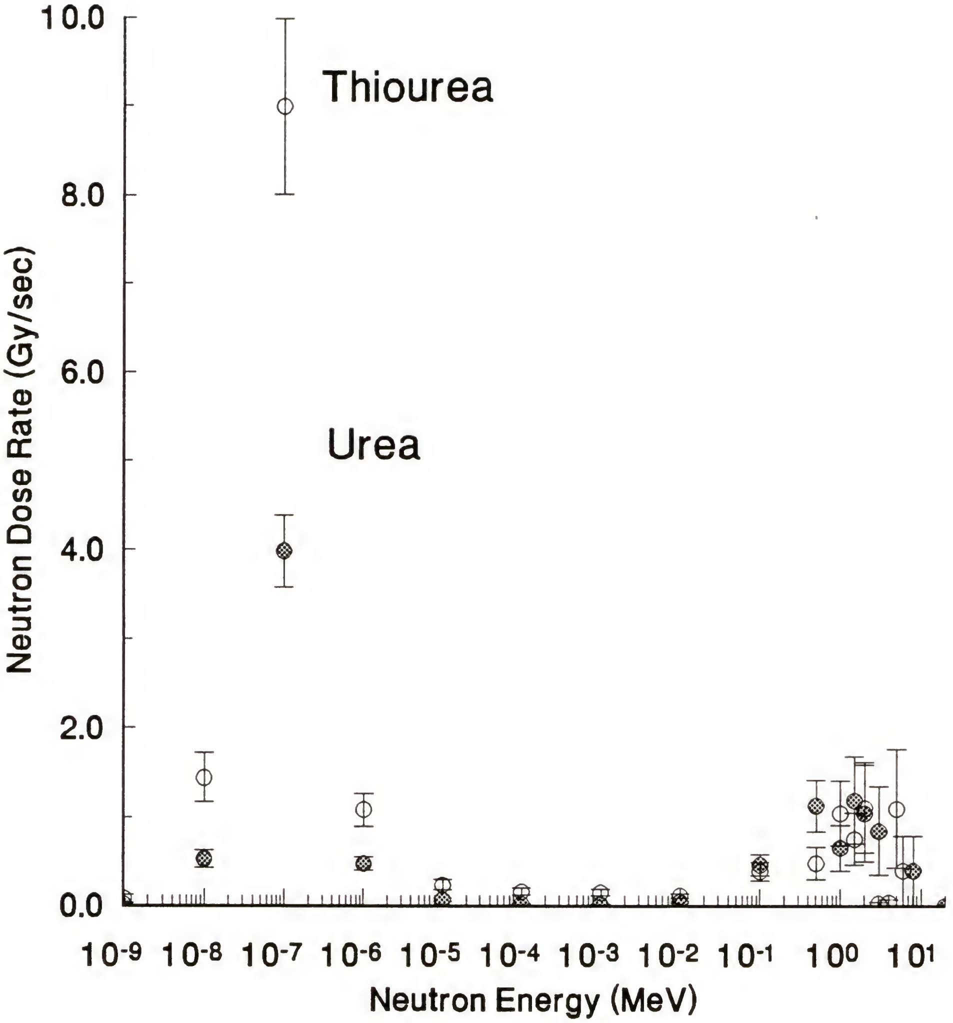

Figure 5-3: The neutron absorbed dose rates in urea and thiourea calculated by MCNP at CVP of the UFTR.

According to the MCNP user's manual an error more than 20% in the values computed by MCNP are believed to be accurate within a factor of a few [55]. Thus, to improve the accuracy in each energy bin one is required to run the MCNP with more histories because the error in MCNP scales as the inverse of the square root of the sample size. A sample output of MCNP for urea is shown in Appendix D. The output has been cut short for convenience. The MCNP calculations are used to quantify neutron reaction rates with the atomic constituents of urea and thiourea in the next section.

Effects of Reactor Neutrons on Urea and Thiourea

Effects on the NQR Signal Amplitude

In order to study the effect of neutrons on urea and thiourea, these compounds were simultaneously exposed to neutrons and photons from a nuclear reactor. As discussed previously, gamma doses do not produce significant changes in the NQR parameters of these samples. Therefore, the effects of neutrons alone on the NQR parameters of these samples were observed while using mixed radiation fields of gammas and neutrons from a nuclear reactor.

Figure 4-6 illustrates the effect of neutron fluence on the NQR amplitude of urea. A trend of decreasing amplitude relative to the standard sample can be observed with increasing neutron fluence. It is observed that the maximum change in the NQR signal amplitudes from urea samples is about

10%. Figure 4-7 shows a significant decrease in the NQR signal amplitude with increasing neutron fluence for thiourea. The decrease in signal amplitude is observed up to about 50% for neutron fluence equal to $17.28\mathrm{x}10^{15}$ cm^{-2} with respect to the amplitude of unirradiated sample.

In general, the amplitude of the NQR signals are proportional to the number of ^{14}N nuclei sending signals within radio frequency bandwidth applied to excite a particular transition frequency. The transition frequency observed near the center of the rf bandwidth gives the highest amplitude and for transition frequencies away from the center of the rf bandwidth the signal amplitudes decrease as shown in figure 4-5. For example, the bandwidth of the rf signal applied in this experiment was about 637 kHz (FWHM) for collecting the thiourea spectra. When transition frequency ν_1 (site-1) for thiourea is excited, the transition frequency ν_2 (site-2) is simultaneously excited since it is only 20.5 kHz from the central frequency ν_1 but the intensity of ν_2 decreases to about 30%. Thus, transition frequencies far from the central frequency ν_1 are not observed. Since the NQR spectroscopy is a technique that observes changes in the efg near ^{14}N nuclei in thiourea and urea, the decrease in the NQR signal amplitude of thiourea shows that changes in the efg near ^{14}N probe nuclei have occurred due to neutrons irradiations.

In order to observe any development or formation of new crystalline structures in urea and thiourea with neutron interactions, X-ray analyses of urea and thiourea samples were carried out. The X-ray spectrographs, figures 4-25 and 4-26, show that the number of significant peaks for irradiated samples are the same as compared to the unirradiated (standard) samples of urea and thiourea, respectively. Since no new, nor significant, peaks appear in figures 4-25 and 4-26, following irradiations it is unlikely that any crystalline structure has been produced in these compounds due to neutron irradiation.

In order to observe whether or not there has been any neutron irradiation change induced in diffracted X-ray intensity (peak amplitude) from different planes in urea and thiourea crystals, a method of internal calibration was employed. For that purpose, the ratio Rx was defined as

$$Rx=\frac{2nd\ Greatest\ peak\ height\ of\ X\text{-}ray\ spectrum}{1st\ Greatest\ peak\ height\ of\ X\text{-}ray\ spectrum} \quad (5\text{-}4)$$

Figure 5-4 shows the ratio Rx for zero (standard), one , and four hour irradiations for urea and thiourea. The ratio Rx was found to be a slow changing function for urea, while for thiourea Rx was found to change dramatically with neutron fluence exhibiting a drastic reduction in the peak ratio although the peaks were not observed to broaden. Such a drastic reduction in Rx for thiourea suggests that the molecular planes are rearranged in the molecular crystal

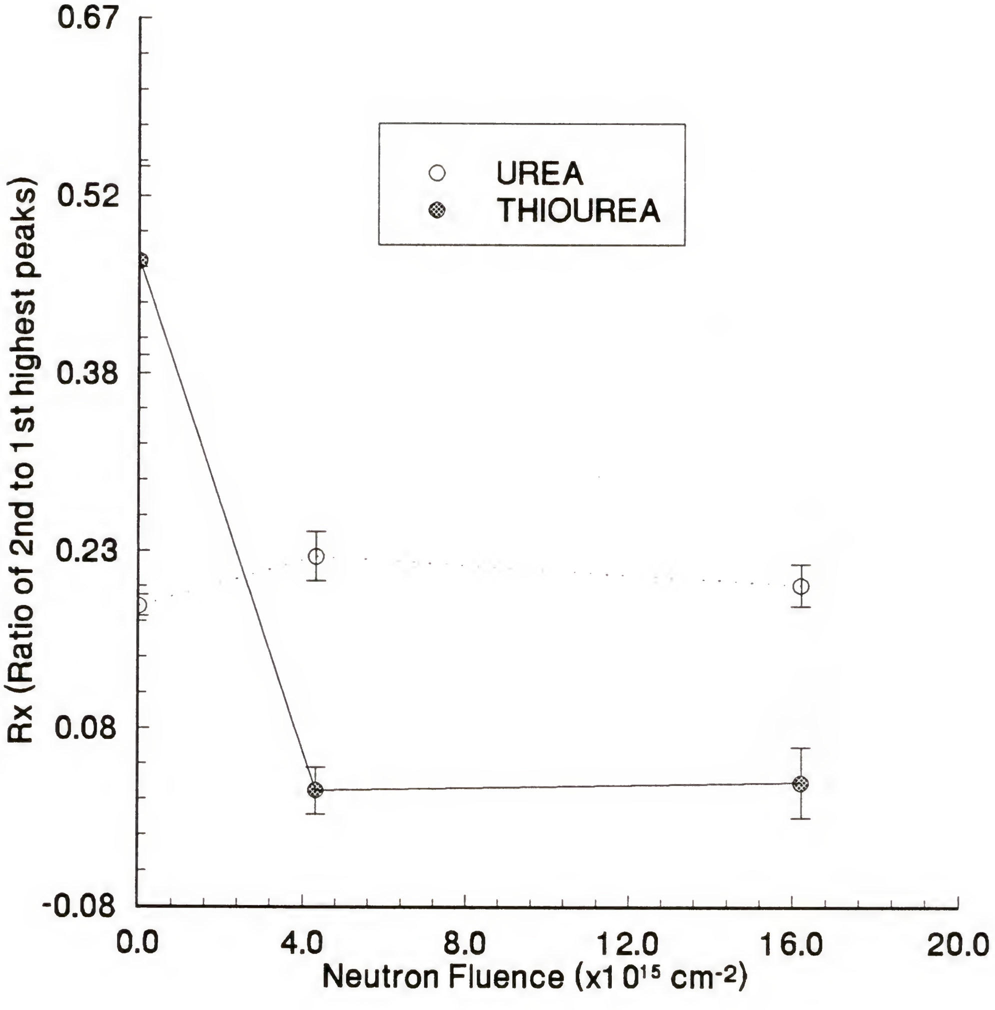

Figure 5-4: The ratio Rx from X-ray spectrographs (figures 4-25 & 4-26) is plotted for urea and thiourea for zero, one, and four hours irradiated samples. The errors are of three standard deviations.

following neutron irradiations, consequently reducing the X-ray peak amplitudes. Such random dispersions in the orientation of the molecular planes would produce, most likely, lattice defects. Lattice defects in turn produce changes in the electronic distributions surrounding ^{14}N nuclei, thus shifting the NQR transition frequency beyond their detection limit (rf frequency bandwidth of 637 KHz). In this way the aforesaid lattice defects could result in a reduction of the NQR signal amplitude. Thus, the results of X-ray analysis of thiourea, lends support for the NQR spectroscopic results, that ^{14}N nuclei are not transmitting signals within the range of detection and, thereby, yielding decreasing amplitudes for the NQR signal with increasing neutron fluences. Figure 5-5 shows d-spacing which is the distance between intermolecular planes corresponding to the strongest peak for urea and thiourea as a function of neutron fluence. The d-spacing is observed to be changing for both urea and thiourea. The change in d-spacing for urea a nearly linear increase, while for thiourea a slower increase is observed. These results are seen to be consistent with the NQR signal amplitude variations shown in figures 4-6 and 4-7.

To further investigate the differences in response of urea and thiourea to neutron irradiations, the Monte Carlo simulation of the experiment on samples of urea and thiourea was employed. The results in Table 1 show that neutrons

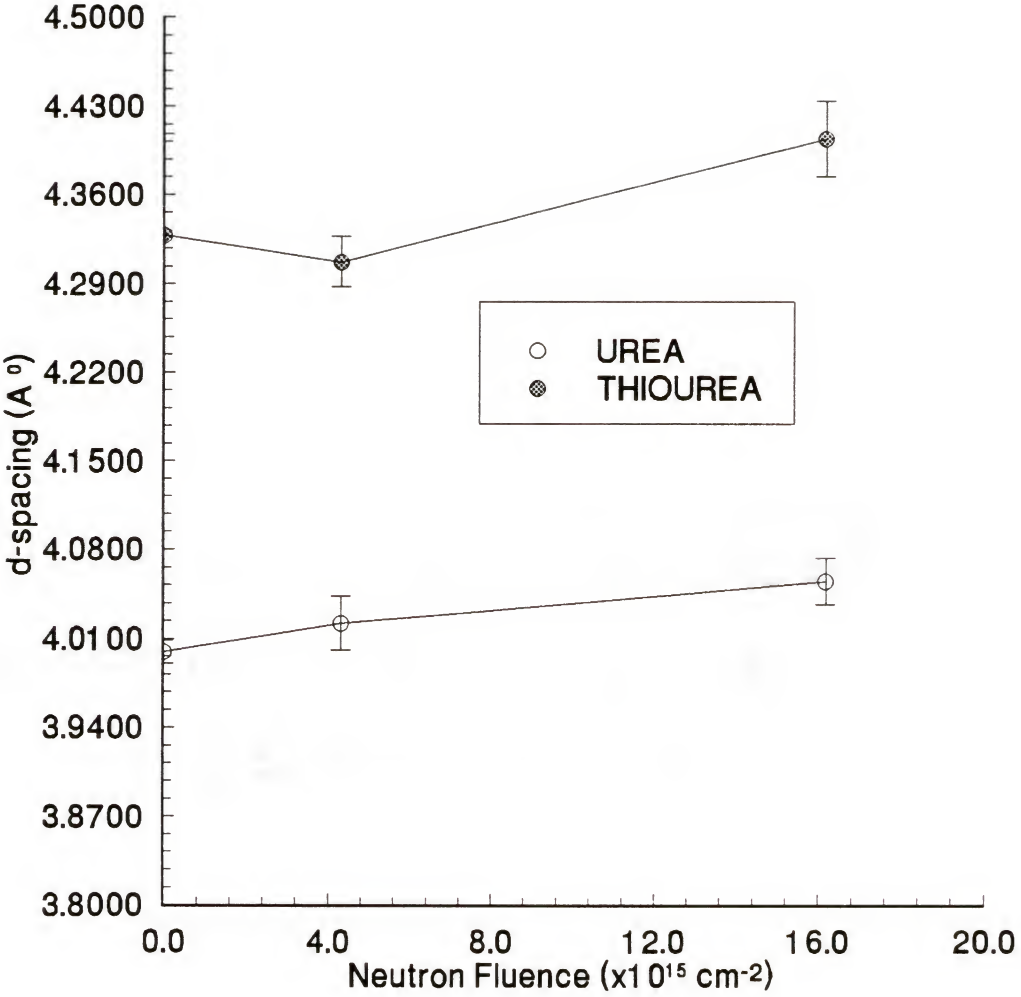

Figure 5-5: The d-spacings for urea and thiourea for the strongest peak are shown varying with neutron fluence.

Table 1. This table is the output of MCNP. RR is the reaction rate (#/sec-molecule). Tot and Scatt represent the total and scattering reaction rates, respectively.

	Urea	Thiourea	H_2O
RR (1) Tot. (2) Scatt.	(1) 4.00×10^{-11} (2) 3.73×10^{-11}	(1) 4.32×10^{-11} (2) 3.71×10^{-11}	- - -
(%) Reaction with			
H	(75.3±6.1)%	(77.8±5.7)%	90.4%
C	(04.3±1.1)%	(03.8±0.8)%	-
N	(17.4±2.5)%	(16.4±1.8)%	-
O	(02.8±0.9)%	-	09.6%
S	-	(01.8±0.7)%	-
$\dot{D}_n$ (Gy/s)	11.9±1.2	15.2±1.6	10.4±2.6

recoil with hydrogen nuclei in about 77% of the total reactions both for urea and thiourea within limits of computational errors. Also, the total reaction rates due to neutrons reacting with urea and thiourea are comparable over the entire energy range of neutrons. The total integrated neutron absorbed dose over the entire neutron energy range for urea and thiourea is 11.9±1.2 and 15.2±1.6 Gy/sec, respectively. The errors shown are for one standard deviation. These neutron doses are comparable within two standard deviations. The Monte Carlo simulations show that urea and thiourea are almost identical for neutron interactions. Thus, the significant reduction of the NQR signal amplitude observed in thiourea can be attributed to its diminished intermolecular forces as compared that in urea. As mentioned in the first chapter, the major difference between the two compounds is in the strength of intermolecular forces. Urea molecules are linked together via hydrogen bonding while thiourea molecules are linked together via van der Waals type of forces [13]. This difference in the intermolecular forces in urea and thiourea has been observed directly by the NQR signal amplitude. Neutrons interact almost equally in molecules of urea and thiourea (Table 1). Neutron interactions in thiourea, however, result in a greater number of due to its weaker intermolecular forces compared to in urea due to neutron interactions. This trend is also evidenced by X-ray analysis as shown in figure 5-4.

In order to be able to better observe the relative density of lattice defects in urea and thiourea, their effects on the experimental values of inverse linewidth T_2^* , which is independent of the NQR signal amplitude, were used.

Effects on Inverse Linewidth

The measurement of the inverse linewidths in this research show that the parameter is sensitive to small changes in efg, independent of the NQR signal amplitude. The random lattice defects produce random distributions in efg in the vicinity of ^{14}N, which are not only observed for thiourea but also for urea by inverse linewidth.

The inverse of T_2^* , the line broadening $\Delta\nu$, provides a measure of the dispersion of the transition frequencies about a mean transition frequency, ν. Then, $\Delta\nu/\nu$ becomes a measure of the degree of lattice defects. $\Delta\nu/\nu$ can be related to $\Delta r_m/r_m$ as

$$\frac{\Delta\nu}{\nu}=k\frac{\Delta r_m}{r_m} \qquad (5\text{-}5)$$

where Δr_m is the dispersion in the mean intermolecular distances, while r_m is the mean intermolecular distances before irradiations [57]. For urea, the mean intermolecular distance is measured from ^{14}N to oxygen atoms of adjacent molecules which is 3.02 Å [12]. Similarly, the mean intermolecular distance for thiourea is the mean distance from ^{14}N to sulfur atoms of the adjacent thiourea molecules which is 3.45 Å [14]. The constant k, in equation (5-5), is known to have a value between 0.3 and 3.0 for most organic compounds [57]. Equation (5-5) can be written in terms of linewidth as

$$\frac{1}{T_2^*\nu}=\frac{\pi k\Delta r_m}{r_m} \qquad (5\text{-}6)$$

Using equation (5-6), one can compare the relative dispersions in intermolecular distances for unirradiated and in radiated samples of either thiourea or urea, independent of the constant k, as

$$\frac{(T_2^*\nu)_r}{(T_2^*\nu)_u}=\frac{(\frac{\Delta r_m}{r_m})_u}{(\frac{\Delta r_m}{r_m})_r} \tag{5-7}$$

where the subscripts u and r represent values for unirradiated and radiated samples, respectively. The above equation can be written, after simplification, as

$$(\Delta r_m)_r=\frac{(T_2^*)_u}{(T_2^*)_r}(\Delta r_m)_u \tag{5-8}$$

Since T_2^*,s can be measured experimentally, using equation (5-8), one finds $(\Delta r_m)_r$ for thiourea and urea, for four hour irradiations, as $2.1(\Delta r_m)_u$ and $1.5(\Delta r_m)_u$, respectively. The values of $(\Delta r_m)_r$ determined from experiments show that neutrons produce relatively larger dispersions in intermolecular distances in thiourea than in urea.

From the experimental data obtained in this research an empirical relationship between T_2^* and neutron fluence, ϕt, has been developed both for urea and thiourea. The empirical relationship using data from figures 4-8 and 4-9 is given as

$$T_2^*(\phi t)=T_0 e^{-\beta[\phi t]} \tag{5-9}$$

where $T_2^*(\phi t)$ is inverse linewidth as a function of neutron fluence, ϕt. The constant, T_0, is the inverse linewidth for unexposed samples and β is a constant having units of number per unit neutron fluence.

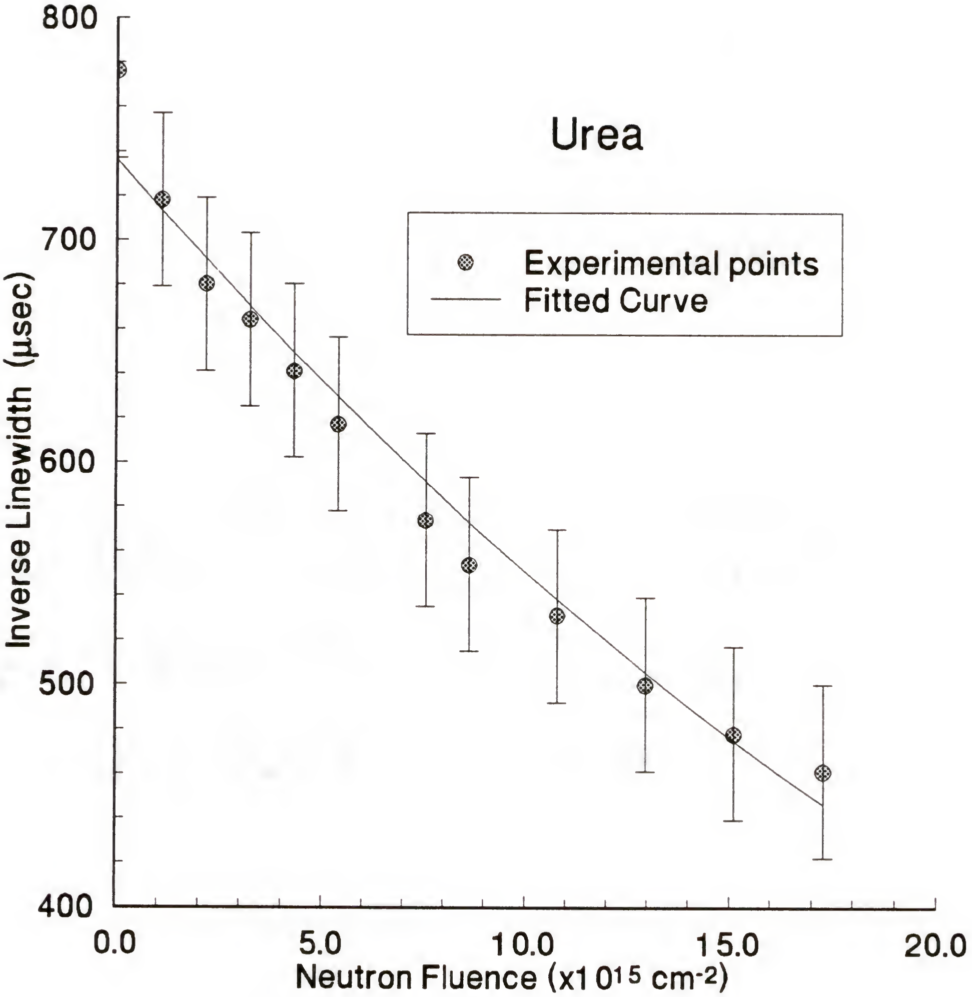

Figure 5-6: The exponential decay of inverse linewidth for urea. The solid line is the fitted curve to experimental data.

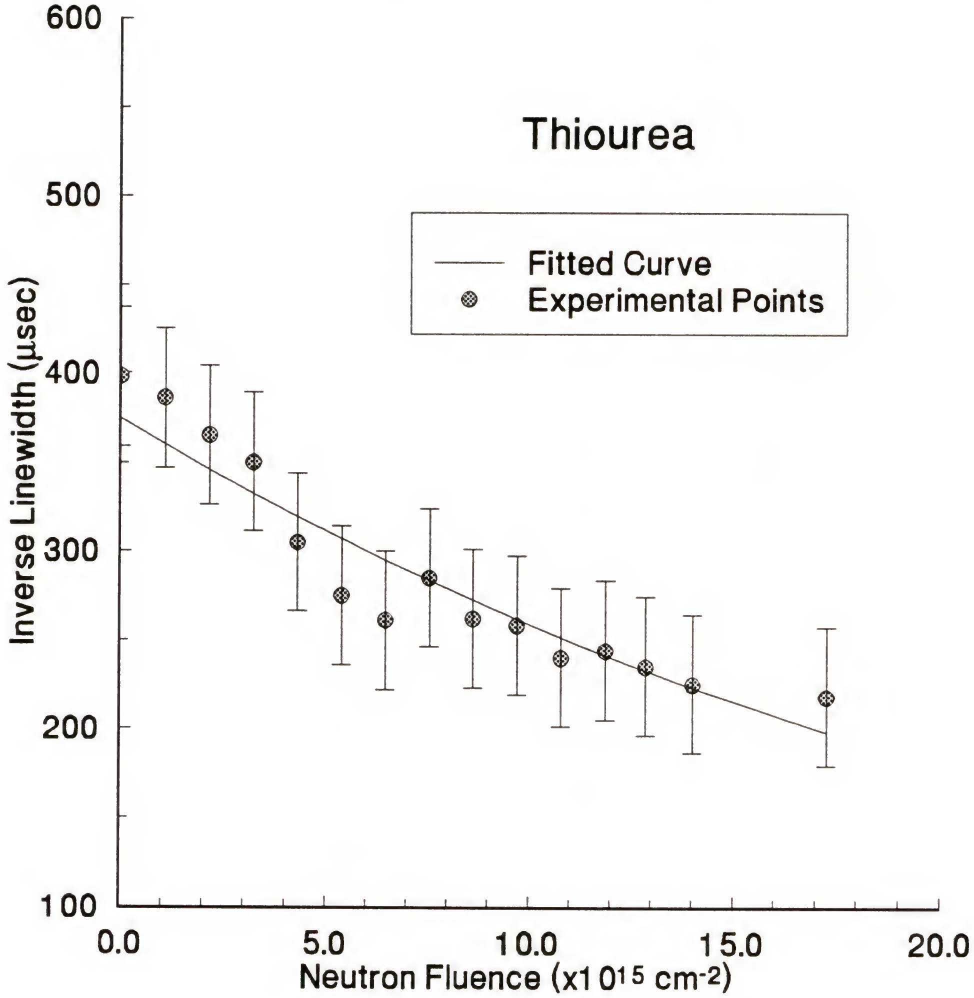

Figure 5-7: The variation of inverse linewidth for thiourea. The solid curve is the fitted to model (equation (5-9)).

Fitting the experimental data gives β equal to $2.9\text{x}10^{-17}$ and $3.7\text{x}10^{-17}$ (per cm^{-2}) for urea and thiourea, respectively. The figures 5-6 and 5-7 show the fit to the experimental data. The empirical relationship expressed by equation (5-9) can be used for calibrating the high neutron fluence (or flux) in a nuclear reactor in the presence of reactor gammas within an accuracy of 30%.

Mathematical Model

In order to determine the number of secondary damage sites per primary damage, irrespective of the shape of the damage, a mathematical model has been developed.

The Monte Carlo program MCNP determined the neutrons energy spectrum at CVP of the UFTR as shown in figure 5-2. These neutrons interact with urea and thiourea molecules through primary interactions. The primary interactions include, (1) absorption reactions which change the atomic constituents of urea and thiourea molecules, and (2) scattering reactions that produce recoil atoms from the molecules of urea and thiourea.

Each primary interaction which changes the electronic distribution in a molecule of urea or thiourea is referred to as primary damage (PD).

Surrounding each site of primary damage, several hundred molecules are forced to change their electronic distributions to adjust the charge inequilibrium created by PD, hence referred to as secondary damage. Similarly, the recoil nucleus from urea or thiourea molecules leaves behind a vacancy. Surrounding each vacancy, several hundred molecules change their electronic distributions which are also included in secondary damage. The energetic recoil nuclei further interact with the atoms and produce cascade displacements of atoms as explained in chapter one. At each site of a displaced atom, the electronic distributions of several hundred molecules are changed and also contribute to secondary damage. It is expected that the cascade displacements of protons following interactions with neutrons will provide the dominant mechanism of lattice damage in urea and thiourea.

In order to estimate the number of molecules damaged at each site of the displaced atom, the following procedure can be adopted.

Neutrons of energy E_n produce on average a recoil atom of energy $\alpha E_n/2$, where $\alpha=4A/(A+1)^2$ and A is the atomic mass of the target atom, at each collision. The number of displacements, N_d, of atoms [5] is given as

$$N_d=\frac{\alpha E_n}{2E_c} \tag{5-10}$$

where E_c is the energy required to irreversibly displace one atom from the molecule.

The primary interactions computed by MCNP with different nuclei in urea and thiourea molecules are shown in table 1.

The table shows that the scattering reactions are about 90% of the total primary reaction for urea and thiourea, respectively. Also, it is shown in table 1 that 77% of the total reaction is with hydrogen atoms. Since the absorption cross section for hydrogen is negligible compared to scattering cross section, the recoil of hydrogen nuclei is a dominant mode of interaction both for urea and thiourea. For most solids E_c can be taken as 25 eV [5]. Therefore, taking E_n= 1 Mev and using equation (5-10), one can find N_d as $2.0x10^4$.

From the measurement of NQR signal amplitude, one cannot determine the individual contribution from each of the secondary mechanisms. However, one can determine the total number of secondary damage molecules, N_{sd}, as explained below.

The number of primary damaged sites, R, can be computed as given in equation (5-11)

$$R=N_t\sum_{i}^{20}\sum_{j}^{4} n^j\sigma_t^j(E_i)\,\phi(E_i)\; tm \qquad (5\text{-}11)$$

where,

R= Number of primary damage

t= Exposure time in reactor (sec)

m= Mass of target material in grams (g)

N_t= Number of original target molecules/g

$\phi(E_i)$ =Energy dependent neutron flux (cm^{-2} sec^{-1})

$\sigma_t^j(E_i)$ = Total energy dependent neutron cross section for jth nucleus (cm^2)

n^j= Fractional abundance of the jth constituent atom in the molecules

i= Subscript i represents the energy groups at CVP of the UFTR considered in the MCNP and

j= Subscript j represents different nuclei in one molecule.

One can compute the fraction of primary damaged sites, r, through primary interactions using the following relationship

$$r = \frac{R}{mN_t} \tag{5-12}$$

Using the Monte Carlo code MCNP, twenty energy group calculations, determined the fraction of primary damaged sites (in %) in urea and thiourea for a neutron fluence $\phi t=17.28\text{x}10^{15}$ cm^{-2}. The fraction of primary damaged sites is determined to be $5.7\text{x}10^{-5}$% and $6.2\text{x}10^{-5}$% for urea and thiourea, respectively. The NQR signal amplitudes are not appreciably affected by such a small fraction of primary damaged sites. Thus, the change in the NQR signal amplitude, figure 4-7, results not only from the primary damage but also because of the secondary damage. Figure 5-8 shows how primary and the secondary damage may occur due to incident neutrons. These secondary damages could produce effects such as lattice defects in urea and thiourea. Such secondary damage could

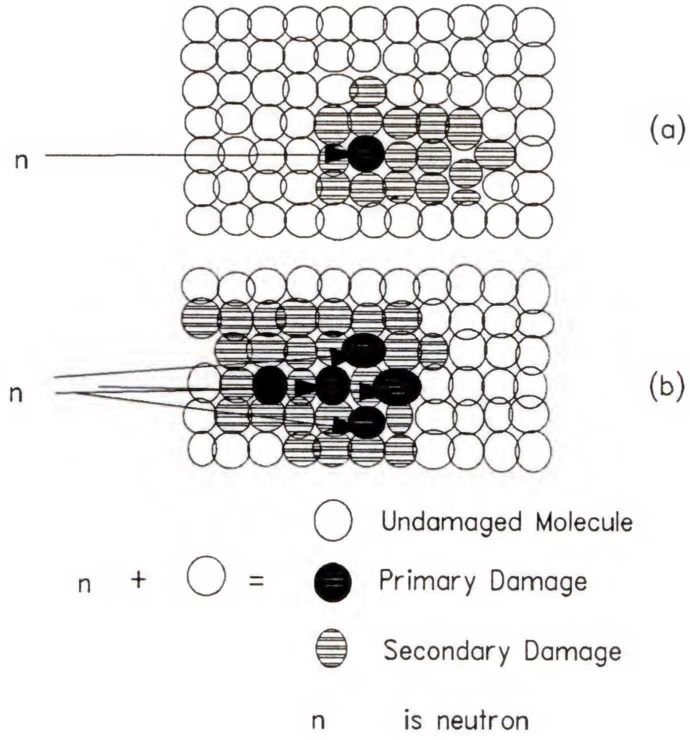

Figure 5-8: (a) The primary and secondary damages are shown with neutron interactions, (b) neutrons are shown interacting with primary and secondary damage molecules.

account for dispersion characteristic of efg near a substantial fraction of the ^{14}N nuclei, thus shifting or changing the transition frequencies out side of the detection limit.

In order to achieve one of the objectives of this research, i.e, to determine the number of secondary damage sites per primary damage, irrespective of the shape of the damage, a mathematical model has been developed. The model can also be used to determine the average value of damaged microvolumes in urea and thiourea due to neutron irradiations.

Development of Mathematical Model

The number of secondary damage sites, N_{sd}, can be estimated by modifying a model developed by Fedin et al., [57]. They developed a model to explain their NQR results for substituted chemical impurities in the organic compound, p-dichlorobenzene using ^{35}Cl [57]. In their research, the NQR signal amplitude variation was attributed to several hundred secondarily damaged molecules near each substitutional impurity site in p-dichlorobenzene. Each substitutional impurity atom had a different electronic distribution. This new electronic distribution forced molecules surrounding each substitutional molecule to rearrange their electronic distributions. This moved the resonance conditions of several hundred molecules out of the detection range, resulting in a decrease NQR signal amplitude.

Since neutrons also produce substitutional and interstitial impurities, it is assumed that Fedin's model, in a modified form would be applicable for this research in determining the number of secondary damage sites in molecules of thiourea and urea. This modified model is based upon two assumptions, (a) primary damage is always produced in an undamaged molecule (not in already primary or secondary damage molecules) and (b) all the damage sites occur at random locations in the material. Thus, knowing the computed fraction of primary damage sites, r, the fraction of undamaged molecules, S, can be written as

$$S=1-r \qquad (5\text{-}13)$$

With the NQR signal amplitude A(r) normalized to the amplitude of the unirradiated sample A_0 i.e., the normalized amplitude, $A(r)/A_0$ is proportional to S, since S is the fraction of the molecules sending the signals. However, the experimental values of the normalized amplitude $A(r)/A_0$ do not vary linearly with r as shown in figure 5-9. This implies that there are significant numbers of secondary damage molecules (or sites) from where NQR signals are not observed to occur within the detection limit.

To determine the number of secondary damaged molecules per primary damaged molecule, one can divide the sample into small control volumes such that one primary damage in the control volume will, on the average, produce, N_{sd}, secondary damaged molecules. Then, the probability that a control

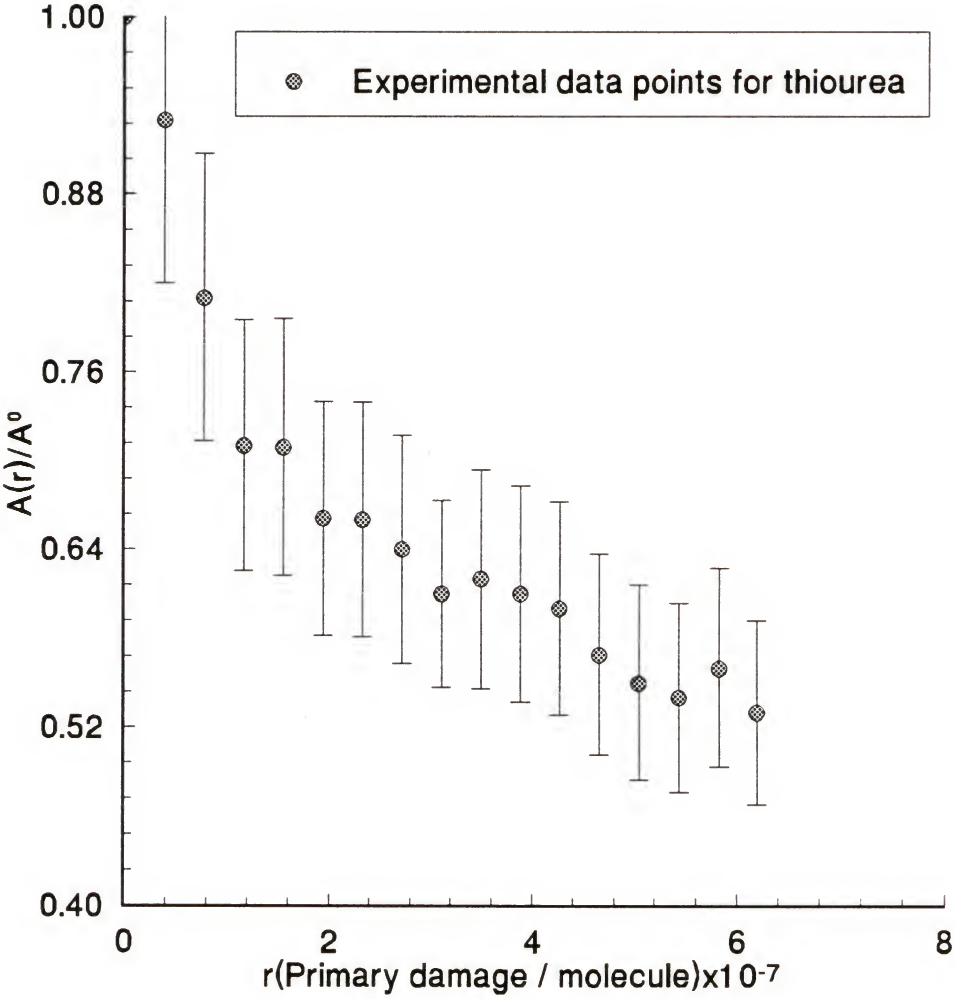

Figure 5-9: The normalized amplitude is shown varying with the fraction of the primary damaged sites, r.

volume will not have secondary damaged molecules is given as

$$\frac{A(r)}{A_0} = (1-r)^{N_{sd}} \qquad (5\text{-}14)$$

Since r<<1 the above equation can be written as

$$\frac{A(r)}{A_0} = e^{-rN_{sd}} \qquad (5\text{-}15)$$

The theoretical model represented by equation (5-15) would be expected to fit experimental data when neutrons interact with only undamaged molecules. For higher neutron fluences neutron interactions with both primary and secondary damaged molecules become significant. In such a case the experimental data depart from the model represented by equation (5-15). Based on the concepts of multiple hit models of microdosimetry [58,59] an additional term P(r) has been added to equation (5-15) which fits the entire range of the experimental data. The term P(r) is the probability of having at least one primary interaction with molecules that have experienced already primary or secondary damaged. Several different forms of P(r), i.e., linear ,linear-quadratic, and quadratic were examined as fitting functions for the experimental data but found not suitable for the present case. However, an expression for P(r) similar to one used by Shyr [58] shows excellent agreement with the experimental data and is given by

$$P(r) = (1 - e^{-\alpha r}) \qquad (5\text{-}16)$$

where α is a constant to adjust the extent of primary interaction with previously damaged molecules. In the limit of this experiment ($r<<1$), variation of P(r), given by equation (5-16), is physically acceptable.

Therefore, a model valid for the entire range of the data is given as

$$\frac{A(r)}{A_0} = (e^{-N_{sd} r}) + (1 - e^{-\alpha r}) \qquad (5\text{-}17)$$

The values of r were determined using the MCNP computer code for twenty energy groups of neutrons. From the best fit of the experimental data for thiourea, the constants N_{sd} and α have been determined as $2.2\text{x}10^6$ (number of secondary damaged molecules / primary damage) and $4.4\text{x}10^5$ respectively. The dot-dashed line in figure 5-10 shows the fit to the model represented by equation (5-17). The solid line represents the model of equation (5-15). Note that the term P(r) has taken into account the decrease in the NQR amplitude due to neutron interactions with previously damaged molecules.

One of the objectives of this work (given in chapter one) to determine the damaged volume in thiourea and urea can, however, be achieved even by using a model represented by equation (5-15). The number N_{sd} can be determined for low values of neutron fluence because higher neutron fluences do not improve the accuracy in determination of N_{sd}.

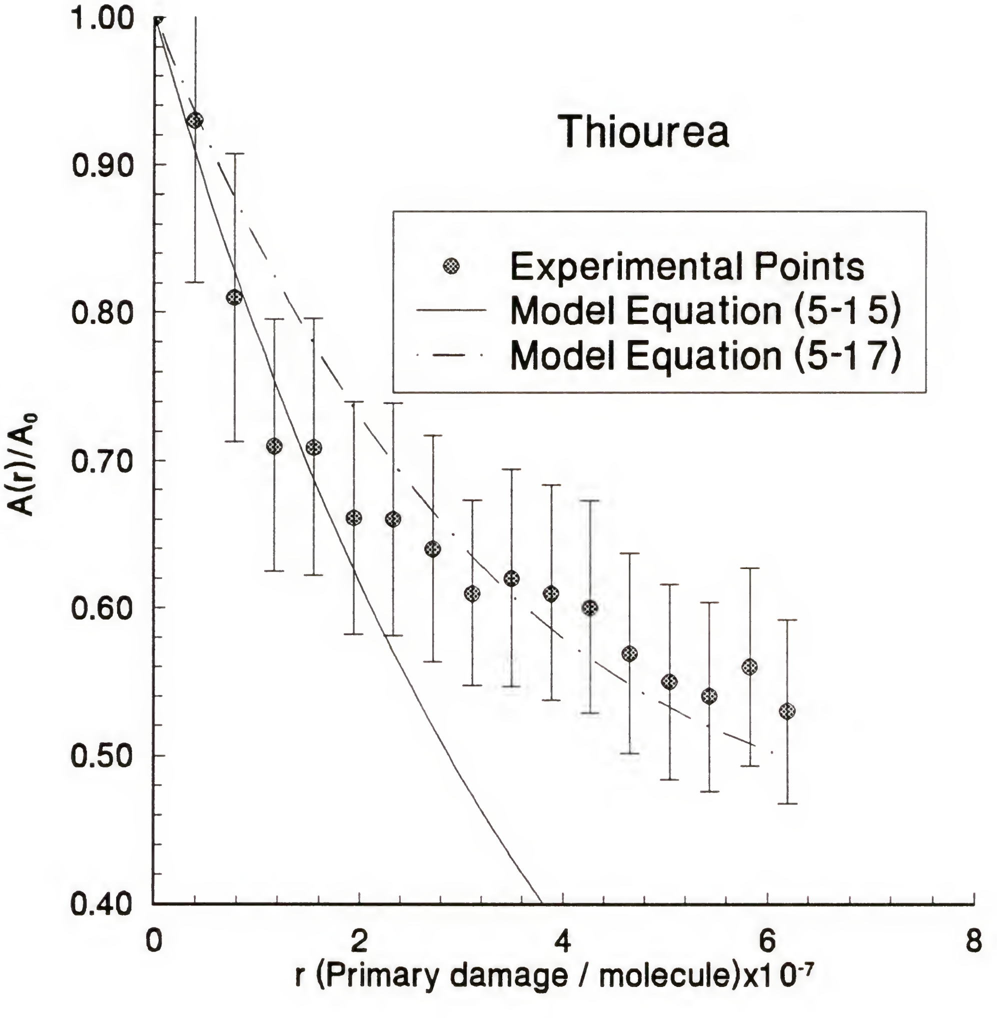

Figure 5-10: A plot of normalized amplitude as a function of r for thiourea. The solid and dot-dashed lines represent the models by equations (5-15) and (5-17), respectively.

The damaged microvolume for thiourea can be determined as follows. The volume of one molecular crystal for thiourea is known to be 351.8 Å^3 [14]. There are four molecules in one molecular crystal for thiourea. One can find the volume of one molecule and then can multiply that volume with the number of N_{sd} molecules which is determined by the model, equation (5-17). The value of the damaged microvolume for thiourea is found to be 2.2×10^{-4} μm^3 per primary damage. The value of the experimentally determined damaged microvolume is required in the field of microdosimetry where doses are calculated on cellular level.

The model, equation (5-17), has been used to find the value of N_{sd} for urea (for $\alpha=0$). A value of N_{sd} has been found as 2.8×10^5 for urea which is low compared to thiourea. The damaged microvolume in the case of urea has been found as 2.1×10^{-5} μm^3 per primary damage.

The different responses of the NQR signal amplitudes for urea and thiourea is postulated to occur because of the differences in the nature of their intermolecular bonding. In urea, molecules are linked by hydrogen bonding, while in thiourea, molecules are held together through van der Waals force. The van der Waals bonding in thiourea is thus much weaker than the hydrogen bonding in urea. Although the number of recoil hydrogen nuclei (protons) that are produced are almost identical, as calculated by MCNP (Table 1), the recoil protons produce more lattice damage by rearranging molecular planes in thiourea than in urea because of weak intermolecular forces (van der Waals) in thiourea as compared to strong intermolecular forces (hydrogen bonding) in urea. This is evident from the results of the NQR signal amplitude for thiourea and urea. Also, X-ray analyses support the presence of more lattice damage in thiourea than in urea, as discussed earlier in this chapter.

Although, the experiments were performed with the aim to employ the results for dosimetry, the NQR amplitude variation has been found to be sensitive for only neutron fluences $\geq 1.02 \times 10^{15}$ cm^{-2} both for urea and thiourea. NQR spectroscopy cannot be used to determine the neutron dose from experiments performed on dry polycrystalline samples of urea and thiourea for neutron fluences lower than 1.02×10^{15} cm^{-2}. It should be noted however that the values of N_{sd} computed for thiourea or urea are independent of the neutron fluence and can be used in microdosimetry where dose is calculated in microvolumes and the knowledge of N_{sd} provides a useful means to define a microvolume.

One can determine the number of secondary damaged molecules from N_{sd} and N_d at each site of displaced atom in thiourea and urea. For example at E_n= 1 MeV about 110 and 14 secondary damaged molecules are present at each site of displaced atom in urea and thiourea, respectively. The combined effects of cascade showers of protons and the approximate 10-100 distorted molecules around each displacement permit NQR to detect neutron interactions from the decreasing NQR signal amplitude.

CHAPTER 6
CONCLUSIONS

This research is an innovative application of a noninvasive state-of-the-art NQR spectroscopy on dry polycrystalline samples of urea and thiourea compounds in mixed radiation fields of gamma and neutron.

The results of NQR spectroscopy have shown that this technique can be applied in mixed radiation fields of gamma and neutron in a nuclear reactor to study the radiation induced changes on microscopic level. In this research it is demonstrated by applying NQR spectroscopy on dry polycrystalline samples of Urea and thiourea exposed at CVP of the UFTR to study the radiation changes.

The neutron fluence $\phi t \geq 1.02\text{x}10^{15}$ cm^{-2} has shown effects on the NQR signal amplitudes for thiourea. The neutron fluence of the same order has show weak effects on the NQR signal amplitude for urea.

The number of secondary damaged sites have been found to be $2.2\text{x}10^6$ and $2.8\text{x}10^5$ for thiourea and urea, respectively. Although, high neutron fluences have been used in this research, useful information about the total number of secondary damaged sites, N_{sd}, has been determined independent of the neutron fluence. This finding also contains information about damaged microvolume of lattice distortion which is important in science and technology, for example in the field of microdosimetry, it is useful to experimentally determine the results of ionizing radiation in regions much smaller than 1 μm. The results are highly valuable for academic and scientific applications such as radiation dosimetry, radiation hardening, and in particular in understanding the radiation interaction on microscopic level.

The NQR signal amplitude has been found to be sensitive to intermolecular forces after neutron irradiations. Thiourea has been found to be more sensitive to neutron radiation than urea. This is attributed to the van der Waals type of forces between thiourea molecules in the molecular crystal while there is hydrogen bonding among urea molecules in urea crystal. The hydrogen bonding is stronger than the van der Waals type of bonding, therefore, neutrons produce a greater number of dispersions in the intermolecular distances in thiourea than urea thus producing more dispersion in efg in the vicinity of ^{14}N nuclei.

Inverse linewidth has been found to be a sensitive NQR parameter for both urea and thiourea. This parameter contains information regarding the inhomogeneity of the efg near the probe nuclei. An empirical relationship [equation (5-9)] has been developed which can be used to find the neutrons fluence even in the presence of high gamma doses.

In case of post nuclear explosions or accidents high neutron fluences can be measured using results of figures 5-6 and 5-7 if someone finds dry polycrystalline urea or thiourea in some laboratory. In addition, the inverse linewidth can also be used to find degree of lattice defects in a crystal by finding $1/T_2^*\nu$ and comparing with the standard sample. Thus, the findings of this research have academic and engineering applications.

APPENDIX A
A SPIN-ECHO OF THIOUREA

Experimentally observed spin-echo of thiourea is shown in figure (A-1) as an example. A $\pi/2$ pulse is applied to thiourea and after a delay time of 3.1 msec a π pulse is applied from the pulsed spectrometer and a spin-echo is observed after 6.2 msec.

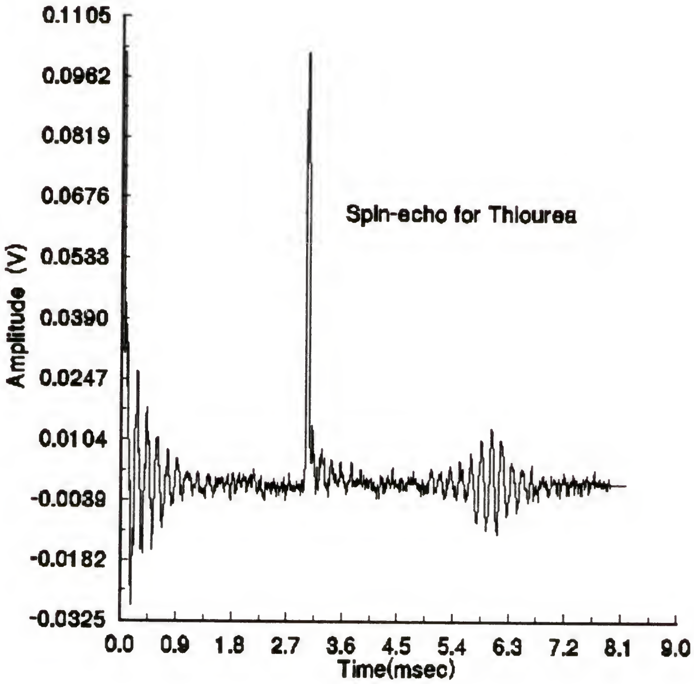

Figure A-1: A spin-echo for thiourea.

APPENDIX B
RAW DATA FILE OF A NQR SPECTRUM

The Nicolet oscilloscope transfers data to the IBM compatible computer using a computer program 4094LTU.EXE written in BASIC and taken from the Henry file transfer software for Nicolet oscilloscope.[1] The data transferred to the IBM compatible computer contains eight columns of voltage values and one value of dwell time.

The raw data for one of the thiourea spectrum is presented as an example. Some useful information can be obtained from the first column. For example forth number in first column gives the dwell time as 2.0×10^{-7} sec. Since there are 16 thousand data points in one file which are neither economical nor beneficial to reproduce here. Therefore, an abridged raw data file is given on the next page as an example.

---

[1] Nicolet Instrument Corporation, Test Instrument Division, Madison, Wisconsin 53711-0288

An example of a part of a raw data file of a NQR spectrum.

```
"wave # 1"     -.000241 -.005147 -.000269 0.000172 -.000894 0.000837 -.000800 -.002200
"PI 1/A"       -.000722 -.005322 -.000400 0.000091 -.000841 0.000772 -.000788 -.002175
 0             -.000694 -.005241 -.000387 0.000106 -.000762 0.000866 -.000747 -.002200
 .0000002      -.001109 -.005322 -.000294 0.000119 -.000709 0.000866 -.000709 -.002256
"From B"       -.001041 -.005481 -.000347 0.000053 -.000816 0.000837 -.000681 -.002347
"  To I"       -.000494 -.005509 -.000269 0.000000 -.000788 0.000878 -.000628 -.002175
"....."        -.000800 -.005588 -.000309 0.000119 -.000762 0.000878 -.000694 -.002387
"" 0.000466 -.005694 -.000334 0.000000 -.000694 0.000931 -.000709 -.002269
"" 0.000106 -.005641 -.000347 0.000091 -.000762 0.000866 -.000681 -.002334
"" 0.002266 -.005734 -.000456 0.000000 -.000816 0.000825 -.000628 -.002547
"" 0.002091 -.005641 -.000416 0.000106 -.000856 0.000919 -.000616 -.002522
"" 0.004506 -.005775 -.000387 0.000025 -.000828 0.000812 -.000616 -.002509
"" 0.004853 -.005694 -.000587 0.000025 -.000841 0.000837 -.000709 -.002469
"" 0.007212 -.005694 -.000428 0.000066 -.000800 0.000837 -.000722 -.002509
"" 0.008091 -.005616 -.000428 0.000025 -.000828 0.000891 -.000722 -.002522
"" 0.010144 -.005588 -.000494 0.000066 -.000934 0.000931 -.000600 -.002588
"" 0.011866 -.005616 -.000469 0.000066 -.000963 0.000784 -.000562 -.002669
"" 0.013253 -.005616 -.000334 0.000159 -.001000 0.000837 -.000775 -.002656
"" 0.015531 -.005441 -.000281 0.000131 -.001056 0.000784 -.000656 -.002747
"" 0.016359 -.005547 -.000347 0.000212 -.001028 0.000812 -.000775 -.002656
"" 0.019119 -.005600 -.000256 0.000237 -.001134 0.000706 -.000722 -.002734
"" 0.019706 -.005575 -.000334 0.000184 -.001000 0.000784 -.000775 -.002588
"" 0.022784 -.005575 -.000441 0.000253 -.001081 0.000719 -.000762 -.002600
"" 0.023131 -.005575 -.000456 0.000278 -.001322 0.000678 -.000709 -.002534
"" 0.026331 -.005481 -.000481 0.000319 -.001200 0.000559 -.000747 -.002469
"" 0.026413 -.005547 -.000522 0.000306 -.001187 0.000491 -.000841 -.002522
"" 0.029825 -.005522 -.000628 0.000266 -.001241 0.000559 -.000841 -.002469
"" .................................................................
"" .................................................................
"" .................................................................
"" 0.038053 -.005694 -.000641 0.000478 -.001363 0.000491 -.000975 -.002375
"" 0.040266 -.005722 -.000681 0.000331 -.001481 0.000400 -.001056 -.002416
"" 0.042266 -.005816 -.000800 0.000453 -.001469 0.000478 -.001163 -.002387
"" 0.043625 -.005856 -.000828 0.000466 -.001534 0.000413 -.001147 -.002416
"" 0.046319 -.005934 -.000641 0.000478 -.001522 0.000453 -.001147 -.002456
"" 0.047253 -.005841 -.000616 0.000600 -.001469 0.000466 -.001122 -.002441
"" 0.050091 -.005894 -.000694 0.000531 -.001562 0.000491 -.001109 -.002441
```

"" These data are formatted using DFCPN for plotting. Other useful physical NQR parameters are extracted by using computer programs COPROC and NOLFIT as explained in chapter four.

APPENDIX C
COMPUTER PROGRAM LISTINGS: NQR PARAMETER EXTRACTION

Computer Program DFCPN

```
CCCCCCCCCCCCCCCCCCCCCCCCCCCCCCCCCCCCCCCCCCCCCCCCCCCCCCCCCCCCCCCCCCC
C                                                                 C
C      DFCPN.FOR IS A FORTRAN 77 PROGRAM                          C
C      DFCPN.FOR COLUMNIZES THE DATA FROM DIGITAL OSCILLOSCOPE    C
C      DEVELOPED BY KHALID JAMIL                                  C
C      VERSION 1.0 (OCTOBER 22,1990)                              C
C                                                                 C
CCCCCCCCCCCCCCCCCCCCCCCCCCCCCCCCCCCCCCCCCCCCCCCCCCCCCCCCCCCCCCCCCCC

      CHARACTER INFILE*20
      DIMENSION X(2048,8),D(32000)
      EQUIVALENCE (X(1,1),D(1))
      WRITE(*,*)'ENTER NAME OF YOUR INPUT FILE'
      READ(5,15)INFILE
15    FORMAT(A20)
      OPEN(1,FILE=INFILE,STATUS='OLD')
      OPEN(2,FILE='DFCPN.OUT')
      WRITE(*,*)'DELETE FIRST M POINTS FROM SPECTRUM ; M=?'
      READ(*,*)NI
      WRITE(*,*)' SKIP N (ALTERNATE) NUMBER OF DATA POINTS N=?'
      READ(*,*)M1
      M=M1+1
      WRITE(*,*)'ENTER DWELL TIME (msec)'
      READ(*,*)DELTA
      WRITE(*,*)'ARE YOU USING FULL SPECTRUM ?  IF YES   :ENTER 1'
      WRITE(*,*)'ARE YOU USING HALF SPECTRUM ?  IF YES   :ENTER 2'
      WRITE(*,*)'ARE YOU USING QUARTER SPECTRUM ? IF YES :ENTER 3'
      READ(*,*)S
      IF(S.EQ.1) GOTO 9
      IF(S.EQ.2) GOTO 11
      IF(S.EQ.3) GOTO 13
      WRITE(*,*)' '
 9    WRITE(*,*)'USING FULL SPECTRUM'
      WRITE(*,*)'READIND INPUT FILE'
      READ(1,10)((X(I,J),J=1,8),I=1,2048)
10    FORMAT(3X,G9.6,G9.6,G9.6,G9.6,G9.6,G9.6
     & ,G9.6,G9.6)
      GOTO 18
11    WRITE(*,*)'USING HALF SPECTRUM'
      WRITE(*,*)'READING INPUT FILE'
      READ(1,12)((X(I,J),J=1,4),I=1,2048)
12    FORMAT(3X,G9.6,G9.6,G9.6,G9.6)
      GOTO 18
13    WRITE(*,*)'USING QUARTER SPECTRUM'
      WRITE(*,*)'READING INPUT FILE'
      READ(1,14)((X(I,J),J=1,2),I=1,2048)
14    FORMAT(3X,G9.6,G9.6)
```

```
18      WRITE(*,*)'COLUMNIZED THE INPUT DATA'
        IF(S.EQ.1)THEN
        II=8
        KK=16384
        ELSE IF(S.EQ.2) THEN
        II=4
        KK=8192
        ELSE
        II=2
        KK=4096
        ENDIF
        K=0
        DO 20 J=1,II
        DO 30 I=1,2048
        K=K+1
        D(K)=X(I,J)
30      CONTINUE
20      CONTINUE
        NF=KK+NI-1
        WRITE(*,*)'WRITING OUTPUT DATA ON TO FILE DFCPN.OUT'
        DO 40 K=NI,NF,M
        T=(FLOAT(K)-FLOAT(NI))*DELTA
        WRITE(2,50)T,D(K)
50      FORMAT(E9.4,1X,F8.6)
40      CONTINUE
        END
```

Computer Program COPROC

```
CCCCCCCCCCCCCCCCCCCCCCCCCCCCCCCCCCCCCCCCCCCCCCCCCCCCCCCCCCCCCCCC
C                                                              C
C       PROGRAM COPROC.FOR (IN FORTRAN 77)                     C
C       BASED ON THE METHOD OF FAST FOURIER TRANSFORM (FFT)    C
C       DEVELOPED BY KHALID JAMIL                              C
C                                                              C
CCCCCCCCCCCCCCCCCCCCCCCCCCCCCCCCCCCCCCCCCCCCCCCCCCCCCCCCCCCCCCCC

        REAL ANS,D1,B,B1,A,K2,S,SS
        INTEGER M,K,J,ISIGN
        DIMENSION  D1(16384),ANS(34000)
        OPEN(1,FILE='DFCPN.OUT',STATUS='OLD')
        OPEN(2,FILE='COPROC.OUT')
        WRITE(*,*)'ENTER NUMBER OF DATA POINTS (MUST BE POWER OF 2)'
        READ(5,*)M
        WRITE(*,*)'SELECT NO WINDOW       :ENTER 0'
        WRITE(*,*)'SELECT HANNING WINDOW  :ENTER 1'
        WRITE(*,*)'SELECT PARZEN WINDOW   :ENTER 2'
        READ(*,*)S
        WRITE(*,*)'FOR AUTOCORRELATION ON , ENTER 1'
        WRITE(*,*)'FOR AUTOCORRELATION OFF, ENTER 0'
        READ(*,*)SS
        WRITE(*,*)' '
        WRITE(*,*)'READING INPUT  DATA'
        READ(1,11)(D1(K),K=1,M)
11      FORMAT(9X,F8.4)
        REWIND(1)
        READ(1,110)DEL
110     FORMAT(/,E9.4)
        CLOSE(1)
        IF(SS.EQ.1)GOTO 12
```

```
       IF(SS.EQ.0)GOTO 13
 12    WRITE(*,*)'AUTOCORRELATION STARTS'
       CALL CORREL(D1,D1,M,ANS)
       WRITE(*,*)'AUTOCORRELATION COMPLETED'
       GOTO 14
 13    WRITE(*,*)'AUTOCORRELATION IS OFF'
 14    IF(S.EQ.0)GOTO 22
       IF(S.EQ.1)GOTO 33
       IF(S.EQ.2)GOTO 44
 33    WRITE(*,*)'HANNING WINDOW STARTS'
       J=0
       DO 9 K=1,M
       K1=K-1
       K2=DFLOAT(K1)
       J=J+1
       ANS(J)=0.5D00*(1.0D00-DCOS((2.0D0*3.141592*K2)
      & /(DFLOAT(M-1))))*ANS(K)
  9    CONTINUE
       WRITE(*,*)'WINDOWING STOPS'
       GOTO 22
 44    WRITE(*,*)'PARZEN WINDOW STARTS'
       J=0
       DO 19 K=1,M
       K1=K-1
       K2=DFLOAT(K1)
       J=J+1
       ANS(J)=(1.0-ABS((K2-0.5*FLOAT(M-1))/
     & (0.5*FLOAT(M+1))))*ANS(K)
 19    CONTINUE
       WRITE(*,*)'WINDOWING STOPS'
 22    WRITE(*,*)'FOURIER TRANSFORMATION STARTS'
       N=M/2
       ISIGN=1
       IF(SS.EQ.1)GOTO 45
       IF(SS.EQ.0) GOTO 46
 45    CALL REALFT(ANS,N,ISIGN)
 46    CALL REALFT(D1,N,ISIGN)
       WRITE(*,*)'FFT COMPLETED'
       WRITE(*,*)'CREATING COPROC.OUT FILE'
       IF(SS.EQ.1)GOTO 23
       IF(SS.EQ.0)GOTO 24
 23    B=0.0
       DO 20 J=1,M,2
       B=B+1.0
       B1=(B-1.0)/(FLOAT(M)*DEL)
       A=SQRT(ANS(J)**2+ANS(J+1)**2)
       WRITE(2,*)B1,A
 20    CONTINUE
       GOTO 26
 24    B=0.0
       DO 25 J=1,M,2
       B=B+1.0
       B1=(B-1.0)/(FLOAT(M)*DEL)
       A=(D1(J)**2+D1(J+1)**2)
       WRITE(2,*)B1,A
 25    CONTINUE
 26    STOP

       SUBROUTINE CORREL(DATA1,DATA2,N,ANS)
       PARAMETER(NMAX=32768)
       DIMENSION DATA1(N),DATA2(N)
       COMPLEX FFT(NMAX),ANS(N)
       CALL TWOFFT(DATA1,DATA2,FFT,ANS,N)
       NO2=FLOAT(N)/2.0
       DO 11 I=1,N/2+1
        ANS(I)=FFT(I)*CONJG(ANS(I))/NO2
11     CONTINUE
       ANS(1)=CMPLX(REAL(ANS(1)),REAL(ANS(N/2+1)))
       CALL REALFT(ANS,N/2,-1)
       RETURN
       END

       SUBROUTINE TWOFFT(DATA1,DATA2,FFT1,FFT2,N)
       DIMENSION DATA1(N),DATA2(N)
       COMPLEX FFT1(N),FFT2(N),H1,H2,C1,C2
       C1=CMPLX(0.5,0.0)
       C2=CMPLX(0.0,-0.5)
       DO 11 J=1,N
        FFT1(J)=CMPLX(DATA1(J),DATA2(J))
11     CONTINUE
       CALL FOUR1(FFT1,N,1)
       FFT2(1)=CMPLX(AIMAG(FFT1(1)),0.0)
       FFT1(1)=CMPLX(REAL(FFT1(1)),0.0)
       N2=N+2
       DO 12 J=2,N/2+1
       H1=C1*(FFT1(J)+CONJG(FFT1(N2-J)))
        H2=C2*(FFT1(J)-CONJG(FFT1(N2-J)))
        FFT1(J)=H1
        FFT1(N2-J)=CONJG(H1)
        FFT2(J)=H2
        FFT2(N2-J)=CONJG(H2)
12     CONTINUE
       RETURN
       END

       SUBROUTINE REALFT(DATA,N,ISIGN)
       REAL*8 WR,WI,WPR,WPI,WTEMP,THETA
       DIMENSION DATA(*)
       THETA=6.28318530717959D0/2.0D0/DBLE(N)
       C1=0.5
       IF (ISIGN.EQ.1) THEN
        C2=-0.5
        CALL FOUR1(DATA,N,+1)
       ELSE
        C2=0.5
        THETA=-THETA
       ENDIF
       WPR=-2.0D0*DSIN(0.5D0*THETA)**2
       WPI=DSIN(THETA)
       WR=1.0D0+WPR
       WI=WPI
       N2P3=2*N+3
       DO 11 I=2,N/2+1
        I1=2*I-1
        I2=I1+1
        I3=N2P3-I2
        I4=I3+1
        WRS=SNGL(WR)
        WIS=SNGL(WI)
        H1R=C1*(DATA(I1)+DATA(I3))
        H1I=C1*(DATA(I2)-DATA(I4))
        H2R=-C2*(DATA(I2)+DATA(I4))
        H2I=C2*(DATA(I1)-DATA(I3))
        DATA(I1)=H1R+WRS*H2R-WIS*H2I
        DATA(I2)=H1I+WRS*H2I+WIS*H2R
        DATA(I3)=H1R-WRS*H2R+WIS*H2I
        DATA(I4)=-H1I+WRS*H2I+WIS*H2R
        WTEMP=WR
        WR=WR*WPR-WI*WPI+WR
        WI=WI*WPR+WTEMP*WPI+WI
11     CONTINUE
       IF (ISIGN.EQ.1) THEN
        H1R=DATA(1)
        DATA(1)=H1R+DATA(2)
        DATA(2)=H1R-DATA(2)
       ELSE
        H1R=DATA(1)
        DATA(1)=C1*(H1R+DATA(2))
        DATA(2)=C1*(H1R-DATA(2))
        CALL FOUR1(DATA,N,-1)
       ENDIF
       RETURN
       END

       SUBROUTINE FOUR1(DATA,NN,ISIGN)
       REAL*8 WR,WI,WPR,WPI,WTEMP,THETA
       DIMENSION DATA(2*NN)
       N=2*NN
       J=1
       DO 11 I=1,N,2
        IF(J.GT.I)THEN
        TEMPR=DATA(J)
        TEMPI=DATA(J+1)
        DATA(J)=DATA(I)
        DATA(J+1)=DATA(I+1)
       DATA(I)=TEMPR
        DATA(I+1)=TEMPI
        ENDIF
        M=N/2
1       IF ((M.GE.2).AND.(J.GT.M)) THEN
        J=J-M
        M=M/2
        GO TO 1
        ENDIF
        J=J+M
11     CONTINUE
       MMAX=2
2      IF (N.GT.MMAX) THEN
        ISTEP=2*MMAX
        THETA=6.28318530717959D0/(ISIGN*MMAX)
        WPR=-2.D0*DSIN(0.5D0*THETA)**2
        WPI=DSIN(THETA)
        WR=1.D0
        WI=0.D0
        DO 13 M=1,MMAX,2
        DO 12 I=M,N,ISTEP
        J=I+MMAX
        TEMPR=SNGL(WR)*DATA(J)-SNGL(WI)*DATA(J+1)
        TEMPI=SNGL(WR)*DATA(J+1)+SNGL(WI)*DATA(J)
        DATA(J)=DATA(I)-TEMPR
        DATA(J+1)=DATA(I+1)-TEMPI
        DATA(I)=DATA(I)+TEMPR
        DATA(I+1)=DATA(I+1)+TEMPI
12      CONTINUE
        WTEMP=WR
        WR=WR*WPR-WI*WPI+WR
        WI=WI*WPR+WTEMP*WPI+WI
13      CONTINUE
        MMAX=ISTEP
       GO TO 2
       ENDIF
       RETURN
       END
```

Nonlinear Fitting (NOLFIT) Program

```
CCCCCCCCCCCCCCCCCCCCCCCCCCCCCCCCCCCCCCCCCCCCCCCCCCCCCCCCCCCCCCCCCC
C                                                                C
C      NONLINEAR FITTING (NOLFIT.FOR) PROGRAM IN FORTRAN 77       C
C      THIS PROGRAM IS BASED UPON LEAST SQUARES FITTING           C
C      OF NONLINEAR FUNCTIONS                                     C
C      DEVELOPED BY KHALID JAMIL                                  C
C                                                                C
CCCCCCCCCCCCCCCCCCCCCCCCCCCCCCCCCCCCCCCCCCCCCCCCCCCCCCCCCCCCCCCCCC

       DIMENSION X(9000),Y(9000),SIGMAY(9000),A(20),DELTAA(20)
       DIMENSION SIGMAA(20),YFIT(9000)
       OPEN(1,FILE='DFCPN.OUT',STATUS='OLD')
       OPEN(2,FILE='NOLFIT.OUT')
       OPEN(3,FILE='YFIT.OUT')
       OPEN(4,FILE='A.IN')
       OPEN(7,FILE='DELAA.IN')
       WRITE(*,*)'ENTER NUMBER OF DATA POINTS TO BE FITTED'
       READ(5,*)NDATA
       WRITE(*,*)'ENTER NO OF FITTING PARAMETERS =?'
       READ(5,*)MA
       READ(4,*)(A(I),I=1,MA)
       READ(7,*)(DELTAA(I),I=1,MA)
       SIG=1.2E-03
       WRITE(*,*)'ENTER RUN NUMBER OR EXPERIMENTAL ID'
       READ(5,*)RN
       WRITE(*,*)'INITIAL DATA POINTS DELETED FROM  SPECTRUM'
       READ(5,*)PD
       WRITE(*,*)'NUMBER OF DATA POINTS SKIPPED FROM SPECTRUM'
       READ(5,*)AP
       WRITE(*,*)'ENTER APPLIED RADIO FREQUENCY (KHz)'
       READ(5,*)RF
       WRITE(*,*)'READING INPUT  DATA'
       READ(1,20)(Y(K),K=1,NDATA)
20     FORMAT(10X,F8.6)
       REWIND(1)
       READ(1,30)(X(J),J=1,NDATA)
30     FORMAT(E9.4)
       CLOSE(1)
       DO 40 K=1,NDATA
       SIGMAY(K)=SIG
40     CONTINUE
       WRITE(*,*)
       WRITE(*,*)'PROGRAM IS ITERATING: WAIT AND RELAX!'
       K=1
41     CALL GRIDLS(X,Y,SIGMAY,NDATA,MA,1,A,DELTAA,
     & SIGMAA,YFIT,CHISQR)
       B(K)=0.0
       B(K+1)=CHISQR
       IF(ABS(B(K)-B(K+1))).LE.0.01)GOTO 43
       WRITE(6,42)K,B(K+1)
```

```
42    FORMAT('+','ON ITERATION NUMBER',I3,',',2X,'CHI-SQUARE
     & IS=',1X,F9.5,)
      K=K+1
      GOTO 41
43    K=1
      B1=0.0
      FLAMDA=0.001
35    CALL CURFIT(X,Y,SIGMAY,NDATA,MA,1,A,DELTAA,SIGMAA,
     & ,FLAMDA,YFIT,CHISQR)
      B2=CHISQR
      C=0.0001
      IF(B1.EQ.0.0)THEN
      STATUS=(1.0-(B2-B1)/B2)*100
      ELSE
      STATUS=(1.0-(B1-B2)/B1)*100
      END IF
      K=K+1
      J=K-1
      WRITE(6,44)J,STATUS
44    FORMAT('+','ON ITERATION NUMBER',I3,',',2X,'CONVERGENCE
      IS',1X,F9.5,1X,'PERCENT')
      IF(ABS(B1-B2).LT.C)GOTO 45
      B1=B2
      GOTO 35
45    WRITE(*,*)'FINAL ITERATION'
      CALL POLISH(SIGMAY,CHISQR,SIG,NDATA)
      CALL CURFIT(X,Y,SIGMAY,NDATA,MA,1,A,DELTAA,SIGMAA,
     & FLAMDA,YFIT,CHISQR)
      QF1=RF-A(3)
      QF2=RF-A(7)
      S=FLOAT(K)
      S2=FLOAT(NDATA)
      WRITE(6,*)(A(I),I=1,MA)
      WRITE(6,*)(SIGMAA(K1),K1=1,MA)
      WRITE(6,*)RN,PD,AP,RF,SIG
      WRITE(6,*)QF1,QF2
      WRITE(2,51)RN
51    FORMAT(1X,'RUN NUMBER=',G12.5)
      WRITE(2,52)PD
52    FORMAT(////////,1X,'INITIAL DATA POINTS
     & DELETED=',G12.5)
      WRITE(2,53)AP
53    FORMAT(1X,'DATA POINTS (ALTERNATIVE) SKIPPED=',G12.5)
      WRITE(2,56)S2
56    FORMAT(1X,'NUMBER OF DATA POINTS FITTED=',G12.5)
      WRITE(2,54)RF
54    FORMAT(1X,'APPLIED RADIO-FREQUENCY (KHz)=',F8.3)
      WRITE(2,*)'  '
      WRITE(2,*)'FITTED PARAMETERS'
46    WRITE(2,*)(A(I),I=1,MA)
      WRITE(2,*)'ERROR IN FITTED PARAMETERS'
      WRITE(2,*)(SIGMAA(K1),K1=1,MA)
      WRITE(2,55)CHISQR
55    FORMAT(//,1X,'CHI-SQUARE=',F5.2)
      WRITE(2,60)SIG
60    FORMAT(1X,'MEAN SIGMA-IN-Y=',G12.5)
      WRITE(2,57)QF1
57    FORMAT(1X,'SITE-1 TRANSITION FREQUENCY (KHz)=',F8.3)
      WRITE(2,58)QF2
58    FORMAT(1X,'SITE-2 TRANSITION FREQUENCY (KHz)=',F8.3)
      WRITE(3,50)(YFIT(I),I=1,NDATA)
```

```
50      FORMAT(1X,F8.6)
        END

        SUBROUTINE GRIDLS(X,Y,SIGMAY,NPTS,NTERMS,MOD,A,DELTAA,SIGMAA
       *,YFIT,CHISQR)
        DIMENSION X(1),Y(1),SIGMAY(1),A(1),DELTAA(1),SIGMAA(1),YFIT(1)
11      NFREE=NPTS-NTERMS
        FREE=NFREE
        CHISQR=0.
        IF(NFREE) 100,100,20
20      DO 90 J=1,NTERMS
21      DO 22 I=1,NPTS
22      YFIT(I)=FUNCTN(X,I,A)
23      CHISQ1=FCHISQ(Y,SIGMAY,NPTS,NFREE,MOD,YFIT)
        FN=0.
        DELTA=DELTAA(J)
41      A(J)=A(J)+DELTA
        DO 43 I=1,NPTS
43      YFIT(I)=FUNCTN(X,I,A)
44      CHISQ2=FCHISQ(Y,SIGMAY,NPTS,NFREE,MOD,YFIT)
45      IF(CHISQ1-CHISQ2) 51,41,61
51      DELTA=-DELTA
        A(J)=A(J)+DELTA
        DO 54 I=1,NPTS
54      YFIT(I)=FUNCTN(X,I,A)
        SAVE=CHISQ1
        CHISQ1=CHISQ2
57      CHISQ2=SAVE
61      FN=FN+1.
        A(J)=A(J)+DELTA
        DO 64 I=1,NPTS
64      YFIT(I)=FUNCTN(X,I,A)
        CHISQ3=FCHISQ(Y,SIGMAY,NPTS,NFREE,MOD,YFIT)
66      IF(CHISQ3-CHISQ2) 71,81,81
71      CHISQ1=CHISQ2
        CHISQ2=CHISQ3
        GOTO 61
81      DELTA=DELTA*((CHISQ3-CHISQ2)/(CHISQ3-2.*CHISQ2+CHISQ1)+.5)
82      A(J)=A(J)-DELTA
83      SIGMAA(J)=DELTAA(J)*SQRT(2./(FREE*(CHISQ3-2.*CHISQ2+CHISQ1)))
84      DELTAA(J)=DELTAA(J)*FN/3.
90      CONTINUE
91      DO 92 I=1,NPTS
92      YFIT(I)=FUNCTN(X,I,A)
93      CHISQR=FCHISQ(Y,SIGMAY,NPTS,NFREE,MOD,YFIT)
100     RETURN
        END

        FUNCTION FCHISQ(Y,SIGMAY,NPTS,NFREE,MOD,YFIT)
        DOUBLE PRECISION CHISQ,WEIGHT
        DIMENSION Y(1),SIGMAY(1),YFIT(1)
11      CHISQ=0.
12      IF(NFREE) 13,13,20
13      FCHISQ=0.
        GOTO 40
20      DO 30 I=1,NPTS
21      IF(MOD) 22,27,29
22      IF(Y(I))25,27,23
23      WEIGHT=1./Y(I)
        GO TO 30
25      WEIGHT=1./(-Y(I))
        GOTO 30
```

```
 27     WEIGHT=1.
        GOTO 30
 29     WEIGHT=1./SIGMAY(I)**2
 30     CHISQ=CHISQ+WEIGHT*(Y(I)-YFIT(I))**2
 31     FREE=NFREE
 32     FCHISQ=CHISQ/FREE
 40     RETURN
        END

        SUBROUTINE CURFIT(X,Y,SIGMAY,NPTS,NTERMS,MODE,A,DELTAA,
       *SIGMAA,FLAMDA,YFIT,CHISQR)
        DOUBLE PRECISION ARRAY
        DIMENSION X(1),Y(1),SIGMAY(1),A(1),DELTAA(1),SIGMAA(1),YFIT(1)
        DIMENSION WEIGHT(8000),ALPHA(20,20),BETA(20),DERIV(20)
       *,ARRAY(20,20),B(20)
 11     NFREE=NPTS-NTERMS
        IF(NFREE)13,13,20
 13     CHISQR=0.
        GOTO 110
 20     DO 30 I=1,NPTS
 21     IF(MODE) 22,27,29
 22     IF(Y(I)) 25,27,23
 23     WEIGHT(I)=1./Y(I)
        GOTO 30
 25     WEIGHT(I)=1./(-Y(I))
        GOTO 30
 27     WEIGHT(I)=1.
        GOTO 30
 29     WEIGHT(I)=1./SIGMAY(I)**2
 30     CONTINUE
 31     DO 34 J=1,NTERMS
        BETA(J)=0.
        DO 34 K=1,J
 34     ALPHA(J,K)=0.
 41     DO 50 I=1,NPTS
        CALL FDERIV(X,I,A,DELTAA,NTERMS,DERIV)
        DO 46 J=1,NTERMS
        BETA(J)=BETA(J)+WEIGHT(I)*(Y(I)-FUNCTN(X,I,A))*DERIV(J)
        DO 46 K=1,J
 46     ALPHA(J,K)=ALPHA(J,K)+WEIGHT(I)*DERIV(J)*DERIV(K)
 50     CONTINUE
 51     DO 53 J=1,NTERMS
        DO 53 K=1,J
 53     ALPHA(K,J)=ALPHA(J,K)
 61     DO 62 I=1,NPTS
 62     YFIT(I)=FUNCTN(X,I,A)
 63     CHISQ1=FCHISQ(Y,SIGMAY,NPTS,NFREE,MODE,YFIT)
 71     DO 74 J=1,NTERMS
        DO 73 K=1,NTERMS
 73     ARRAY(J,K)=ALPHA(J,K)/SQRT(ALPHA(J,J)*ALPHA(K,K))
 74     ARRAY(J,J)=1.+FLAMDA
 80     CALL MATINV(ARRAY,NTERMS,DET)
 81     DO 84 J=1,NTERMS
        B(J)=A(J)
        DO 84 K=1,NTERMS
 84     B(J)=B(J)+BETA(K)*ARRAY(J,K)/SQRT(ALPHA(J,J)*ALPHA(K,K))
 91     DO 92 I=1,NPTS
 92     YFIT(I)=FUNCTN(X,I,B)
 93     CHISQR=FCHISQ(Y,SIGMAY,NPTS,NFREE,MODE,YFIT)
        IF(CHISQ1-CHISQR)95,101,101
 95     FLAMDA=10.*FLAMDA
        GOTO 71
```

```
101     DO 103 J=1,NTERMS
        A(J)=B(J)
103     SIGMAA(J)=SQRT(ARRAY(J,J)/ALPHA(J,J))
        FLAMDA=FLAMDA/10.
110     RETURN
        END

        FUNCTION FCHISQ(Y,SIGMAY,NPTS,NFREE,MOD,YFIT)
        DOUBLE PRECISION CHISQ,WEIGHT
        DIMENSION Y(1),SIGMAY(1),YFIT(1)
11      CHISQ=0.
12      IF(NFREE) 13,13,20
13      FCHISQ=0.
        GOTO 40
20      DO 30 I=1,NPTS
21      IF(MOD) 22,27,29
22      IF(Y(I))25,27,23
23      WEIGHT=1./Y(I)
        GO TO 30
25      WEIGHT=1./(-Y(I))
        GOTO 30
27      WEIGHT=1.
        GOTO 30
29      WEIGHT=1./SIGMAY(I)**2
30      CHISQ=CHISQ+WEIGHT*(Y(I)-YFIT(I))**2
31      FREE=NFREE
32      FCHISQ=CHISQ/FREE
40      RETURN
        END

        SUBROUTINE MATINV(ARRAY,NORDER,DET)
        DOUBLE PRECISION ARRAY,AMAX,SAVE
        DIMENSION ARRAY(20,20),IK(20),JK(20)
10      DET=1.
11      DO 100 K=1,NORDER
        AMAX=0.
21      DO 30 I=K,NORDER
        DO 30 J=K,NORDER
23      IF(DABS(AMAX)-DABS(ARRAY(I,J))) 24,24,30
24      AMAX=ARRAY(I,J)
        IK(K)=I
        JK(K)=J
30      CONTINUE
31      IF(AMAX) 41,32,41
32      DET=0.
        GOTO 140
41      I=IK(K)
        IF(I-K) 21,51,43
43      DO 50 J=1,NORDER
        SAVE=ARRAY(K,J)
        ARRAY(K,J)=ARRAY(I,J)
50      ARRAY(I,J)=-SAVE
51      J=JK(K)
        IF(J-K) 21,61,53
53      DO 60 I=1,NORDER
        SAVE=ARRAY(I,K)
        ARRAY(I,K)=ARRAY(I,J)
60      ARRAY(I,J)=-SAVE
61      DO 70 I=1,NORDER
        IF(I-K) 63,70,63
63      ARRAY(I,K)=-ARRAY(I,K)/AMAX
70      CONTINUE
```

```
71    DO 80 I=1,NORDER
      DO 80 J=1,NORDER
      IF(I-K) 74,80,74
74    IF(J-K) 75,80,75
75    ARRAY(I,J)=ARRAY(I,J)+ARRAY(I,K)*ARRAY(K,J)
80    CONTINUE
81    DO 90 J=1,NORDER
      IF(J-K) 83,90,83
83    ARRAY(K,J)=ARRAY(K,J)/AMAX
90    CONTINUE
      ARRAY(K,K)=1./AMAX
100   DET=DET*AMAX
101   DO 130 L=1,NORDER
      K=NORDER-L+1
      J=IK(K)
      IF(J-K) 111,111,105
105   DO 110 I=1,NORDER
      SAVE=ARRAY(I,K)
      ARRAY(I,K)=-ARRAY(I,J)
110   ARRAY(I,J)=SAVE
111   I=JK(K)
      IF(I-K) 130,130,113
113   DO 120 J=1,NORDER
      SAVE=ARRAY(K,J)
      ARRAY(K,J)=-ARRAY(I,J)
120   ARRAY(I,J)=SAVE
130   CONTINUE
140   RETURN
      END

      SUBROUTINE POLISH(SIGMAY,CHISQR,SIG,NDATA)
      DIMENSION SIGMAY(1)
      SIG=SQRT(CHISQR*SIG**2)
      DO 70 K=1,NDATA
70    SIGMAY(K)=SIG
      RETURN
      END

C     DEFINE YOUR FUNCTION :A THEORETICAL MODEL FOR FITTING
      FUNCTION FUNCTN(X,I,A)
      DIMENSION X(1),A(1)
      X1=X(I)
      PI=2.0*3.1415926
      F1=A(1)*EXP(-X1/A(2))*COS(A(3)*PI*X1+A(4))
      F2=A(5)*EXP(-X1/A(6))*COS(A(7)*PI*X1+A(8))
      FUNCTN=F1+F2+A(9)
      RETURN

      SUBROUTINE FDERIV(X,I,A,DELTAA,NTERMS,DERIV)
      DIMENSION X(1),A(1),DERIV(1)
      X1=X(I)
      PI=3.1415926*2.0
      DERIV(1)=+EXP(-X1/A(2))*COS(A(3)*PI*X1+A(4))
      DERIV(2)=(X1*EXP(-X1/A(2))*COS(A(3)*PI*X1+
     & A(4))*A(1))/(A(2)**2)
      DERIV(3)=-EXP(-X1/A(2))*SIN(A(3)*PI*X1+A(4))*A(1)*X1*PI
      DERIV(4)=-EXP(-X1/A(2))*SIN(A(3)*PI*X1+A(4))*A(1)
      DERIV(5)=+EXP(-X1/A(6))*COS(A(7)*PI*X1+A(8))
      DERIV(6)=(X1*EXP(-X1/A(6))*COS(A(7)*PI*X1
     & +A(8))*A(5))/(A(6)**2)
      DERIV(7)=-EXP(-X1/A(6))*SIN(A(7)*PI*X1+A(8))*A(5)*X1*PI
      DERIV(8)=-EXP(-X1/A(6))*SIN(A(7)*PI*X1+A(8))*A(5)
      DERIV(9)=1.0
      RETURN
      END
```

APPENDIX D
MONTE CARLO NEUTRON PHOTON TRANSPORT CODE (MCNP)

An Example of MCNP Input for the UFTR

```
UFTR : INPUT DATA FOR MCNP
1        1  -1.4050 -1
2        2 -1.59  2 -3 -4 5 6 -7
3        2 -1.59  8 -3 -9 5 6 -7
4        2 -1.59  10 -3 -11 5 6 -7
5        2 -1.59  2 -12 -4 13 6 -7
6        2 -1.59  8 -12 -9 13 6 -7
7        2 -1.59  10 -12 -11 13 6 -7
8       3 -1.6 ((14 -5 -16 12 6 -7) (1)):(14 -13 -16 17 6 -7)
         :(4 -15 -16 17 6 -7):(14 -15 -16 3 6 -7)
         :(9 -15 -2 17 6 -7):(11 -15 -8 17 6 -7):(14 -15 -10
         17 6 -7):(14 -15 -16 17 18 -6):(14 -15 -16 17 7 -19)
9        0  -18:19:-17:15:-14:16

1      S   76.2 76.2 76.2 1.905
2      PY  86.677
3      PX  104.77
4      PY  102.552
5      PX  91.44
6      PZ  43.656
7      PZ  108.744
8      PY  68.262
9      PY  84.137
10     PY  49.847
11     PY  65.722
12     PX  60.96
13     PX  47.63
14     PY  0.0
15     PX  152.4
16     PY  152.4
17     PX  0.0
18     PZ  0.0
19     PZ  152.4

IN     1 1 1 1 1 1 1 1 0
KCODE  1000 1 2 30 4500
KSRC   98 94 76 53 53 55
CUTN   100000000 .0
VOL    28.9583   13773.3 13773.3 13773.3 13773.3 13773.3
```

```
      13773.3  3456937.1  0
M1     6012.10 -0.158 16032.01 -0.421 7014.04 -0.368 1001.04
     -.053
M2     92235.19 -0.0200 13027.04 -0.5438 1001.04 -0.0515
       8016.04 -0.3845 48000.01 -0.0002
M3     6012.10 -1
MT3    GRPH.01
E0     1.0E-09 1.0E-08 1.0E-07 1.0E-06 1.0E-05 1.0E-04
       .001 0.01 0.1 0.5 1.0 1.5 2.0 3.0 4.0 5. 6. 7. 8. 10. 20
FM2    7.44E+15
FM4    7.44E+15
FM6    1.1919E+06
F2     1 3
F4     1 3
F6     1 3
PRINT
```

Explanations of Input Cards

The input cards for MCNP are divided into three major sections. Each section is separated by one blank card. The first section, cell cards, contains information about the cells defined in the problem. The second section, surface cards, defines the surface equations in the problems. The last section, data cards, defines all other aspects of the problem. All cards have open format for input with mnemonic or cell/surface numbers in columns 1 through 5. The data are supplied in columns 6 through 72. The first line of the input is for problem identification or heading of the problem. All sections of input will be described as follows:

Cell Cards

In section one, the first column represents the cell number. The second column shows the material numbers which are explicitly defined in section three. The third column represents the material density. The negative sign indicates that the material density is in the unit of gram/cm^3. The material density with positive sign stands for the atomic density in the units of 10^{24} atoms/cm^3. Whatever is the case MCNP gives the density in both units in the output. All other numbers show the surfaces bounding the cell. Since a cell is bounded by surfaces, therefore different regions are connected by using Boolean operators of intersection (space between surface numbers), union (symbol is :), and complement (symbol is #) [55]. The plus sign for positive is optional before a surface. A signed surface number represents the region on the other side of the surface where the points have the indicated sense. Cell #1 is the CVP in UFTR. Cells #2 to #7 are the fuel boxes. Cell #8 is graphite in which fuel boxes and sample are embedded. Cell #9 is all other space but the core.

Surface Cards

The general form of the surface card is of the form:

j n a list

Where j is the surface number given in the first column. If there is an asterisk it is a reflecting surface. n is absent if there is no coordinates transformation. a is the surface mnemonic given in MCNP users' manual [55]. For example S indicates the sphere. The Cartesian coordinates (x,y,z) of its origin and the radius of the sphere are given after S. PX, PY, and PZ are the equations of the planes perpendicular to the x-, y-, and z-axes, respectively and the numbers are the distances of the planes from the respective axis. All these planes are shown in figure 5-1.

Data Cards

The first card IN shows the importance of cells. The general form of this card is:

$$\mathrm{Im}\ X_1\ X_2\ \ldots\ X_j \ldots X_n$$

where m=N stands for neutron and m=P stands for photon. X_j is the importance for cells j=1,2,3...,n. In this problem all cells have importance equal to one except cell #9 which has zero importance because this cell is extended out side the core upto infinity.

The general form of the k-code input is as follows:

KCODE NSRCK RKK IKZ KCT MSRK KNRM

where NSRCK = nominal source size per cycle

RKK = initial guess for K_{eff}

IKZ = number of cycle to be skipped before tally accumulation

KCT = number of cycle to be done

MSRK = number of source points to allocate storage for

and KNRM = source normalization

0 means normalization by weight

1 means normalization tallies to number of particles.

The first number in KCODE card shows the nominal source size. The nominal source size for each cycle is in the range of 300 to 3000. The source size is 2000 in this simulation problem. The second number is the initial guess of k_{eff}. The third number shows the number of cycles skipped before tallies accumulation which has a value of 2 in the input card. The forth number shows the number of cycles to be done which is 30. The product of RKK and KCT is the number of histories for which MCNP was run. This simulation has sixty thousand histories. The computer allocates storage for 4500 source points. The card KSRC defines the locations of the initial source points in Cartesian coordinates (x,y,z). At least one source point must be included in the input. The present simulation has two source points.

The cutoff card has the general form:

CUTm T E WC1 WC2 SWTM

where m is taken as N or P for neutron and photon, respectively. T is the time cutoff in shake while one shake is 10^{-8} sec. E is the energy cutoff in MeV. WC1 and WC2 are the weight cutoffs. SWTM is the minimum source weight. In this simulation, CUTN is the time cutoff for neutron in 10^8 shake. Energy cutoff is 0.0 MeV. All other parameters have the default values.

The VOl card gives the volume of all the cells. MCNP generally calculates the volumes of all cells that are rotationally symmetric about any axis. The code calculated the cell volumes for all the cells from 1 to 7 which were generated by surface of revolution except cell #8 which was not rotationally symmetric about any axis.

The cards M1, M2, and M3 are the materials cards. These cards give the material identifier as ZZZAAA.nn. The proton number, z, and the mass number of an element are given by ZZZ and AAA , respectively. The number nn shows the library identifier [55]. The number next to ZZZAAA.nn with negative sign shows the weight fraction of the element in the material. MT3 specifies that $S(\alpha,\beta)$ thermal data are used for graphite at room temperature. This card also take into account the molecular bonding while slowing down in graphite.

The E0 card specifies the single energy bin structure for all the tallies. The general tallies mnemonic for neutron are Fm. For neutron transport only one digit numbers are used. Therefore, F2, F4, and F6 are the tallies counting the flux averaged over a surface, the flux averaged over a cell, and energy deposition over a cell, respectively. The cards FM2, FM4, and FM6 are the multiplier cards to tallies F2, F4, and F6 with the number given in the seventh column. The last card is the PRINT card to save output in the output file for printout.

MCNP was run for urea and thiourea by changing the material compositions in cell #1. All other cards remain the same. A sample output for MCNP is given as follows.

Abridged Sample Output of MCNP

```
MCNP     VERSION 3                       05/22/93   17:07:19.31
 ************************************************************************                                    PROBID = 05/22/93
17:07:19.31
  INP=uftr.u OUTP=kurea XSDIR=XSDIR2
    1-       UFTR : DATA FOR UFTR SIMULATION BY MCNP
    2-       1       1 -1.323 -1
    3-       2       2 -1.59  2 -3 -4 5 6 -7
    4-       3       2 -1.59  8 -3 -9 5 6 -7
    5-       4       2 -1.59  10 -3 -11 5 6 -7
    6-       5       2 -1.59  2 -12 -4 13 6 -7
    7-       6       2 -1.59  8 -12 -9 13 6 -7
    8-       7       2 -1.59  10 -12 -11 13 6 -7
    9-       8       3 -1.6 ((14 -5 -16 12 6 -7) (1)):(14 -13 -16 17 6 -7)
   10-               :(4 -15 -16 17 6 -7):(14 -15 -16 3 6 -7)
   11-               :(9 -15 -2 17 6 -7):(11 -15 -8 17 6 -7):(14 -15 -10
   12-               17 6 -7):(14 -15 -16 17 18 -6):(14 -15 -16 17 7 -19)
   13-       9       0  -18:19:-17:15:-14:16
   14-
   15-       1     S   76.2 76.2 76.2 1.905
   16-       2     PY  86.677
   17-       3     PX  104.77
   18-       4     PY  102.552
   19-       5     PX  91.44
   20-       6     PZ  43.656
   21-       7     PZ  108.744
   22-       8     PY  68.262
   23-       9     PY  84.137
   24-       10    PY  49.847
   25-       11    PY  65.722
   26-       12    PX  60.96
   27-       13    PX  47.63
   28-       14    PY  0.0
   29-       15    PX  152.4
   30-       16    PY  152.4
   31-       17    PX  0.0
   32-       18    PZ  0.0
   33-       19    PZ  152.4
   34-
   35-       IN    1 1 1 1 1 1 1 1 0
   36-       KCODE 2000 1 2 30 4500
 WARNING.  TALLIES ARE NORMED PER FISSION NEUTRON FOR ONE GENERATION.
   37-       KSRC  98 94 76 53 53 55
   38-       CUTN  100000000 .0
   39-       VOL   28.9583   13773.3 13773.3 13773.3 13773.3 13773.3
   40-             13773.3  3456937.1  0
   41-       M1    6012.10 -0.1999 8016.04 -0.2668 7014.04 -0.4662 1001.04 -.0671
   42-       M2    92235.19 -0.0201 13027.04 -0.5467 1001.04 -0.0475
   43-             8016.04 -0.3855  48000.01 -0.0002
   44-       M3    6012.10 -1
   45-       E0    .000000001 0.00000001 1.0E-07 0.000001 0.00001 0.0001
   46-             .001 0.01 0.1 0.5 1.0 1.5 2.0 3.0 4.0 5. 6. 7. 8. 10. 20
   47-       FM4   7.44E+15
   48-       FM2   7.44E+15
   49-       FM6   1.1919E+06
   50-       F2    1 5
   51-       F4    1 3
   52-       F1    1 5
   53-       F6    1 3
   54-       PRINT
   55-
1     INITIAL SOURCE FROM KSRC CARD.                                                     PRINT TABLE 90
 ORIGINAL NUMBER OF POINTS                               2
    POINTS NOT IN ANY CELL                         0
    POINTS IN CELLS OF ZERO IMPORTANCE             0
    POINTS IN VOID CELLS                           0
    POINTS IN AMBIGUOUS CELLS                      0
 TOTAL POINTS REJECTED                                   0
 POINTS REMAINING                                        2
 POINTS AFTER EXPANSION OR CONTRACTION                2000
 NOMINAL SOURCE SIZE                                  2000

 INITIAL GUESS FOR K(EFF.)                        1.000000

 CYCLES TO SKIP BEFORE TALLYING                          2

 TOTAL FISSION NUBAR DATA ARE BEING USED.

 SOURCE DISTRIBUTION WRITTEN TO FILE SRCTP           CYCLE =   0
                                                PRINT TABLE 30
          NEUTRON TALLY TYPE 4:    TRACK LENGTH ESTIMATE OF PARTICLE FLUX.
 CELLS             1     3


 ALL SCORES ARE MULTIPLIED BY   7.44000E+15

 ENERGY BINS
       0.00000E+00  TO  1.00000E-09 MEV
       1.00000E-09  TO  1.00000E-08 MEV
       1.00000E-08  TO  1.00000E-07 MEV
       1.00000E-07  TO  1.00000E-06 MEV
       1.00000E-06  TO  1.00000E-05 MEV
       1.00000E-05  TO  1.00000E-04 MEV
       1.00000E-04  TO  1.00000E-03 MEV
       1.00000E-03  TO  1.00000E-02 MEV
       1.00000E-02  TO  1.00000E-01 MEV
       1.00000E-01  TO  5.00000E-01 MEV
       5.00000E-01  TO  1.00000E+00 MEV
       1.00000E+00  TO  1.50000E+00 MEV
       1.50000E+00  TO  2.00000E+00 MEV
       2.00000E+00  TO  3.00000E+00 MEV
       3.00000E+00  TO  4.00000E+00 MEV
       4.00000E+00  TO  5.00000E+00 MEV
       5.00000E+00  TO  6.00000E+00 MEV
       6.00000E+00  TO  7.00000E+00 MEV
       7.00000E+00  TO  8.00000E+00 MEV
       8.00000E+00  TO  1.00000E+01 MEV
       1.00000E+01  TO  2.00000E+01 MEV
       TOTAL BIN
1TALLY   6                                                                          PRINT TABLE 30
            NEUTRON TALLY TYPE 6:   TRACK LENGTH ESTIMATE OF HEATING.

 CELLS             1     3


 ALL SCORES ARE MULTIPLIED BY   1.19190E+06

 ENERGY BINS
       0.00000E+00  TO  1.00000E-09 MEV
       1.00000E-09  TO  1.00000E-08 MEV
       1.00000E-08  TO  1.00000E-07 MEV
       1.00000E-07  TO  1.00000E-06 MEV
       1.00000E-06  TO  1.00000E-05 MEV
       1.00000E-05  TO  1.00000E-04 MEV
```

```
          1.00000E-04  TO  1.00000E-03 MEV
          1.00000E-03  TO  1.00000E-02 MEV
          1.00000E-02  TO  1.00000E-01 MEV
          1.00000E-01  TO  5.00000E-01 MEV
          5.00000E-01  TO  1.00000E+00 MEV
          1.00000E+00  TO  1.50000E+00 MEV
          1.50000E+00  TO  2.00000E+00 MEV
          2.00000E+00  TO  3.00000E+00 MEV
          3.00000E+00  TO  4.00000E+00 MEV
          4.00000E+00  TO  5.00000E+00 MEV
          5.00000E+00  TO  6.00000E+00 MEV
          6.00000E+00  TO  7.00000E+00 MEV
          7.00000E+00  TO  8.00000E+00 MEV
          8.00000E+00  TO  1.00000E+01 MEV
          1.00000E+01  TO  2.00000E+01 MEV
          TOTAL BIN
 MATERIAL COMPOSITION                                                          PRINT TABLE 40

  MATERIAL
   NUMBER      COMPONENT NUCLIDE, ATOM FRACTION

     1          6012.10 ,0.12505    8016.04 ,0.12522    7014.04 ,0.24992    1001.04 ,0.49981
     2         92235.19 ,0.00093   13027.04 ,0.22125    1001.04 ,0.51464    8016.04 ,0.26316
               48000.01 ,0.00002
     3          6012.10 ,1.00000

  MATERIAL
   NUMBER      COMPONENT NUCLIDE, MASS FRACTION

     1          6012.10 ,0.19990    8016.04 ,0.26680    7014.04 ,0.46620    1001.04 ,0.06710
     2         92235.19 ,0.02010   13027.04 ,0.54670    1001.04 ,0.04750    8016.04 ,0.38550
               48000.01 ,0.00020
     3          6012.10 ,1.00000

  THERMAL FREE GAS TREATMENT FOR NUCLIDES

                1001
                6012
                7014
                8016
1     CELL VOLUMES AND MASSES                                                PRINT TABLE 50
```

```
 PROGR PROBL     ATOM          GRAM         INPUT       CALCULATED                                 REASON VOLUME
  NAME  NAME    DENSITY       DENSITY       VOLUME        VOLUME         MASS         PIECES     NOT CALCULATED

     1     1 1.06130E-01   1.32300E+00   2.89583E+01   2.89583E+01   3.83118E+01       1

     2     2 8.76891E-02   1.59000E+00   1.37733E+04   1.37735E+04   2.18995E+04       0

     3     3 8.76891E-02   1.59000E+00   1.37733E+04   1.37735E+04   2.18995E+04       0

     4     4 8.76891E-02   1.59000E+00   1.37733E+04   1.37735E+04   2.18995E+04       0

     5     5 8.76891E-02   1.59000E+00   1.37733E+04   1.37735E+04   2.18995E+04       0

     6     6 8.76891E-02   1.59000E+00   1.37733E+04   1.37735E+04   2.18995E+04       0

     7     7 8.76891E-02   1.59000E+00   1.37733E+04   1.37735E+04   2.18995E+04       0

     8     8 8.02933E-02   1.60000E+00   3.45694E+06   0.00000E+00   5.53110E+06       0    ASYMMETRIC
     9     9 0.00000E+00   0.00000E+00   0.00000E+00   0.00000E+00   0.00000E+00       0    INFINITE
1      SURFACE AREAS                                                                          PRINT TABLE 50

 PROGR PROBL     INPUT       CALCULATED    REASON AREA
  NAME  NAME     AREA           AREA       NOT CALCULATED

     1     1 0.00000E+00   4.56037E+01
     2     2 0.00000E+00   1.73525E+03
     3     3 0.00000E+00   3.09982E+03
     4     4 0.00000E+00   1.73525E+03
     5     5 0.00000E+00   3.09982E+03
     6     6 0.00000E+00   0.00000E+00   ASYMMETRIC
     7     7 0.00000E+00   0.00000E+00   ASYMMETRIC
     8     8 0.00000E+00   1.73525E+03
     9     9 0.00000E+00   1.73525E+03
    10    10 0.00000E+00   1.73525E+03
    11    11 0.00000E+00   1.73525E+03
    12    12 0.00000E+00   3.09982E+03
    13    13 0.00000E+00   3.09982E+03
    14    14 0.00000E+00   2.32258E+04
    15    15 0.00000E+00   2.32258E+04
    16    16 0.00000E+00   2.32258E+04
    17    17 0.00000E+00   2.32258E+04
    18    18 0.00000E+00   2.32258E+04
    19    19 0.00000E+00   2.32258E+04
```

```
1                9 CELLS                                                                    PRINT TABLE 60
 PROGR PROBL
  NAME  NAME  MAT   ATOM DEN      GRAM DEN     IMPORTANCE    PHOTON WT     VOLUME        MASS

     1     1    1 1.06130E-01  1.32300E+00  1.00000E+00  0.00000E+00  2.89583E+01  3.83118E+01
     2     2    2 8.76891E-02  1.59000E+00  1.00000E+00  0.00000E+00  1.37733E+04  2.18995E+04
     3     3    2 8.76891E-02  1.59000E+00  1.00000E+00  0.00000E+00  1.37733E+04  2.18995E+04
     4     4    2 8.76891E-02  1.59000E+00  1.00000E+00  0.00000E+00  1.37733E+04  2.18995E+04
     5     5    2 8.76891E-02  1.59000E+00  1.00000E+00  0.00000E+00  1.37733E+04  2.18995E+04
     6     6    2 8.76891E-02  1.59000E+00  1.00000E+00  0.00000E+00  1.37733E+04  2.18995E+04
     7     7    2 8.76891E-02  1.59000E+00  1.00000E+00  0.00000E+00  1.37733E+04  2.18995E+04
     8     8    3 8.02933E-02  1.60000E+00  1.00000E+00  0.00000E+00  3.45694E+06  5.53110E+06
     9     9    0 0.00000E+00  0.00000E+00  0.00000E+00  0.00000E+00  1.00000E+00  0.00000E+00

 TOTAL                                                               3.53961E+06  5.66253E+06
1               19 SURFACES                                                               PRINT TABLE 70
 PROGR PROBL
  NAME  NAME       TRANS  TYPE   SURFACE COEFFICIENTS

     1     1               S     7.6200000E+01   7.6200000E+01   7.6200000E+01   1.9050000E+00
     2     2              PY     8.6677000E+01
     3     3              PX     1.0477000E+02
     4     4              PY     1.0255200E+02
     5     5              PX     9.1440000E+01
     6     6              PZ     4.3656000E+01
     7     7              PZ     1.0874400E+02
     8     8              PY     6.8262000E+01
     9     9              PY     8.4137000E+01
    10    10              PY     4.9847000E+01
    11    11              PY     6.5722000E+01
    12    12              PX     6.0960000E+01
    13    13              PX     4.7630000E+01
    14    14              PY     0.0000000E+00
    15    15              PX     1.5240000E+02
    16    16              PY     1.5240000E+02
    17    17              PX     0.0000000E+00
    18    18              PZ     0.0000000E+00
    19    19              PZ     1.5240000E+02
```

```
1  THERMAL LIMIT =  2.0000E+02

     TIME:      0.0000E+00

     CELL         TMP 1
       1        2.5300E-08
       2        2.5300E-08
       3        2.5300E-08
       4        2.5300E-08
       5        2.5300E-08
       6        2.5300E-08
       7        2.5300E-08
       8        2.5300E-08

          1 WARNING MESSAGE SO FAR.
1CROSS-SECTION TABLES

     TABLE    LENGTH

                        TABLES FROM FILE BMCCS2

   1001.04C    1416  H-1   ENDF/B IV (T404 REV.1) 10NOV75 NEW GP FORMAT          (  1269)     11 DEC 75
   6012.10C    6900  C-12 LASL SUBLIBRARY MAT 102 13 APR 1976  POINTWISE T=0.0  (   102)     15 APR 76
   7014.04C   15730   N-14 ENDF/B-IV   NEW GAMMA PRODUCTION FORMAT              (  1275)     14 OCT 75
   8016.04C   17278   O-16 ENDF/B-IV   NEW GAMMA PRODUCTION FORMAT              (  1276)     14 OCT 75
  13027.04C   25761   AL-27 ENDF/B-IV  NEW GAMMA PRODUCTION FORMAT              (  1193)     14 OCT 75
  48000.01C    6584  CD       LLL-HOWERTON   1/73                               (   534)      7 MAY 75
  92235.19C   16173  U-235 ENDF/B-IV T=3*E+4  24 FEBRUARY 1976        TOTAL NU  (  1261)      8 MAR 78

  TOTAL       89842

 WARNING.  NEUTRON ENERGY CUTOFF IS BELOW SOME CROSS-SECTION TABLES.

 USE OF DYNAMICALLY ALLOCATED STORAGE


     GENERAL              55084
     TALLIES               1056
     CROSS SECTIONS       89842

     TOTAL               145982
 ************************************************************************
 DUMP NO.  1 ON FILE   RUNTPE          NPS =       0          CTM =   0.00


        2 WARNING MESSAGES SO FAR.
1   STARTING MCRUN.      FIELD LENGTH =      0      CP0 =  0.66                                    PRINT
TABLE 110

 CYCLE    1  K(COLLISION)  0.993387  REMOVAL LIFETIME(ABS)  7.5136E+04  SOURCE POINTS GENERATED   1937

 ************************************************************************
 DUMP NO.  2 ON FILE   RUNTPE          NPS =    2000          CTM =  34.55


 CYCLE    2  K(COLLISION)  0.994567  REMOVAL LIFETIME(ABS)  7.5510E+04  SOURCE POINTS GENERATED   1986

 SOURCE DISTRIBUTION WRITTEN TO FILE SRCTP           CYCLE =   2

 ************************************************************************
 DUMP NO.  3 ON FILE   RUNTPE          NPS =    3937          CTM =  69.53


 CYCLE    3  K(COLLISION)  1.014181  REMOVAL LIFETIME(ABS)  7.8501E+04  SOURCE POINTS GENERATED   2124

 SOURCE DISTRIBUTION WRITTEN TO FILE SRCTP           CYCLE =   3

 ************************************************************************
 DUMP NO. 10 ON FILE   RUNTPE          NPS =   17963          CTM = 322.37


  ESTIMATOR     CYCLE   10     AVE OF     8 CYCLES     COMBINATION     SIMPLE AVERAGE COMBINED AVERAGE
CORR

K(COLLISION)   1.025930     1.004554 0.0074     K(COL/ABS)       1.002217 0.0043     1.001561   0.0044-0.1251

K(ABSORPTION)  1.015418     0.999880 0.0053     K(ABS/TK LN)     1.002219 0.0045     1.001412 0.0046  -0.0968
 K(TRK LENGTH)  1.024974     1.004559 0.0079     K(TK LN/COL)     1.004557 0.0076     1.004544 0.0074   0.9887
 REM LIFE(COL)    6.7590E+04  7.3897E+04 0.0191   K(COL/ABS/TK LN)    1.002998 0.0052     1.001696 0.0046
 REM LIFE(ABS)    6.9530E+04  7.4186E+04 0.0149    LIFE(COL/ABS)     7.4042E+04 0.0167    7.4405E+04 0.0148
0.9310

 SOURCE POINTS GENERATED   2111
SOURCE DISTRIBUTION WRITTEN TO FILE SRCTP           CYCLE =  10

*************************************************************************
DUMP NO. 20 ON FILE   RUNTPE           NPS =    37607          CTM = 675.91


 ESTIMATOR        CYCLE   20     AVE OF    18 CYCLES      COMBINATION          SIMPLE AVERAGE      COMBINED AVERAGE
  CORR
K(COLLISION)       0.980799        0.993595 0.0068     K(COL/ABS)           0.998518 0.0042       1.001162 0.0038
0.1516
K(ABSORPTION)      0.975575        1.003441 0.0041     K(ABS/TK LN)         0.998482 0.0044       1.001362 0.0039
0.1639
K(TRK LENGTH)      0.983718        0.993522 0.0071     K(TK LN/COL)         0.993559 0.0069       0.993780 0.0066
0.9939
REM LIFE(COL)    7.5663E+04      7.4846E+04 0.0131     K(COL/ABS/TK LN)     0.996853 0.0050       1.000982 0.0040
REM LIFE(ABS)    7.4553E+04      7.5011E+04 0.0105     LIFE(COL/ABS)      7.4929E+04 0.0116     7.5130E+04 0.0102
0.9336
SOURCE POINTS GENERATED    1980

SOURCE DISTRIBUTION WRITTEN TO FILE SRCTP           CYCLE =  20

*************************************************************************
DUMP NO. 30 ON FILE   RUNTPE           NPS =    58020          CTM =1039.52


 ESTIMATOR        CYCLE   30     AVE OF    28 CYCLES      COMBINATION          SIMPLE AVERAGE      COMBINED AVERAGE
  CORR
K(COLLISION)       1.015640        0.996798 0.0050     K(COL/ABS)           1.000208 0.0032       1.001877 0.0029
0.1660
K(ABSORPTION)      0.977099        1.003617 0.0032     K(ABS/TK LN)         1.000266 0.0032       1.001996 0.0029
0.1346
K(TRK LENGTH)      1.024480        0.996915 0.0052     K(TK LN/COL)         0.996857 0.0051       0.996597 0.0049
0.9905
REM LIFE(COL)    7.3616E+04      7.4481E+04 0.0110     K(COL/ABS/TK LN)     0.999110 0.0037       1.001921 0.0031
REM LIFE(ABS)    7.3559E+04      7.4545E+04 0.0091     LIFE(COL/ABS)      7.4513E+04 0.0099     7.4601E+04 0.0087
0.9490
SOURCE POINTS GENERATED    2111

SOURCE DISTRIBUTION WRITTEN TO FILE SRCTP           CYCLE =  30
1     RUN TERMINATED WHEN    30 KCODE CYCLES WERE DONE.                05/23/93   11:00:48.29
      UFTR : INPUT FOR UFTR                                            PROBID = 05/22/93   17:07:19.31
```

```
                         LEDGER OF NET NEUTRON CREATION AND LOSS (FOR ACCOUNTING ONLY)
                   TRACKS      WEIGHT        ENERGY                                   TRACKS     WEIGHT
 ENERGY
                              (PER SOURCE PARTICLE)                                               (PER SOURCE
 PARTICLE)

  SOURCE            59881     1.0020E+00    1.9823E+00        ESCAPE                 16990     2.3490E-01
 1.3454E-02
  SCATTERING            0     0.            6.4084E-07        SCATTERING                 0     0.
 1.9490E+00
  FISSION               0     0.            0.                CAPTURE                    0     3.5182E-01
 1.8178E-02
  (N,XN)                1   1.2828E-05    2.5679E-06       ENERGY CUTOFF          0     0.               0.

  FORCED COLLISION      0   0.            0.               TIME CUTOFF            0     0.               0.

  WEIGHT CUTOFF         0     1.9379E-02    4.0819E-08        WEIGHT CUTOFF      42892     1.9658E-02
 4.3219E-08
  WEIGHT WINDOW         0   0.            0.               WEIGHT WINDOW          0     0.               0.

  CELL IMPORTANCE       0   0.            0.               CELL IMPORTANCE        0     0.               0.

  ENERGY IMPORT.        0   0.            0.               ENERGY IMPORT.         0     0.               0.

  DXTRAN                0   0.            0.               DXTRAN                 0     0.               0.

  EXP. TRANSFORM        0   0.            0.               EXP. TRANSFORM         0     0.               0.

                                                             DEAD FISSION              0     4.1500E-01
 1.6454E-03
     TOTAL          59882     1.0214E+00    1.9823E+00            TOTAL             59882     1.0214E+00
 1.9823E+00

   PREDICTED AVG OF SRC FUNCTION ZERO      0.0000E+00     AVERAGE LIFETIME, SHAKES                   CUTOFFS
   TRACKS PER NEUTRON STARTED              1.0000E+00       ESCAPE                1.7968E+05         TCO
   1.0000E+08
   COLLISIONS PER NEUTRON STARTED          1.5089E+02    CAPTURE             9.2488E+04  ECO   0.0000E+00
   TOTAL COLLISIONS                           9035650    CAPTURE OR ESCAPE 1.2740E+05  WC1  -5.0000E-01
   NET MULTIPLICATION                  1.0000E+00 0.0002    ANY TERMINATION   1.2482E+05  WC2  -2.5000E-01
 COMPUTER TIME SO FAR IN THIS RUN  1073.43 MINUTES                 TOTAL NEUTRONS BANKED                1
 COMPUTER TIME IN MCRUN (4C0)      1072.77 MINUTES                    PER SOURCE PARTICLE       1.6700E-05
 SOURCE PARTICLES PER MINUTE            5.5819E+01                 TOTAL PHOTONS BANKED                 0
 FIELD LENGTH                                    0                    PER SOURCE PARTICLE       0.0000E+00
 RANDOM NUMBERS GENERATED                103493923                 MAXIMUM NUMBER EVER IN BANK          1
 LAST STARTING RANDOM NUMBER        125569591092041                 BANK OVERFLOWS TO BACKUP FILE        0
 NEXT STARTING RANDOM NUMBER        141936460798597

 TALLY LIST-SCORING WAS ABANDONED AT NPS =      3938
1    PROBLEM ACTIVITY IN EACH CELL, NEUTRONS ONLY

    CELL          TRACKS      POPULATION   COLLISIONS   COLLISIONS     NUMBER         FLUX         AVERAGE
AVERAGE
 PROGR PROBL    ENTERING                               * WEIGHT     WEIGHTED      WEIGHTED    TRACK WEIGHT   TRACK
MFP
  NAME  NAME                                           (PER HISTORY)    ENERGY         ENERGY     (RELATIVE)
(CM)

     1     1         324           254         1399    1.8097E-02   4.5429E-05   1.3608E-01   8.1183E-01
8.5852E-01
     2     2       35547         16446       370607    5.2665E+00   2.2048E-04   5.3969E-01   8.9943E-01
1.7400E+00
     3     3       36251         17761       371860    5.2522E+00   2.0865E-04   5.2077E-01   8.9437E-01
1.7107E+00
     4     4       28478         13187       284439    3.9990E+00   1.9463E-04   5.0641E-01   8.9019E-01
1.6830E+00
     5     5       28080         12894       282190    3.9618E+00   1.9865E-04   5.1561E-01   8.9045E-01
1.6951E+00
     6     6       34536         16831       349295    4.9491E+00   2.0650E-04   5.0992E-01   8.9698E-01
1.7011E+00
     7     7       32207         14901       323794    4.5890E+00   2.1229E-04   5.2194E-01   8.9804E-01
1.7197E+00


     8     8      152596         53034      7052066    1.0041E+02   2.7222E-05   1.0871E-01   8.5858E-01
2.7723E+00

    TOTAL       348019        145308      9035650    1.2845E+02
1    NEUTRON WEIGHT BALANCE IN EACH CELL -- EXTERNAL EVENTS                                 PRINT TABLE 130

    CELL          SOURCE       ENTERING       TIME         ENERGY       EXITING        TOTAL
 PROGR PROBL                                 CUTOFF       CUTOFF
```

```
     1     1  0.0000E+00   4.6644E-03   0.0000E+00   0.0000E+00  -4.2601E-03   4.0433E-04
     2     2  1.9806E-01   3.5196E-01   0.0000E+00   0.0000E+00  -4.1566E-01   1.3436E-01
     3     3  1.7895E-01   3.7922E-01   0.0000E+00   0.0000E+00  -4.2388E-01   1.3430E-01
     4     4  1.4026E-01   2.9535E-01   0.0000E+00   0.0000E+00  -3.2968E-01   1.0593E-01
     5     5  1.3909E-01   2.9161E-01   0.0000E+00   0.0000E+00  -3.2576E-01   1.0493E-01
     6     6  1.7086E-01   3.6187E-01   0.0000E+00   0.0000E+00  -4.0640E-01   1.2633E-01
     7     7  1.7477E-01   3.2157E-01   0.0000E+00   0.0000E+00  -3.7804E-01   1.1831E-01
     8     8  0.0000E+00   2.2837E+00   0.0000E+00   0.0000E+00  -2.2411E+00   4.2531E-02

     TOTAL    1.0020E+00   4.2899E+00   0.0000E+00   0.0000E+00  -4.5248E+00   7.6709E-01

   TOTAL OVER ALL CELLS FOR EACH NUCLIDE

                 1001.04C                    1687834     2.3695E+01   1.3328E-01   0.0000E+00   0.0000E+00
                 6012.10C                    7052127     1.0041E+02   4.2694E-02   0.0000E+00   0.0000E+00
                 7014.04C                        244     3.1671E-03   2.9164E-04   0.0000E+00   0.0000E+00
                 8016.04C                     164154     2.4321E+00   1.3928E-03   0.0000E+00   0.0000E+00
                13027.04C                      85740     1.3269E+00   4.1366E-02   0.0000E+00   0.0000E+00
                48000.01C                       4405     5.6199E-02   5.5792E-02   0.0000E+00   0.0000E+00
                92235.19C                      41146     9.3449E-01   4.9201E-01   0.0000E+00   1.2828E-05
1TALLY    1      NPS =     59881
           NEUTRON TALLY TYPE 1:   NUMBER OF PARTICLES CROSSING A SURFACE.

 SURFACE  1

      ENERGY
    1.0000E-09   1.68519E-05 1.0000
    1.0000E-08   2.02809E-04 0.2519
    1.0000E-07   4.03516E-03 0.0920
    1.0000E-06   1.12353E-03 0.1806
    1.0000E-05   5.18146E-04 0.2693
    1.0000E-04   4.97669E-04 0.2276
    1.0000E-03   5.01275E-04 0.2595
    1.0000E-02   3.11722E-04 0.2721
    1.0000E-01   5.77617E-04 0.2301
    5.0000E-01   6.79818E-04 0.2276
    1.0000E+00   2.27967E-04 0.3506
    1.5000E+00   2.08841E-04 0.3712
    2.0000E+00   1.18376E-04 0.5127
    3.0000E+00   8.84056E-05 0.6009
    4.0000E+00   0.00000E+00 0.0000
    5.0000E+00   0.00000E+00 0.0000
    6.0000E+00   0.00000E+00 0.0000
    7.0000E+00   0.00000E+00 0.0000
    8.0000E+00   0.00000E+00 0.0000
    1.0000E+01   3.21112E-05 1.0000
    2.0000E+01   0.00000E+00 0.0000
      TOTAL      9.14030E-03 0.0709
          NEUTRON TALLY TYPE 2:   PARTICLE FLUX AVERAGED OVER A SURFACE.

          THIS TALLY IS ALL MULTIPLIED BY  7.44000E+15

          AREAS
              SURFACE:        1           5

                      4.56037E+01  3.09982E+03

 SURFACE  1

     ENERGY
    1.0000E-09   7.59796E+09 1.0000
    1.0000E-08   6.62412E+10 0.3131
    1.0000E-07   1.31847E+12 0.1349
    1.0000E-06   3.96824E+11 0.2476
    1.0000E-05   1.72256E+11 0.3076
    1.0000E-04   1.53314E+11 0.2802
    1.0000E-03   1.34800E+11 0.3001
    1.0000E-02   7.38128E+10 0.2940
    1.0000E-01   1.42551E+11 0.2566
    5.0000E-01   2.40704E+11 0.2809
    1.0000E+00   5.39255E+10 0.3690
    1.5000E+00   4.99044E+10 0.4081
    2.0000E+00   2.35831E+10 0.5063
    3.0000E+00   2.36134E+10 0.6498
    4.0000E+00   0.00000E+00 0.0000
    5.0000E+00   0.00000E+00 0.0000
    6.0000E+00   0.00000E+00 0.0000
    7.0000E+00   0.00000E+00 0.0000
    8.0000E+00   0.00000E+00 0.0000
    1.0000E+01   7.95304E+09 1.0000
    2.0000E+01   0.00000E+00 0.0000
      TOTAL      2.86555E+12 0.0892
1TALLY    4        NPS =     59881
          NEUTRON TALLY TYPE 4:   TRACK LENGTH ESTIMATE OF PARTICLE FLUX.

          THIS TALLY IS ALL MULTIPLIED BY  7.44000E+15
          VOLUMES
                   CELL:         1              3

                          2.89583E+01  1.37733E+04

CELL   1

      ENERGY
    1.0000E-09    6.03537E+08 0.6030
    1.0000E-08    7.04990E+10 0.1947
    1.0000E-07    1.32245E+12 0.1034
    1.0000E-06    3.57268E+11 0.1639
    1.0000E-05    1.80331E+11 0.3512
    1.0000E-04    1.59708E+11 0.2562
    1.0000E-03    1.90317E+11 0.2651
    1.0000E-02    1.36783E+11 0.2543
    1.0000E-01    1.94622E+11 0.2469
    5.0000E-01    1.75959E+11 0.2536
    1.0000E+00    5.11751E+10 0.4056
    1.5000E+00    6.88243E+10 0.4127
    2.0000E+00    4.98047E+10 0.5258
    3.0000E+00    3.59468E+10 0.6058
    4.0000E+00    0.00000E+00 0.0000
    5.0000E+00    0.00000E+00 0.0000
    6.0000E+00    0.00000E+00 0.0000
    7.0000E+00    0.00000E+00 0.0000
    8.0000E+00    0.00000E+00 0.0000
    1.0000E+01    1.03526E+10 1.0000
    2.0000E+01    0.00000E+00 0.0000
      TOTAL       3.00465E+12 0.0819


CELL   3

      ENERGY
    1.0000E-09    6.19381E+08 0.0587
    1.0000E-08    5.26064E+10 0.0169
    1.0000E-07    8.15509E+11 0.0126
    1.0000E-06    2.65515E+11 0.0131
    1.0000E-05    1.67824E+11 0.0148
    1.0000E-04    1.69306E+11 0.0148
    1.0000E-03    1.72474E+11 0.0145
```

```
      1.0000E-02   1.79181E+11 0.0145
      1.0000E-01   2.19155E+11 0.0141
      5.0000E-01   2.81563E+11 0.0148
      1.0000E+00   2.07843E+11 0.0182
      1.5000E+00   1.38322E+11 0.0222
      2.0000E+00   1.10591E+11 0.0258
      3.0000E+00   1.48614E+11 0.0244
      4.0000E+00   6.85449E+10 0.0346
      5.0000E+00   3.96714E+10 0.0503
      6.0000E+00   1.89105E+10 0.0669
      7.0000E+00   9.40361E+09 0.0948
      8.0000E+00   4.85485E+09 0.1377
      1.0000E+01   3.71278E+09 0.1703
      2.0000E+01   1.07356E+09 0.2941
        TOTAL      3.07529E+12 0.0088
1TALLY   6         NPS =    59881
           NEUTRON TALLY TYPE 6:   TRACK LENGTH ESTIMATE OF HEATING.

           THIS TALLY IS ALL MULTIPLIED BY  1.19190E+06

           MASSES
                   CELL:       1            3

                         3.83118E+01  2.18995E+04

 CELL  1

        ENERGY
      1.0000E-09   1.40270E-02 0.5634
      1.0000E-08   5.27052E-01 0.1921
      1.0000E-07   3.98578E+00 0.1050
      1.0000E-06   4.71127E-01 0.1617
      1.0000E-05   6.61450E-02 0.3365
      1.0000E-04   1.75768E-02 0.2703
      1.0000E-03   1.14302E-02 0.2646
      1.0000E-02   3.97982E-02 0.2811
      1.0000E-01   4.58830E-01 0.2602
      5.0000E-01   1.31012E+00 0.2603
      1.0000E+00   6.53797E-01 0.4032
      1.5000E+00   1.19237E+00 0.4138
      2.0000E+00   1.04503E+00 0.5264
      3.0000E+00   8.47558E-01 0.5977
      4.0000E+00   0.00000E+00 0.0000
```

```
       5.0000E+00   0.00000E+00 0.0000
       6.0000E+00   0.00000E+00 0.0000
       7.0000E+00   0.00000E+00 0.0000
       8.0000E+00   0.00000E+00 0.0000
       1.0000E+01   3.96298E-01 1.0000
       2.0000E+01   0.00000E+00 0.0000
         TOTAL      1.10369E+01 0.1243

  CELL  3

         ENERGY
       1.0000E-09   3.87019E+00 0.0576
       1.0000E-08   1.03232E+02 0.0169
       1.0000E-07   5.68610E+02 0.0127
       1.0000E-06   6.96501E+01 0.0136
       1.0000E-05   8.16262E+00 0.0180
       1.0000E-04   1.09630E+01 0.0159
       1.0000E-03   4.27301E+00 0.0149
       1.0000E-02   1.43906E+00 0.0149
       1.0000E-01   1.01507E+00 0.0142
       5.0000E-01   2.10224E+00 0.0151
       1.0000E+00   2.26833E+00 0.0183
       1.5000E+00   1.94256E+00 0.0223
       2.0000E+00   1.74064E+00 0.0258
       3.0000E+00   2.60150E+00 0.0245
       4.0000E+00   1.41209E+00 0.0347
       5.0000E+00   8.67723E-01 0.0503
       6.0000E+00   4.48047E-01 0.0671
       7.0000E+00   2.33324E-01 0.0951
       8.0000E+00   1.38861E-01 0.1368
       1.0000E+01   1.11642E-01 0.1696
       2.0000E+01   3.81906E-02 0.2934
         TOTAL      7.85120E+02 0.0120
 TALLY FLUCTUATION CHARTS

               TALLY    1                           TALLY    2                           TALLY    4
       NPS       MEAN       ERROR      FOM            MEAN       ERROR      FOM            MEAN       ERROR      FOM
       4000    1.37194E-02 0.9999 1.4E-02        2.61370E+12 0.9999 1.4E-02        9.99207E+12 0.9999 1.4E-02
       8000    5.12109E-03 0.3294 6.4E-02        1.52329E+12 0.3523 5.6E-02        9.57496E+11 0.3546 5.6E-02
      12000    9.30407E-03 0.1903 1.3E-01        3.04411E+12 0.2372 8.3E-02        3.13213E+12 0.2264 9.1E-02
      16000    9.51680E-03 0.1532 1.5E-01        3.07203E+12 0.1837 1.0E-01        3.07498E+12 0.1830 1.0E-01
```

```
    20000     9.24445E-03 0.1344 1.5E-01       2.91977E+12 0.1578 1.1E-01       3.02807E+12 0.1583 1.1E-01
    24000     9.05379E-03 0.1216 1.6E-01       2.75108E+12 0.1401 1.2E-01       2.99809E+12 0.1442 1.1E-01
    28000     8.66912E-03 0.1121 1.6E-01       2.60761E+12 0.1281 1.2E-01       2.83355E+12 0.1333 1.1E-01
    32000     8.76219E-03 0.1015 1.7E-01       2.61683E+12 0.1155 1.3E-01       2.88507E+12 0.1204 1.2E-01
    36000     8.56043E-03 0.0950 1.7E-01       2.54471E+12 0.1081 1.3E-01       2.85457E+12 0.1125 1.2E-01
    40000     8.73572E-03 0.0885 1.8E-01       2.72054E+12 0.1149 1.1E-01       2.91458E+12 0.1045 1.3E-01
    44000     9.46730E-03 0.0827 1.8E-01       2.93851E+12 0.1042 1.2E-01       3.15198E+12 0.0957 1.4E-01
    48000     9.13342E-03 0.0801 1.8E-01       2.97131E+12 0.1022 1.1E-01       2.96741E+12 0.0936 1.3E-01
    52000     8.90390E-03 0.0773 1.8E-01       2.84635E+12 0.0986 1.1E-01       2.95275E+12 0.0897 1.3E-01
    56000     8.98687E-03 0.0739 1.8E-01       2.81851E+12 0.0936 1.1E-01       2.97727E+12 0.0857 1.4E-01
    59881     9.14030E-03 0.0709 1.9E-01       2.86555E+12 0.0892 1.2E-01       3.00465E+12 0.0819 1.4E-01

              TALLY    6
     NPS        MEAN       ERROR      FOM
     4000     4.20190E+01 0.9999 1.4E-02
     8000     2.82688E+00 0.4286 3.8E-02
    12000     1.41778E+01 0.4159 2.7E-02
    16000     1.17002E+01 0.3411 3.0E-02
    20000     1.08223E+01 0.2809 3.5E-02
    24000     1.03528E+01 0.2441 3.9E-02
    28000     9.68051E+00 0.2223 4.0E-02
    32000     1.16544E+01 0.1918 4.7E-02
    36000     1.10418E+01 0.1786 4.8E-02
    40000     1.11315E+01 0.1650 5.1E-02
    44000     1.22020E+01 0.1460 5.9E-02
    48000     1.13845E+01 0.1425 5.7E-02
    52000     1.12289E+01 0.1352 5.9E-02
    56000     1.08744E+01 0.1301 5.9E-02
    59881     1.10369E+01 0.1243 6.0E-02

*************************************************************************
DUMP NO. 31 ON FILE   RUNTPE          NPS =    59881          CTM =1072.77


        2 WARNING MESSAGES SO FAR.

RUN TERMINATED WHEN    30 KCODE CYCLES WERE DONE.

MCNP     VERSION 3                          05/23/93   11:00:57.02      PROBID = 05/22/93   17:07:19.31
```

REFERENCES

[1] J. E. Turner, Atoms, Radiation, and Radiation Protection (1986), Pergamon Press Inc., New York.

[2] H. Vargas, J. Pelzl, and C. Dimitropoulos, "^{35}Cl NQR Studies of Irradiation Defects in Chlorates," Journal of Magnetic Resonance, 30 (1978), 423.

[3] R. G. Lerner and G. L. Trigg, Encyclopedia of Physics 2nd edition (1991), VCH Publishers. Inc., New York.

[4] W. S. C. Williams, Nuclear and Particle Physics (1991), Oxford Science Publications, Oxford.

[5] B. T. Kelly, Irradiation Damage to Solids (1966), Pergamon Press Inc., Oxford.

[6] D. S. Billington and J. H. Crawford Jr., Radiation Damage in Solids (1961), Princeton University Press, New Jersey.

[7] J. Randall, W. Moulton, and W. Ard, " Effects of Crystalline Defects on Pure Quadrupole Resonances," Journal of Chemical Physics, 31 (1959), 730.

[8] J. Pelzl, H. Vargas, D. Dautreppe, and H. Schulz, "Influence of Point Defects on the Nuclear Quadrupole Resonance of ^{35}Cl in $KClO_3$ and $NaClO_3$," Journal of Physics and Chemistry in Solids, 36 (1975), 791.

[9] J. Duchesne, M. Monfils, and J. Garsou,"Nuclear Quadrupole Resonance of γ-irradiated para-dichlorobenze," Journal of Chemical Physics, 23 (1955), 1969.

[10] D. E. Hintenlang and G. A. Higgins, "Radiation Response of Hydrated Urea Evaluated Using ^{14}N Nuclear Quadrupole Resonance," Nuclear Science and Engineering, 112 (1992), 181.

[11] R. D. Dyson, Cell Biology, A Molecular Approach (1974), Allyn and Bacon Inc., Boston.

[12] R. Dovesi, M. Causa, R. Orlando, C. Roetti, and V. R. Saunders, "Ab Initio Approach to Molecular Crystals: A Periodic Hartee-Fock Study of Crystalline Urea," Journal of Chemical Physics, 92 (1990), 7402.

[13] S. Swaminathan, B. M. Craven, and R. K. Mc Mullan, "The Crystal Structure and Molecular Thermal Motion of Urea at 12, 60 and 123 K from Neutron Diffraction," Acta Crystallographica, B40 (1984), 300.

[14] G. J. Goldsmith and J. G. White,"Ferroelectric Behavior of Thiourea," Journal of Chemical Physics, 31 (1959), 1175.

[15] D. H. Smith and R. M. Cotts,"Nitrogen Electric Quadrupole and Proton Magnetic Resonances in Thiourea," Journal of Chemical Physics, 41 (1964), 2403.

[16] H. C. Ohanian, Physics (1985), W.W. Norton and Company, Inc., New York and London.

[17] A. Foderaro, The Element of Neutron Interaction Theory (1971), MIT Press, Cambridge, Massachusetts, and London.

[18] R. D. Evan, The Atomic Nucleus (1955), Robert E. Krieger Publishing Company, Malabar, Florida.

[19] E. A. C. Lucken, Nuclear Quadrupole Coupling Constants (1969), Academic Press, London and New York.

[20] G. L. Catchen, L. H. Menke, Jr., K. Jamil, M. Blaszkiewicz, and B. E. Scheetz,"Anomalous Asymmetry of the Electric Field Gradient at the Ti Site in $Ba_2(Ti_{0.95}Hf_{0.05})(Ge_{2x}Si_{2-2x})O_8$ Ceramics Measured by Perturbed-

Angular-Correlation Spectroscopy," Physical Review B, 39 (1989), 3826.

[21] A. G. Marshall, Fourier, Hadamard, and, Hilbert Transforms in Chemistry (1981), Plenum Press, New York and London.

[22] N. F. Ramsey, Nuclear Moments (1953), Wiley, New York.

[23] T. P. Das and E. L. Hahn, Nuclear Quadrupole Resonance spectroscopy (1958), Solid State Physics Supplement 1. Academic Press, New York and London.

[24] C. P. Slichter, Principles of Magnetic Resonance (1990), Springer-Verlag, Berlin, New York, and London.

[25] E. P. Wigner, "Gruppentheorie (F. Vieweg and Sohn, Braunschweg,1931);" , Group Theory and its Application to Quantum Mechanics of Atomic Spectra (1959), Academic Press, New York.

[26] J. J. Sakurai, Modern Quantum Mechanics (1985), Benjamin/Cummings Publishing Company, Inc., New York.

[27] K. Sieghbahn, Alpha-, Beta- and Gamma-Ray Spectroscopy Volume 2 (1965), North-Holland Publishing Company, Amsterdam.

[28] E. Schempp and P. J. Bray, Physical Chemistry Volume 4 (1970), edited by D. Henderson, Academic Press Inc., New York.

[29] E. Schempp and P. J. Bray, "Nuclear Quadrupole Resonance in 5 -Membered Heterocycles: Pyrazole, Imidazole, 1,2,4 -Triazole," Physics Letters, 25 (1967), 414.

[30] F. Bloch, "Nuclear Induction," Physical Review, 70 (1946), 460.

[31] L. C. Hebel and C. P. Slichter, " Nuclear Spin Relaxation in Normal and Superconducting Aluminium," Physical Review, 113 (1959), 1504.

[32] D. Wolf, Spin-Temperature and Relaxation in Matter: Basic Principles and Applications (1979), Clarendon Press, Oxford.

[33] R. Kubo and K. Tomita, " A General theory of Magnetic Resonance Absoption," Journal of the Physical Society of Japan, 9 (1954), 888.

[34] A. A. koukoulas and M. A. Whitehead," Experimental Considerations in Determining Spin-Lattice Times in NQR Spectroscopy," Journal of Magnetic Resonance, 86 (1990), 555.

[35] N. Bloembergen, E. M. Purcell, and R. V. Pound, " Relaxation Effects in Nuclear Magnetic Resonance Absorption," Physical Review, 73 (1948), 679.

[36] P. M. Anderson, N. S. Sullivan, and B. Andraka, " Nuclear Quadrupole Resonance Spectroscopy for Ultra-low Temperature Thermometry, " American Institute of Physics: Temperature, its Measurements and Control in Science and Industry, 6 (1992), 1013.

[37] P. J. Bray, S. J. Gravina, D. E. Hintenlang, and R. V. Mulkern, " Nuclear Magnetic Resonance of Glasses," Magnetic Resonance Review, 13 (1988), 263.

[38] N. Bloembergen, Nuclear Magnetic Relaxation (1961), Benjamin, New York.

[39] W. G. Clark, " Pulsed Nuclear Resonance Apparatus," Review of Scientific Instruments, 35 (1964), 316.

[40] J. A. S. Smith, Advances in Nuclear Quadrupole Resonance Volume 1 (1974), Heyden and Son Ltd., London, New York.

[41] E. L. Hahn,"Spin Echoes," Physical Review, 80 (1950), 580.

[42] G. Paic, Inonizing Radiation: Protection and Dosimetry (1988), CRC Press, Florida.

[43] W. L. McLaughlin, A. W. Boyd, K. H. Chadwick, J. C. McDonald, A. Miller, Dosimerty for Radiation Processing (1989), Taylor and Francis, London, New York.

[44] E. P. Blizard and L. S. Abbott, Reactor Handbook 2nd Edition Volume iii Part B (1962), Interscience/John Wiley and sons, New York.

[45] E. O. Brigham, Fast Fourier Transform (1974), Prentice-Hall, Inc., Englewood Cliffs.

[46] W. H. Press, B. P. Flannery, S. A. Teukolsky, and W. T. Vetterling, Numerical Recipes, The Art of Scientific Computing (1988), Cambridge University Press, Cambridge and New York.

[47] E. R. Cohen and B. N. Taylor, " The 1986 Adjustment of the Fundamental Physical Constants," Review of Modern Physics, 59 (1987), 1121.

[48] P. R. Bevington, Data reduction and Error Analysis for Physical Sciences (1969), McGraw-Hill Book Company, New York.

[49] D. W. Marquardt, "An Algorithm for Least-square Estimation of Nonlinear Parameters," Journal of the Society for Industrial and Applied Mathematics, 11 (1963), 431.

[50] A. R. Gallant, " Nonlinear Regression," The American Statistician, 29 (1975), 73.

[51] L. H. Iselin, " An analytical Method for Estimating the ^{14}N Nuclear Quadrupole Resonance Parameters of Organic Compounds with Complex Free Induction Decays for Radiation Effects Studies," ME Thesis (1992), University of Florida, Gainesville.

[52] Y. Ueda, T. Okazaki, and T. Ichikawa, " ESR Study of Radicals Produced with 60Co-γ Rays at 77K in Thiourea Single Crystals," Miroshima Daigaku K-Ogakubu Kenky-u h-okoku' : Bulletin of the Faculty of Engineering, Hiroshima University 32 (1984), 145.

[53] E. D. Cashwell and C. J. Everett, A Practical Manual on the Monte Carlo Method for Random Walk Problems (1959), Pergamon Press, New York and London.

[54] J. Spanier and E. M. Gelbard, Monte Carlo Principles and Neutron Transport Problems (1969), Addison-Wesley, New York.

[55] W. L. Thomson, MCNP-A General Monte Carlo Code for Neutron and Photon Transport, Revised Edition (1990), Las Alamos Monte Carlo Group, Los Alamos National Laboratory, New Mexico.

[56] N. J. Diaz and W. G. Vernetson, Safety Analysis Report University of Florida Training Reactor Revised Edition (1989), Department of Nuclear Engineering Sciences, University of Florida, Gainesville.

[57] E. I. Fedin and A. I. Kitaigorodskii, "Nuclear Quadrupole Resonance Studies of Solid Solutions of Some Organic Compounds," Soviet Physics- Crystallography 6 (1960), 322.

[58] L. J. Shyr, "Risk Estimate of Low-Level Radiation Exposure Using Stochastic Concepts," Ph.D. dissertation, (1988), The University of North Carolina, Chapel Hill.

[59] V. Beir, Health Effects of Exposure to Low Levels of Ionizing Radiation (1990), National Academic Press Washington D.C.

BIOGRAPHICAL SKETCH

Khalid Jamil was born on December 16, 1956, at Lahore, Pakistan. His mother died when he was a toddler and his father, Mr. Hifzur Rehman Wahidi, brought him up. He learned languages, basics of physics, chemistry, and mathematics at home from his father and did his matriculation from Lahore board of intermediate and secondary education in 1970. He was formally admitted to Mohammadan Anglo Oriental (MAO) college at Lahore, where he passed his Fellow of Science, F.Sc., in 1972. He received his B.Sc. degree from Government College Lahore in 1974. He continued his graduate studies and accomplished his master's degree in physics from University of the Punjab, Lahore, in 1976. He was selected for a fellowship from the Center for Nuclear Studies (CNS) for doing his M.Sc. in nuclear engineering which he completed in 1979. Mr. Jamil stood first class throughout his academic career and received meritorious scholarships.

In 1980, Mr. Jamil accepted a position as a researcher at Pakistan Institute of Nuclear Science and Technology (PINSTECH). There, he was associated with research for the development and applications of solid state nuclear track detectors (SSNTD) in various disciplines of nuclear physics and nuclear engineering. He authored and coauthored over forty research papers in refereed journals of international repute.

In 1984, he went to Philipps University Marburg, then in West Germany, on a training program as a Pakistani scientist in radon measurements and heavy ions physics. He completed his training successfully and produced several papers during his stay in West Germany. He returned to Pakistan in 1985.

In fall 1985, he won a scholarship from the ministry of science and technology, Pakistan, in an open competition for doctoral studies in nuclear engineering. He was sent to Pennsylvania State University (PSU) in fall 1986 where he continued his Ph.D. work in the area of Perturbed Angular Correlation (PAC) spectroscopy and coauthored three papers on PAC spectroscopy in Physical Review B. However, as a result of conflicts between his research mentor and the PSU administration, Mr. Jamil decided to transfer his studies to the University of Florida continuing his doctoral studies in the similar spectroscopic technique of Nuclear Quadrupole Resonance (NQR).

Khalid and his wife, Farhat Fatma, had their 11th marriage anniversary on October 5, 1993. They have a nine-year-old son, Ashar and a five-year-old daughter, Anam.

I certify that I have read this study and that in my opinion it conforms to acceptable standards of scholarly presentation and is fully adequate, in scope and quality, as a dissertation for the degree of Doctor of Philosophy.

David E. Hintenlang, Chairman
Assistant Professor of
Nuclear Engineering Sciences

I certify that I have read this study and that in my opinion it conforms to acceptable standards of scholarly presentation and is fully adequate, in scope and quality, as a dissertation for the degree of Doctor of Philosophy.

William H. Ellis

William H. Ellis
Associate Professor of
Nuclear Engineering Sciences

I certify that I have read this study and that in my opinion it conforms to acceptable standards of scholarly presentation and is fully adequate, in scope and quality, as a dissertation for the degree of Doctor of Philosophy.

Samim Anghaie

Samim Anghaie
Professor of
Nuclear Engineering Sciences

I certify that I have read this study and that in my opinion it conforms to acceptable standards of scholarly presentation and is fully adequate, in scope and quality, as a dissertation for the degree of Doctor of Philosophy.

Robert J. Hanrahan
Professor of Chemistry

I certify that I have read this study and that in my opinion it conforms to acceptable standards of scholarly presentation and is fully adequate, in scope and quality, as a dissertation for the degree of Doctor of Philosophy.

E. Dow Whitney

E. Dow Whitney
Professor of Materials Science
and Engineering

This dissertation was submitted to the Graduate Faculty of the College of Engineering and to the Graduate School and was accepted as partial fulfillment of the requirements for the degree of Doctor of Philosophy.

December 1993

Winfred M. Phillips
Dean, College of Engineering

Karen A. Holbrook
Dean, Graduate School